# DEEP-ETCHED WAVEGUIDE GRATINGS FOR PHOTONIC DEVICES

# ANALYSIS AND DESIGN OF THIN FILM COATINGS AND DEEP-

# ETCHED WAVEGUIDE GRATINGS

# FOR INTEGRATED PHOTONIC DEVICES

By

GUIRONG (RONA) ZHOU, B.Eng. (EE), M.Eng. (EE)

A Thesis

Submitted to the School of Graduate Studies in

Partial Fulfillment of the Requirements

For the Degree

Master of Engineering

McMaster University

© Copyright by Gui-Rong Zhou, Apr. 2002

i

MASTER OF ENGINEERING (2002)    McMaster University

(Electrical and Computer Engineering)    Hamilton, Ontario

TITLE:    Analysis and Design of Thin Film Coatings and Deep-etched

Waveguide Gratings for Integrated Photonic Devices

AUTHOR:    Gui-Rong (Rona) Zhou, M.Eng. (Nanjing Univ. of Sci. & Tech.)

SUPERVISOR:    Professor Xun Li

CO-SUPERVISOR:    Professor Wei-Ping Huang

NUMBER OF PAGES: Xviii, 139

# ABSTRACT

This thesis aims at investigating the feasibility of realizing antireflection (AR) and high-reflection (HR) to the semiconductor waveguide end facet using monolithically integratable deep-etching technology to replace the conventional thin film dielectric coating counterpart.

Conventional AR coating and HR coatings are the building blocks of semiconductor optical amplifier and semiconductor lasers. In this thesis, the AR coating and HR coating are first studied systematically and comprehensively using two computational electromagnetics approaches: plane wave transmission matrix method (TMM) and finite difference time domain (FDTD) method. The comparison of the results from the two approaches are made and discussed. A few concepts are clarified based on the different treatment between the AR coatings for bulk optics and those for semiconductor waveguide laser structure.

The second part uses the same two numerical tools and more importantly, the knowledge gained from the first part to analyze and design deep-etched waveguide gratings for the advantage of ease of monolithic integration. A variational correction to the TMM is provided in order to consider effect of the finite etching depth also in the plane wave model. Specially, a new idea of achieving AR using deep-etched waveguide gratings is proposed and analyzed comprehensively. A preliminary design is obtained by TMM optimization and FDTD verifications, which provides a minimum power reflectivity in the order of $10^{-5}$ and a bandwidth of 45nm for the power reflectivity less than $10^{-3}$. In order to eliminate the non-physical reflections from the boundary, the perfectly matched layer (PML) absorbing condition is employed and pre-tested for antireflection analysis. The effects of etching depth and number of etching grooves are specifically analyzed for the performance of proposed structures.

Numerical results obtained by FDTD method indicate a promising potential for this alternative technologies.

# ACKNOWLEDGEMENT

# CONTENTS

# LIST OF GLOSSARY

## Symbols

$n_{co}$ : Refractive index of the core active layer of the three-layer optical slab waveguide

$n_{cl}$ : Refractive index of the cladding layer

$d$ : Thickness of the core layer (in $\mu$m units)

$n_i$ : Refractive index of the $i^{th}$ thin film antireflection coating layer, $i$ =1, 2, 3…

$d_i$ : Physical thickness of the $i^{th}$ thin film antireflection coating layer, $i$ =1, 2, 3…

$n_{L,H}$ : Refractive indices of Low (L) and high index (H) layer for high-reflection coatings

$N_{eff}$ : Effective modal index of the waveguide.

$n_L$ : Refractive index of the deep-etched waveguide groove layer.

$d_{Hi}$ : Physical thickness of the $i^{th}$ waveguide barrier layer, $i$ =1, 2, 3…

$d_{Li}$ : Physical thickness of the $i^{th}$ deep-etched waveguide groove layer, $i$ =1, 2, 3…

$r_{s,p}$ : Reflection coefficient for $s$ or $p$ wave, $s$ or $p$ is an alternative symbol for TE or TM often used in thin film optics.

$t_{s,p}$ : Transmission coefficient for $s$ or $p$ wave, $s$ or $p$ is an alternative symbol for TE or TM.

$R_{s,p}$ : Reflectance or power reflectivity for $s$ or $p$ wave.

$T_{s,p}$ : Transmittance or power transmission for $s$ or $p$ waves.

$R$　　: Reflectance or power reflectivity from TMM at normal incidence or modal reflectance (power reflectivity) from FDTD.

## Acronyms

AR: anti-reflection

HR: high-reflection

QWOT: quarter-wave optical thickness

TMM: transmission matrix method

FDTD: finite difference time domain

FD: finite difference

EIM: effective index method

PML: perfectly matched layer

DE: deep-etched

SABAR: semiconductor/air Bragg reflector

TE: transverse electric

TM: transverse magnetic

# LIST OF FIGURES

# LIST OF TABLES

# 1 Introduction

## 1.1 RESEARCH BACKGROUND

Optical communication is the key answer to the ever-increasing demand for data transmission capacity. Thin film optical coating technology provides huge number of optical components such as bandpass filters, antireflection (AR) coatings, high-reflection (HR) coatings, beam-splitters, etc [1]-[6],[9]. Among the various applications, the antireflection coating, which is crucial for travelling wave semiconductor optical amplifier (SOA)[8]-[29], has the greatest importance and most stringent requirements on precision control, and hence is costly. Driven by the significant cost-effective advantages provided by the photonic integrated circuits (PICs) [41]-[45], this thesis is aimed at searching for a monolithic integration alternative solution to conventional AR coatings, as well as a continue study on the integration replacement for HR coatings based on some existing publications[69]-[79].

### 1.1.1 Thin Film Optical Coatings

An optical thin film has been defined in mathematical terms as in [1]:

*A thin film is one whose thickness is of the order of the wavelength of light and whose extent is infinite compared to its thickness; we assume it is bounded by semi-infinite planes. The film is characterized by its refractive index, its absorption coefficient and its thickness (assumed to be uniform).*

The so-called classical thin film optical coatings consists of a sequence of dielectric layers with thickness comparable to the wavelength, and exhibit one of the spectral characteristics shown in Fig. 1-1, where R stands for reflectance and T stands for transmittance [6].
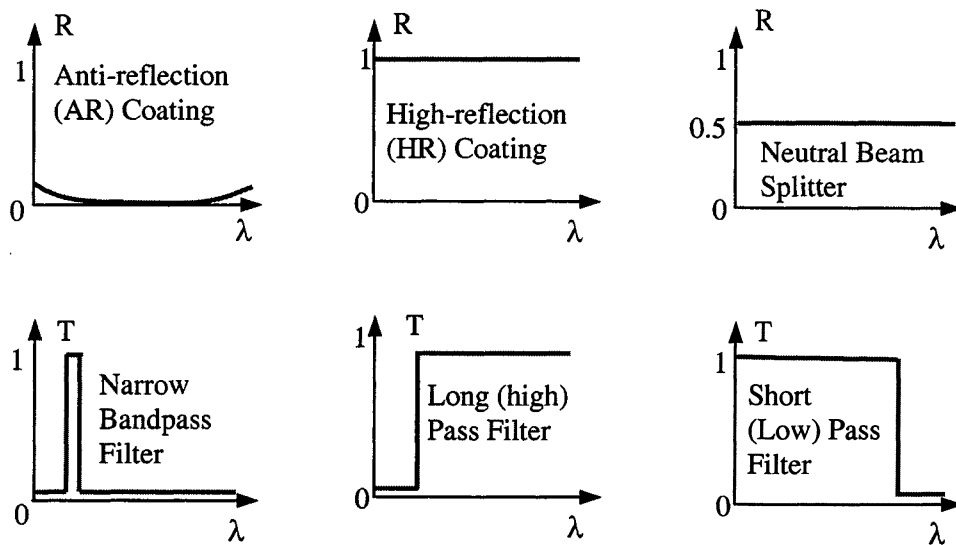


**Fig. 1-1 Characteristics of so-called classical optical coatings [6]**

Thin film coatings are used to alter the reflectance, transmittance, absorbance, or polarization properties of optical components. In Bulk optics, the medium to be coated is usually called the *substrate*. Thin film coatings are deposited in high vacuum ($<10^{-6}$ Torr) using the processes such as evaporation, thermal vaporization, sputtering, etc.[1], [5], [12]. The accurate controls of layer thickness and layer refractive index are crucial in the deposition of optical coatings. Therefore, *In-situ* monitoring is highly desired in the thin film coating manufacturing, especially for antireflection coatings. The higher the requirement is, the more fabrication cost is needed.

In the great majority of cases the thin films are completely transparent, so that no energy

is absorbed. The thin film coatings studied in this thesis is also based on this assumption.

A simple antireflection coating should, therefore, consist of a single film of refractive

index equal to the square root of that of the substrate, and of the optical thickness one quarter of a

wavelength. As it will be explained in the next part briefly and in the specific chapter (Chap. 3)

in detail, there are other improved coatings covering wider wavelength ranges involving more

coating layers.



**(a)**                                                                                                                        **(b)**
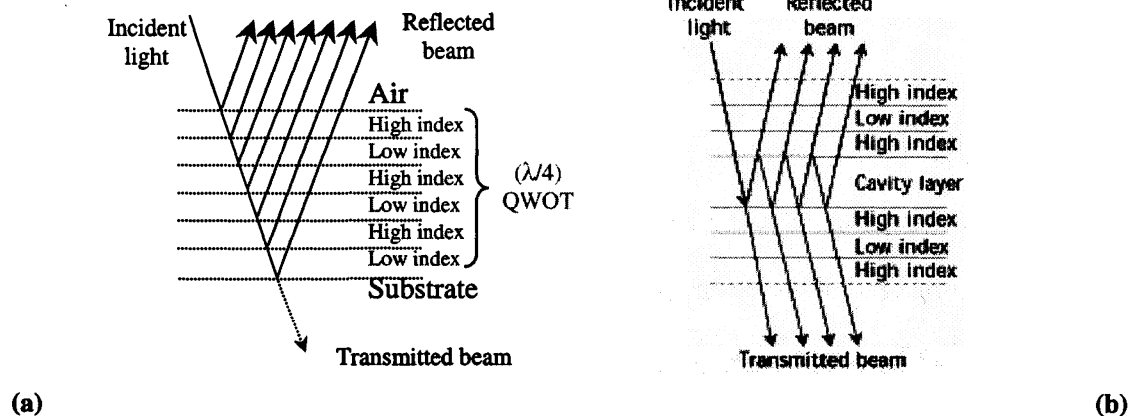
**Fig. 1-2 (a) Schematic view of thin film high-reflection coating; (b) A Fabry-Perot filter showing multiple reflections in the spacer layer.**

Another basic type of thin-film structure is a stack of alternating high- and low-index

films, all one-quarter wavelength thick (see Fig. 1-2 (a)). Light reflected within the high-index

layers will not suffer any phase shift on reflection, while that reflected within the low-index

layers will suffer a change of $180^0$ or $\pi$ phase shift. It is fairly easy to see that the various

components of the incident light produced by the reflection at successive boundaries throughout

the assembly will reappear at the front surface all in phase so that they will recombine

constructively. This implies that the effective reflectance of this assembly can be made very high

indeed, as high as may be desired, merely by increasing the number of layers. This is the basic form of the high-reflection (HR) coatings. When such a coating is constructed, it is found that the reflectance remains high over only a limited range of wavelengths, depending on the ratio of high and low refractive indices. Outside this zone, the reflectance changes abruptly to a low value. Because of this behaviour, the quarter-wave stack is used as a basic building block for many types of thin-film filters. It can be used as a longwave- (high) pass filters, a shortwave-(low) pass filter, a bandpass filter, a straightforward high-reflection coating as shown in Fig. 1-1. The application examples can be found in semiconductor laser mirrors, and as reflectors in a thin-film Fabry-Perot interferometer, which is another fundamental filter type.

A thin film bandpass filter consists of a spacer or cavity layer, which is usually a half a wavelength thick, bounded by two high-reflection coatings (see Fig. 1-2 (b)). Multiple-beam interference in the spacer or cavity layer causes the transmission of this filter to be extremely high over a narrow band of wavelengths around that for which the spacer is a multiple of one half wavelength thick. A more rectangular pass band shape can be achieved by coupling two more Fabry-Perot filters in series, similarly to lumped electric circuits.

### 1.1.2 Semiconductor Optical Amplifier and Antireflection Coatings

With the increasing bandwidth demand, the construction of optical packet-switching nodes targeting optical routers would benefit from fast optical switches. Semiconductor-optical-amplifier (SOA) technology provides this high-speed switching capability as well as gain, high extinction ratio, and high integration potential. Moreover, it is a key technology for several other functions, including all-optical wavelength conversion, regeneration, wavelength selection,

booster and in-line amplification, in-node optical pre-amplification, and mid-span spectral inversion [9], [11].

An SOA is based on the same technology as a Fabry-Perot diode laser. Such a laser consists of an amplifying medium located inside a resonant (Fabry-Perot type) cavity. The amplification function is achieved by externally pumping the energy levels of the material. In order to obtain this amplification function only, it is necessary to protect the device against self-oscillations generating the laser effect. This is accomplished by blocking cavity reflections using both an antireflection (AR) coating and techniques such as angle cleaving the chip facets [8]-[11].

Depending on the efficiency of the AR coating, SOAs can be classified as resonant devices or traveling-wave (TW) devices. Resonant SOAs are manufactured using an AR coating with a reflectivity around $10^{-2}$. They typically feature a gain ripple of 10 to 20 dB and a bandwidth of 2 to 10 GHz. TW devices incorporate a coating with a reflectivity less than $10^{-4}$, which show a gain ripple of a few dB and a bandwidth better than 5 THz (e.g., 40 nm in the 1550 nm window). From now on, the SOAs discussed in this thesis refer to TW devices, which place a stringent requirement on AR coatings.

AR coated, R=0

$P_{in}$

$P_{out} = P_{in}\ e^{g_{net}L}$

L
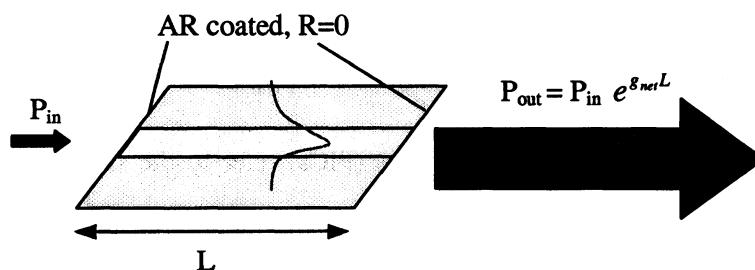
**Fig. 1-3 A Schematic view of a standard SOA**

As shown in Fig. 1-3, the input optical power $P_{in}$ injected into the SOA waveguide is amplified according to $P_{out} = G_{sp} P_{in}$, where $G_{sp}$ is the single pass gain over the length L of the TW SOA such that $G_{sp} = \exp(g_{net} L)$. The net gain $g_{net}$ is given by $g_{net} = \Gamma g - \alpha$, where $\Gamma$, $g$, and $\alpha$ are the optical confinement factor, the material gain, and the optical loss, respectively.

Using single or multiple layers of coating materials ($SiO_x$, $MgF_2$, $TiO_2$, $Al_2O_3$, etc.) for the AR coating technologies, as shown in Fig. 1-4, it is possible to achieve reflectivities on the order of $10^{-5}$, where QWOT stands for quarter wavelength optical thickness and the half wavelength optical thickness is abbreviated to HWOT. The HWOT layer is often called *cavity* of *spacer* in the thin film optics. By combining tilted facets (about a 7° angle) with an AR coating, a device with a highly reproducible and extremely low residual reflectivity can be achieved, leading to gain ripples as low as 0.5 dB [8]-[11].
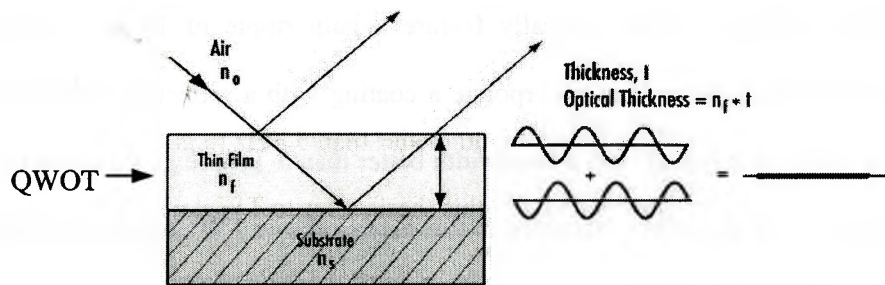


**Fig. 1-4 Single layer antireflection (AR) coating**

## 1.1.3  Photonic Integrated Circuits and Distributed Bragg Reflectors

Semiconductor photonic integrated circuits (PICs) refer to the subset of optoelectronic integrated circuits (OEICs), which focus primarily on the monolithic integration of optically interconnected guided-wave optoelectronic devices. The primary objectives for photonic integration are similar to those for electronic integration: increase functionality and decrease the

cost and size. Meanwhile, PICs are also expected to achieve packaging robustness, associated with replacing individually aligned, single-mode optical connections between discrete optoelectronic devices with lithographically produced integrated waveguides [70].

Manufacturing processes of monolithic PICs are based on semiconductor industry techniques, and can be applied to optics industry through changes to the photo-mask design with pre-knowledge obtained from the computer aided design (CAD) results and related practical experiences. Nowadays, the electronics industry has successfully evolved from discrete transistors to Very Large Scale Integrated Circuits (VLSI), and the significant cost and reliability improvements have been achieved accordingly. Photonic devices are largely based on similar materials, typically III-V semiconductor materials, and are processed or fabricated using many of the same technologies that form the basis for silicon-integrated circuits fabrication. However, optical components rely both on the optical and electronic properties of the materials they are fabricated from, and they often require heteroepitaxial material with accurately controlled composition to achieve optimum performance. As a result, PICs are typically more complicated in structure than silicon ICs [43].

PICs have gained significant progress during the last two decades. Among all these advances, one of the major improvements is the routine fabrication of grating-based distributed feedback (DFB) and distributed Bragg reflector (DBR) lasers [69], allowing high-Q on-chip resonators without cleaved facets. Critical to the success of PIC technology is the ability to make reproducible, high-quality active-passive waveguide transitions. The early approaches in PICs employed butt-coupling, where the active waveguide was removed, and followed by a regrowth of an aligned passive waveguide. Spot-size converter integrated lasers and electroabsorption (EA) modulator integrated DFB lasers have been developed and introduced for practical

applications. If some active devices are integrated within one small area, however, power consumption will be a more crucial issue. Therefore, the reduction of threshold current in lasers is indispensable by combining short cavity and high-reflection coatings. Facet coating applied to short-cavity laser facets, however, may cause overspreading on the surface of lasers, which results in both die-and wire-bonding. In order to overcome these problems, multiple etched mirrors consisting of semiconductor/air pairs are applied into the short cavity laser and their characteristics are numerically calculated [73]-[79]. This distributed reflector shows a very wide high-reflectivity bandwidth due to the large refractive index contrast between semiconductor and air, which allows us to have the advantages of higher fabrication tolerance to lithographic error, imperfect etching, etc. Shin et al first proposed and demonstrated new type low threshold laser due to multiple reflectors consisting of semiconductor/air pairs [71]. Baba et al. proposed a novel short-cavity laser with deep-grating distributed Bragg reflectors (DBRs), and predicted ultimate performance, theoretically [74]. Yuan et al. demonstrated a short-cavity edge-emitting 0.98-μm GaAs-based laser with semiconductor/air DBR mirrors made by reactive ion etching (RIE) [75]. They obtained an effective reflectivity of ~60%. Fig. 1-5 shows a typical application example for semiconductor/air Bragg reflector (SABAR) fabricated in [78].
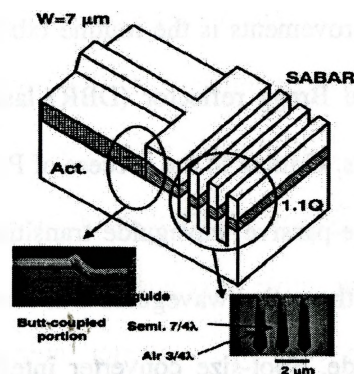


**Fig. 1-5 A schematic view of fabricated integrated laser with butt-coupled waveguide and SABAR is displayed. SEM photographs of butt-coupled waveguide and SABAR are inserted [78].**

## 1.1.4  Main Goal and Challenges

The thesis is attempted to investigate the feasibility of achieving an antireflection by deeply etching the waveguide, instead of cleaving and depositing the dielectric coatings. The main advantage it offers is the significant cost reduction with easier fabrication. From another point of view, the goal of this thesis is to build a complete transition bridge between the thin film coating applications and the on-chip deeply etching waveguide applications, especially when this transition has been partially achieved from HR coating to HR waveguide grating as discussed in the previous part. The question becomes:

1) For an end deep-etched semiconductor laser waveguide structure, can this become a traveling wave amplifier, if we re-design the etching profile by varying the groove width and etching depth? More technically, the problem could be described as, whether we can achieve the very low reflection ($<10^{-4}$) with this deep-etched waveguide grating structure?

2) If answer is yes to the above question, how wide this low reflection bandwidth is?

The first major challenge is the large refractive index contrast provided by semiconductor/air pairs in our proposed new structure, which ever worked as a big advantage for high-reflection applications. As we all know, in the thin film coating structure, the anti-reflection is achieved by complete destructive interference introduced by the multiple dielectric boundaries. In our problem here, the interference mechanism is similar, but only with two fixed media, one is semiconductor waveguide (refractive index around 3.2), the other is the air (1.0). This can be roughly viewed as a coating design problem with two uniform layers with equivalent indices of $n_L$ and $n_H$.

The second challenge is to find a reliable simulation tool to simulate this structure. The conventional simulation tools of thin film coating devices are based on plane wave model and represented mathematically in a transmission matrix method (TMM)[5]-[10] or its equivalent forms. However, this model has been proved to be sufficiently valid only for glass substrate, which occurs in bulk optics. When the thin film coating is deposited at the optical waveguide end facet (in the cases of semiconductor lasers and amplifiers), the plane wave model is no longer sufficient for accurately simulating the wave propagations within the structure. The structure we are about to study has finite etching depth, and the resulted electromagnetic radiations can not be neglected. A more accurate model is needed in order to provide reliable predictions with the thin film coating design as well as deep-etched waveguide grating structures for the integration photonic devices.

The finite difference time domain (FDTD) method has been believed to be a reliable electromagnetic analysis tool [46]-[57]. This method can be easily employed to analyze our structure. However, FDTD simulation normally takes a large amount of computation time, and hence contradicts somehow with the design requirement, that an efficient tool is highly desired.

In summary, the main challenges of this research are:

1) How to accurately simulate the deep-etched waveguide grating structure.

2) How to combine this time-consuming FDTD simulation, with the desired broadband antireflection (BBAR) design.

Another important issue is the QWOT and HWOT are no longer valid in antireflection coatings to the optical amplifier waveguide end, which will be discussed in more detail both in Chapter 3 and Chapter 5.

## 1.2 MAJOR CONTRIBUTIONS

1) Systematic study of the characterization and design of thin film coating devices, especially for the antireflection (AR) coatings, by employing two different numerical methods (TMM and FDTD), comparisons and possible improvements are made.

2) Employ all the experiences gained with thin film coating design to analyze and design of deep-etched waveguide grating structure. Specifically, for the relatively difficult part, antireflection design, the optimum conditions and solutions solved with TMM work as an initial design. The more reliable design is achieved by a refinement with FDTD method.

3) Theoretically prove that deep-etched semiconductor/air gratings can provide not only high-reflection (HR) facet application, but also antireflection (AR) application by using conventional thin film coatings analysis method. Numerically verifying by more accurate finite difference time domain method. Broadband design is preliminarily achieved by applying more grooves design.

4) Effect of etching depth on the field distribution and modal reflectance is studied by FDTD method. The contribution from radiation mode can be clearly observed from the calculated field distribution.

## 1.3 THESIS OUTLINE

The arrangement of this thesis can be read from Fig. 1-6. The whole contents can be divided into two parts, with one part as thin film coating applications (Chapter 3 and 4) and the other part as deep-etched waveguide applications (Chapter 5 and 6). Before discussing any of the applications, the numerical methods to be employed in simulation and design are introduced in Chapter 2, which includes plane wave transmission matrix method (TMM), the finite difference

time domain (FDTD) method, and the effective index method (EIM). These three sections compose the body part of Chapter 2, and are used in every part of the later chapters. The following chapter contains the simulation and design for anti-reflection (AR) coatings both for glass substrate and semiconductor amplifier waveguide. The chapter followed is the similar treatment for high-reflection coatings. Due to the fact that the HR coating for glass substrate is trivial from a theoretical design point of view, we only dealt with HR coated laser facet. For both chapters, TMM and FDTD and combined with refining method to achieve proper coating design. After we have gained the experience of applying these two numerical tools into thin film coating structure, in Chapter 5, we studied the deep-etched waveguide grating for antireflection application. The numerical design results have theoretically proved that a low reflectivity at center wavelength of $1 \times 10^{-5}$ and a bandwidth as wide as 45 nm ($R < 10^{-3}$) can be achieved by applying two deeply etching grooves at the waveguide end. In Chapter 6, the same waveguide structure is used for HR design. Effects of grating period and etching depths on the power reflectivity as well as the bandwidth are considered.
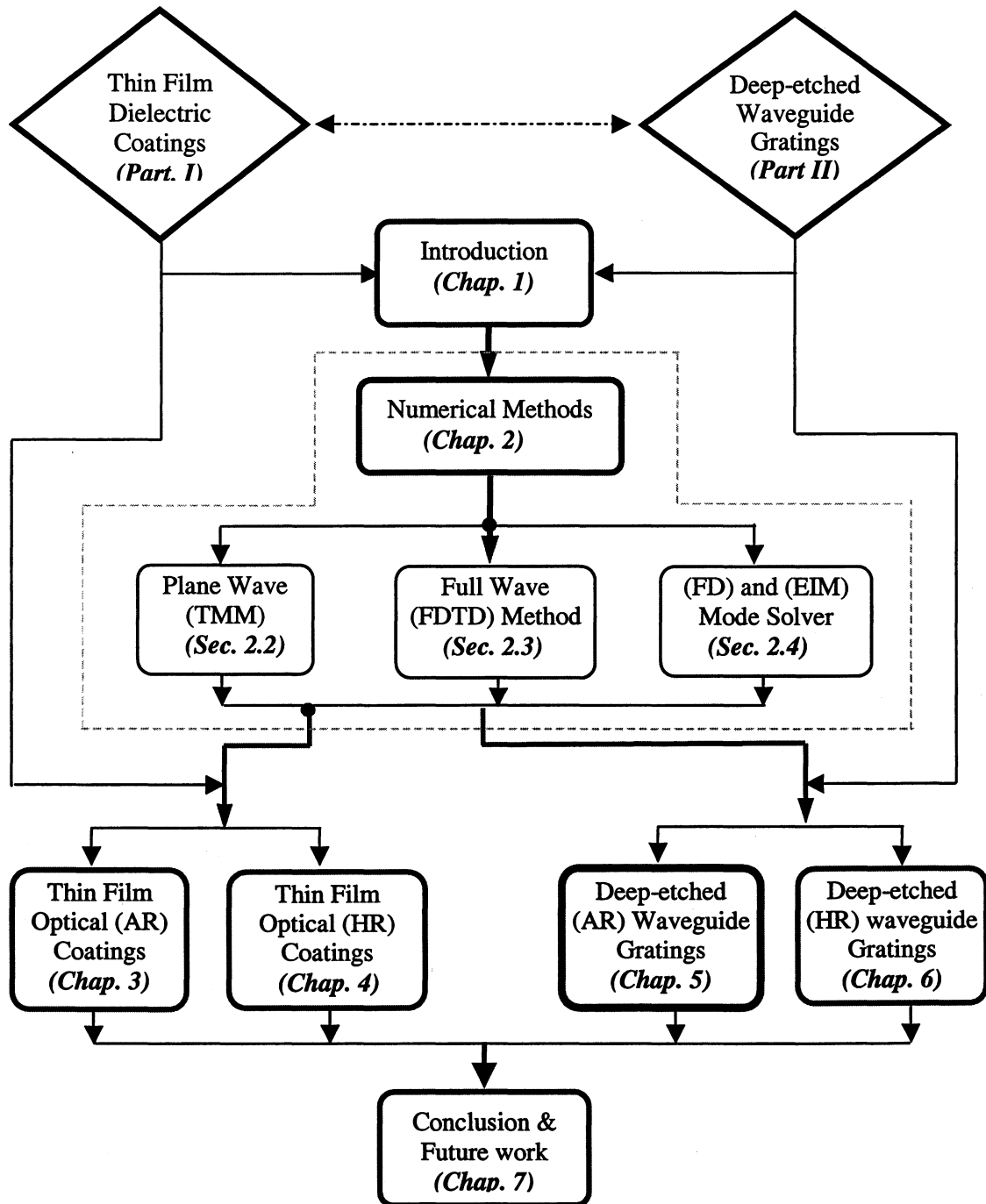
**Fig. 1-6 Block Diagram of the outline of this thesis**

## REFERENCE

[1]  Z. Knittl. *Optics of Thin Films*, John Wiley, New York, 1976.

[2]  J. A. Dobrowolski, Coatings and filters, in *Handbook of Optics*, W. G. Driscoll, eds., McGraw-Hill, New York, 1978.

[3]  H. M. Liddell, Computer-aided Techniques for the Design of Multilayer Filters. Adam Hilger, Bristol, 1981.

[4]  H. Haus, *Waves and Fields in Optoelectronics*. Englewood Cliffs, Nf: Prentice-Hall, 1984.

[5]  H. A. Macleod, *Thin-Film Optical Filters*, 1$^{st}$ ed. (1982), 2$^{nd}$ ed. (1985), 3$^{rd}$ ed. (2001), Chap. 1-4, McGraw-Hill, New York.

[6]  A. Thelen, *Design of optical interference coatings*, McGraw-Hill Optical and Electro-Optical Engineering Series, Chap. 1-5, McGraw-Hill, 1989.

[7]  S. Ramo, J. R. Whinnery, and T. van Duzer, *Fields and Waves in Communication Electronics*, John Wiley, New York, 1984.

[8]  G. P. Agrawal, *Fiber-optic Communication Systems*, second edition, John Wiley, New York, 1995.

[9]  R. Ramaswami and K. N. Sivarajan, *Optical Networks: A Practical Perspective*, Morgan Kaufmann Publishers, Inc., San Francisco, CA, 1998.

[10] P. Yeh, *Optical Waves in Layered Media*, John Wiley, New York, 1988.

[11] J. -J. Bernard and M. Renaud, "SOAs offer a key technology for amplification, switching, wavelength conversion, and regeneration in optical networks", *Alcatel* on-line tutorial, copyrighted by *Alcatel*, Sept. 2001.

[12] Edmund Industrial Optics, "An introduction to optical coatings", on-line tutorial from *Edmund industrial optics*, copyrighted by *Edmund*, Barrington, NJ, 2001.

[13] J. A. Dobrowolski, D. Poitras, et al, "Towards 'perfect' antireflection coatings", *Optical Interference Coatings*, OSA Technical Digest (Optical Society of America), pp. TuA2-1–TuA2-3, July 15-20, 2001.

[14] R. H. Clarke, "Theoretical performance of an anti-reflection coating for a diode laser amplifier, " *Int. J. Electron.*, vol.53, no. 5, pp.495-499, 1982.

[15] G. Eisenstein, "Theoretical design of single layer antireflection coatings, " *Bell Syst. Tech. J.*, vol. 63, no.2, pp.357-364, 1984.

[16] D. R. Kaplan, and P. P. Delmel, "Exact calculation of the reflection coefficient for coated optical waveguide devices," *AT&T Bell Laboratories Technical Journal*, vol.63, no.6, pp.857-877, July-Aug. 1984.

[17] C. Vassalo, "Rigorous and approximate calculations of antireflection layer parameters for travelling-wave diode laser amplifiers", *Electronics Lett.*, vol.21, no.8, Apr. 1985.

[18] T. Sitoh, T. Mukai, and O. Mikami, "Theoretical analysis and fabrication of antireflection coatings on laser-diode facets," *IEEE J. Lightwave Technol.*, vol. LT-3, pp.288-293, 1985.

[19] C. Vassallo, "Polarization-independent antireflection coatings for semiconductor coatings for semiconductor optical amplifiers," *Electronic Lett.*, vol.24, no.1, pp.61-62, Jan. 1988.

[20] L. Atternas and L. Thylen, "Single-layer antireflection coating of semiconductor lasers: polarization properties and the influence of the laser structure", *IEEE J. Lightwave Technol.*, vol. LT-7, no. 2, pp.426-430, 1989.

[21] C. Vassallo, "Theory and practical calculation of antireflection coatings on semiconductor laser diode optical amplifiers", Optical Amplifier Commun., *IEE Proc.*, vol.137, pt. J, no.4, pp.193-202, Aug. 1990.

[22] D. M. Braun, and R. L. Jungerman, "Broadband multiplayer antireflection coating for semiconductor laser facets," *Opt. Lett.*, vol.20, no.10, pp.1154-1156, 1995.

[23] C. Cole, "Broadband antireflection coatings for spaceflight optics," *Ph.D thesis* (#R7123), University of reading, UK. Sept. 1995.

[24] R. Prakasam, S. Fox, et al, "Practical approach to design and fabrication of antireflection coatings for semiconductor optical amplifiers", *IEEE Photon. Technol. Lett.*, vol.8, no.4, pp.509-511, Apr. 1996.

[25] D. J. Gallant, M. L. Tilton, D. J. Bossert, J. D. Barrie, and G. C. Dente, "Optimized single-layer antireflection coatings for semiconductor lasers", *IEEE Photon. Technol. Lett.*, vol.9, pp.300-302, Mar. 1997.

[26] J. Lee, T. Tanaka, S. Sasaki, S. Uchiyama, "Novel design procedure of broadband multilayer antireflection coatings for optical and optoelectronic devices", *IEEE J. Lightwave Technol.*, vol. LT-16, no.5, pp.884-891, 1998.

[27] J. Lee, T. Kamiya, "Improved characterization of multilayer antireflection coatings for broad-band semiconductor optical amplifiers", *IEEE J. Lightwave Technol.*, vol. LT-18, pp.2158-2166, 2000.

[28] J. Yamauchi, M. Mita, S. Aoki, and H. Nakano, "Analysis of antireflection coatings using the FD-TD method with the PML absorbing boundary condition," *IEEE Photon. Technol. Lett.*, vol.8, pp.239-241, 1996.

[29] P. Sewell, M. Reed, T. M. Benson, and P.C. Kendall, "Full vector analysis of two-dimensional angled and coated optical waveguide facets," *IEEE J. Quantum Electron.*, vol.33, pp.2311-2318, Dec. 1997.

[30] C. A. Brackett, "Dense wavelength division multiplexing networks: Principles and applications, "*IEEE J. Selected Area Commun.*, vol. 8, pp. 948-964, 1990.

[31] R. E. Wagner, R. C. Alferness, M. Saleh, and M. S. Goodman, "MONET: Multiwavelength optical networking," *J. Lightwave Technol.*, vol.14, pp.1349-1355, 1996.

[32] R. Magnusson and S. S. Wang, "New principle for optical filters," *Appl. Phys. Lett.*, vol.61, 1022, 1992.

[33] C. He, D. Ma, and W. -Z. Li, "Thin-film filters are the building blocks of multiplexing devices", *WDM Solutions*, Penwell, May 2001.

[34] M. A. Scobey and D. E. Spock, "Passive DWDM components using microplasma optical interference filters," *OFC'96 Technical Digest*, pp. 242-243, San Jose, Feb. 1996.

[35] M. Ettenberg, "A new dielectric facet reflector for semiconductor lasers," *Appl. Phys. Lett.*, vol.32, no.11, pp. 724-725, 1978.

[36] J. Yamauchi, H. Kanbara, and H. Nakano, "Analysis of optical waveguides with high-reflection coatings using the FD-TD method," *IEEE Photon. Technol. Lett.*, vol.10, pp.11-13, 1998.

[37] A.G. Sveshnikov, A.V. Tikhonravov, and M. Trubetskov, "Modern methods for synthesizing multiplayer optical coatings", *J. of Communications Technology and Electronics*, v. 45, No Suppl. 2, pp. S151-S159, 2000.

[38] J. A. Dobrowolski, D. Poitras, et al, "Towards 'perfect' antireflection coatings", in *Optical Interference Coatings*, OSA Technical Digest (Optical Society of America), pp. TuA2-1–TuA2-3, July 15-20, 2001.

[39] William H. Southwell, "Comparison of needle-function predictions to exact calculations", in *Optical Interference Coatings*, OSA Technical Digest (Optical Society of America, Washington DC, 2001), pp.TuA10-1– TuA10-3, July, 2001.

[40] A. Thelen, A. Tikhonravov, et.al., "Results of Optical Interference Coatings 2001 Meeting Design Contest", in *Optical Interference Coatings*, OSA Technical Digest (Optical Society of America, Washington DC, 2001), pp. TuC1-1 - TuC1-3.

[41] T. Tamir, *Integrated Optics*, 2$^{nd}$. Topics Appl. Phys., vol.7, Ch. 1, Springer, New York 1979.

[42] R. G. Hunsperger, *Integrated Optics: Theory and Technology*, Ch. 1, Springer-Verlag, New York 1982.

[43] M. Dagenais, R. F. Leheny, and J. Crow, *Integrated Optoelectronics*, Quantum Electronics Principles and Applications, Academic Press Ltd., 1995.

[44] L. A Coldren, S. W. Corzine, *Diode lasers and photonic integrated circuits*, Chap. 3 and 6, John Wiley & Sons, Inc., 1995.

[45] C. M. Herzinger, C. C. Liu, T. A. DeTemple, and W. C. Chew. "The semiconductor waveguide facet reflectivity problem," *IEEE J. Quantum Electron.*, vol. 29, pp. 2273-2281, 1993.

[46] K. S. Yee, "Numerical solution of initial boundary value problem involving Maxwell's equations," *IEEE Trans. Antenna Propagat.*, vol. AP-14, pp.302-307, 1966.

[47] S. T. Chu and S. K. Chaudhuri, "A finite difference time-domain method for the design and analysis of guide-wave optical structures," *J. Lightwave Technol.*, vol.7, pp.2033-2038, 1989.

[48] R. Y. Chan and J. M. Liu, "Time-domain wave propagation in optical structures," *IEEE Photon. Technol. Lett.*, vol. 18, pp. 1001–1003, 1994.

[49] A. Taflove, Computational Electrodynamics: The Finite-Difference Time-Domain Method. Norwood, MA: Artech House, 1995.

[50] W. P. Huang, C. L. Xu, S. K. Chaundhuri, "A finite difference vector beam propagation method for three dimensional waveguide structures", *IEEE Photon. Technol. Lett.*, 4, pp.148-151, 1992.

[51] D. G. Fang, "Computational electromagnetics", *Lecture Notes* in Milimeterwave Technique Lab, Nanjing University of Sci. & Tech. Nanjing, China, Chap. 4, 2000.

[52] J. P. Berenger, "A perfectly matched layer for the absorption of electromagnetic waves," *J. Comput. Phys.*, vol.114, pp.185-200, 1994.

[53] W. P. Huang, S. T. Chu, A. Goss, and S. K. Chaudhuri, "A scalar finite-difference time-domain approach to guided-wave optics",. *IEEE Photon. Technol Lett.*, vol.3, no.6, June.1991.

[54] W. P. Huang, S. T. Chu and S. K. Chaudhuri, "A semivectorial finite-difference time-domain method," *IEEE Photon. Technol. Lett.*, vol. 3, pp. 803-806, Sept. 1991.

[55] W. C. Chew and W. H. Weedon, "A 3-D perfectly matched medium from modified Maxell's equations with stretched coordinates," *Microwave and Optical Tech. Lett.*, vol. 7, pp. 599-604, Sept. 1994.

[56] N. Georgieva and E. Yamashita, "Time-domain vector-potential analysis of transmission line problems," *IEEE Trans. on Microwave Theory and Techniques*, vol. 46, No 4, pp. 404-410, April 1998.

[57] D. Zhou, W. -P. Huang, C. -L. Xu, D.G. Fang,, B. Chen, "The perfectly matched layer boundary condition for scalar finite-difference time-domain method", *IEEE Photon. Technol. Lett.*, pp. 454-456, May. 2001.

[58] A. Yariv, *Quantum Electronics*, 2$^{nd}$ ed. New York: Wiley, 1975, pp.512.

[59] M. S. Stern, "Semivectorial polarized finite difference method for optical waveguides with arbitrary index profiles," *IEE Proc. J.* 135, pp.56-63, 1988.

[60] E. A. J. Marcatili, "Dielectric rectangular waveguide and directional coupler for integrated optics," *Bell Syst. Tech. J.*, vol.48, no.7, pp.2071-2102, 1969.

[61] R. Ulrich, and R. J. Martin, "Geometrical optics in thin film lightguides," Applied Optics, vol.10, pp.2077-2085, 1971.

[62] V. Ramaswamy, "Strip-loaded film waveguide," *Bell Syst. Tech. J.*, vol.53, pp.697-704, 1974.

[63] J. Buus, "The effective index method and its application to semiconductor lasers," *IEEE J. Quantum Electron.*, QE-18, pp.1279-1286, 1982.

[64] A. Hardy, "Formulation of two-dimensional reflectivity calculations based on the effective-index method", *J. Opt. Soc. Am.* Part A, vol.1, no.5, pp. 550-555, May 1984.

[65] K. S. Chiang, "Dual effective index method for the analysis of rectangular dielectric waveguides," *Applied Optics*, vol.25, pp.2169-2174, 1986.

[66] E. A. J. Marcatili, and A. A. Hardy, "The azimuthal effective index method," *IEEE J. Quantum Electron.*, QE-24, pp.766-774,1988.

[67] P. C. Kendall, "Layered theory of the rib waveguide", in *Rib waveguide Theory by the spectral index method*, Optoelectronics Series, eds P. N. Robson and P.C. Kendall, Research Studies Press and Wiley, ch. 2, pp.9-34, 1990.

[68] D. Marcuse, *Theory of dielectric optical waveguide*, 2$^{nd}$ ed., Academic Press, San Diego, 1991,pp.307-318.

[69] Y. Suematsu, S. Arai, and K. Kishino, "Dynamic single-mode semiconductor lasers with a distributed reflector," *J. Lightwave Technol.*, vol. LT-1, pp.161-176, 1983.

[70] T. L. Kock and U. Koren, "Semiconductor photonic integrated circuits," *IEEE J. Quantum Electron.*, vol.27, no.3, pp.641-653, Mar. 1991.

[71] K. C. Shin, M. Tamura, A. Kasukawa, N. Serizawa, S. Kurihashi, S. Tamura, and S. Arai, "Low threshold current density operation of GaInAsP–InP laser with multiple reflector microcavities," *IEEE Photon. Technol. Lett.*, vol. 7, no.10, pp. 1119–1121, 1995.

[72] P. Vettiger, et al, "Full wave technology – A new approach to large-scale laser fabrication and integration," *IEEE J. Quantum Electron.*, vol.27, no.6, pp.1319-1331, June 1991.

[73] I. Vurgaftman and J. Singh, "Laser cavity mirror imperfections and reflectivity: A time-dependent numerical approach," *Appl. Phys. Lett.*, vol. 66, pp. 288–290, 1995.

[74] T. Baba, M. Hamasaki, et al, "A novel short-cavity laser with deep-grating distributed Bragg reflectors," *Jpn, J. Appl. Phys.*, vol.35, pp. 1390-1394, 1996.

[75] Y. Yuan, T. Brock, P. Bhattacharya, C. Caneau, and R. Bhat, "Edge-emitting lasers with short-period semiconductor/air distributed Bragg reflector mirrors," *IEEE Photon. Technol. Lett.*, vol.9, no.7, pp.881-883, July 1997.

[76] R. Jambunathan and J. Singh, "Design studies for distributed Bragg reflectors for short-cavity edge-emitting lasers," *IEEE J. Quantum Electron.*, vol.33, pp.1180-1189, July 1997.

[77] T. Mukaihara, et al, "1.3 μm GaInAsP lasers integrated with butt-coupled waveguide and high reflective semiconductor/air Bragg reflector (SABAR)," *Electron. Lett.*, vol.34, pp.882-883, 1998.

[78] T. Mukaihara, et al, "Integrated GaInAsP laser diodes with monitoring photodiodes through semiconductor/air Bragg reflector (SABAR*)", IEEE J. Select. Quantum E*lectron, vol. 5, no.3, pp.469-475, May/June, 1999.

[79] P. Modh, N. Eriksson, M.Q.Teixeiro, A.Larsson, and T. Suhara, "Deep-etched distributed Bragg reflector lasers with curved mirrors-experiments and modeling", *IEEE J. Quantum Electron.,* vol.37, pp.752-761, June 2001.

[80] K. Magari, M. Okamoto, et al, "Poloarizatiion-insensitive optical amplifier with tensile-strained-barrier MQW structure", *IEEE J. Quantum Electron.,* vol.30, no.3, pp.695-702, July 1997.

# 2 Numerical Methods

## 2.1 INTRODUCTION

. This chapter presents the numerical methods for the simulation and design of the thin film coating components, including anti-reflection (AR) coatings, bandpass filters, and high-reflection (HR) coatings, etc., as well as the semiconductor waveguide. The first part of the chapter will discuss the transmission matrix method (TMM), which assumes plane waves in all dielectric media[1],[8], [4],[6]. It starts from the fundamental electromagnetic theory, derives the reflection and transmission coefficients for a single boundary, followed by the formulas of calculating the reflection and transmissions of plane waves propagating in one thin film layer and multilayer dielectric stacks. The formulations introduced in this part will be employed in the numerical analysis of thin film coating components, which will be treated in Chapter 3 and 4. The second part of this chapter is another important numerical techniques in electromagnetic simulation, which is, the finite difference time domain (FDTD) method[49],[46],[52]. Unlike the previous plane wave TMM, which assumed all dielectric layers to be homogenous, this method is able to treat with layered waveguide structure. FDTD method will be used to verify some results with antireflection coating structures in chapter 3 and simulate the deep-etched antireflective and high-reflective waveguide gratings structures in Chapter 5 and Chapter 6.

## 2.2 PLANE WAVE TRANSMISSION MATRIX METHOD

### 2.2.1 Maxwell's Equations and Plane Electromagnetic Waves

In this section, we review some of the basic properties of the propagation of optical wave (one special case of electromagnetic wave), beginning with Maxwell's equations and boundary conditions. These are followed by a derivation of the wave equations and an analysis of the propagation of monochromatic plane waves and some of their properties.

#### 2.2.1.1    Maxwell's Equations

$$\nabla \times \vec{E} = -\frac{\partial \vec{B}}{\partial t} \qquad\qquad (2.2\text{-}1)$$

$$\nabla \times \vec{H} = \frac{\partial \vec{D}}{\partial t} + \vec{J} \qquad\qquad (2.2\text{-}2)$$

$$\nabla \cdot (\vec{D}) = q \qquad\qquad (2.2\text{-}3)$$

$$\nabla \cdot (\vec{B}) = 0 \qquad\qquad (2.2\text{-}4)$$

In these equations, $\vec{E}$ and $\vec{H}$ are the electric field vector and magnetic field vector, respectively. These two field vectors are often used to describe an electromagnetic field. The quantities $D$ and $B$ are called the electric displacement and the magnetic induction, respectively. These two quantities are introduced to include the effect of the field on matter. The quantities $q$ and $\vec{J}$ are the electric charge and current densities, respectively, and maybe considered as the sources of the fields $\vec{E}$ and $\vec{H}$. These four Maxwell's equations completely determine the electromagnetic field and are the fundamental equations of the theory of such fields, that is, of electrodynamics.

In optics, one often deals with propagation of electromagnetic radiation in regions of space where both charge density and current density are zero. In fact, if we set $q = 0$ and $\vec{J} = 0$ in Maxwell's equations, we find the nonzero solution exist. This means that an electromagnetic field can exist even in the absence of any charges and currents. Electromagnetic fields occurring in media in the absence of charges are called electromagnetic waves.

In order to uniquely solve the 12 variables, 3 for each of the 4 vectors $\vec{E}$, $\vec{H}$, $\vec{D}$ and $\vec{B}$, Maxwell's equations must be supplemented by the so-called constitutive equations (or material equations)

$$\vec{D} = \varepsilon \vec{E} = \varepsilon_0 \vec{E} + \vec{P} \tag{2.2-5}$$

$$\vec{B} = \mu \vec{H} = \mu_0 \vec{H} + \vec{M} \tag{2.2-6}$$

$\varepsilon$ and $\mu$ are known as the dielectric permittivity and permeability tensors, respectively. If the material is isotropic, both $\varepsilon$ and $\mu$ reduce to scalars, which is true for the problems studied in this thesis. $\vec{P}$ and $\vec{M}$ are electric and magnetic polarizations, respectively. The constant $\varepsilon_0$ is called the permittivity of a vacuum and has a value of $8.854 \times 10^{-12} \, F/m$. The constant $\mu_0$ is known as the permeability of a vacuum with a value of $4\pi \times 10^{-7} \, H/m$. Since our study in this thesis assumes no non-linear optical effects, the dependence of $\varepsilon$ and $\mu$ on $\vec{E}$ and $\vec{H}$ is neglected.

### 2.2.1.2    Boundary Conditions

One of the most important problems in determining the reflection and transmission of electromagnetic radiation through a layered medium (for example, thin films) is the continuity of some components of the field vectors at the dielectric boundaries between the layers. Although

the physical properties (characterized by $\varepsilon$ and $\mu$) may change abruptly across the dielectric interfaces, there exist continuity relationships of some of the components of the field vectors at the dielectric boundary. These continuity conditions can be derived directly from Maxwell's equations. The derivations can be found in any book on classical electromagnetic theory and therefore are omitted here. The continuity relations on the interface between medium 1 and medium 2 are expressed as

$$\vec{n} \times \left( \vec{E}_2 - \vec{E}_1 \right) = 0 \tag{2.2-7}$$

$$\vec{n} \times \left( \vec{H}_2 - \vec{H}_1 \right) = \vec{K} \tag{2.2-8}$$

These two relations tell us that the tangential components of electric field vector $\vec{E}$ is always continuous at the boundary surface, and the difference between the tangential components of the magnetic field vector $\vec{H}$ is equal to the surface current density $\vec{K}$. In many areas of optics, one often deals with situations in which the surface charge density $\sigma$ and surface current density $\vec{K}$ both vanish. It follows that, in such a case, the tangential components of $\vec{E}$ and $\vec{H}$ and the normal components of $\vec{D}$ and $\vec{B}$ are all continuous across the interface separating media 1 and 2 as shown in Fig. 2-1, which can be expressed mathematically as:

$$\vec{E}_{2t} = \vec{E}_{1t} \tag{2.2-9}$$

$$\vec{H}_{2t} = \vec{H}_{1t} \tag{2.2-10}$$

$$\vec{D}_{2n} = \vec{D}_{1n} \tag{2.2-11}$$

$$\vec{B}_{2n} = \vec{B}_{1n} \tag{2.2-12}$$
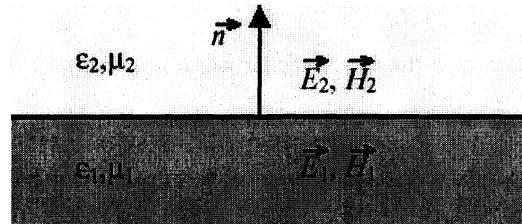
**Fig. 2-1 Discontinuity boundary in material properties**

These boundary conditions are extremely important and the foundation to solve any electromagnetic problem, including the wave propagation in optical media.

## 2.2.2 Reflection of plane waves at a dielectric boundary

In this part, the problem of reflection and transmission of monochromatic plane waves at a plane boundary between two homogeneous isotropic media. When a plane wave incident on the interface will, in general, be split into two waves: a transmitted wave proceeding into the second medium and a reflected wave propagating back into the first medium. The existence of these two waves is a direct consequence of the boundary conditions on the field vectors.

Thin film coatings usually consist of a number of boundaries between various homogeneous media and it is the effect, which these boundaries will have on an incident wave, which we will wish to calculate. A single boundary is the simplest case, which is sketched in Fig. 2-2.

The boundary conditions tell us that, at this boundary, the tangential components of E and H, that is, the components along the boundary, are continuous across it. In this case, the boundary is defined by $z = 0$, and the tangential components must be continuous for all values of x, y and t.
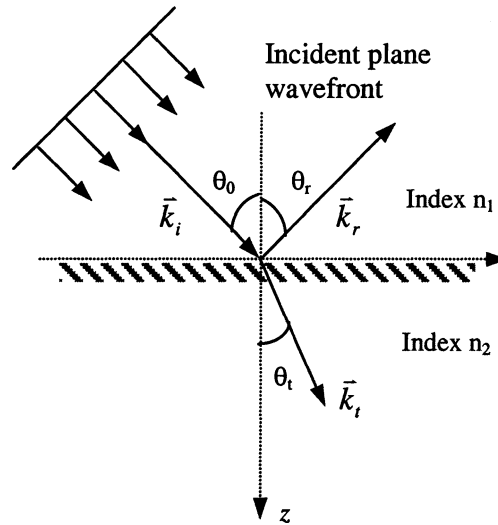


**Fig. 2-2 Plane wavefront incident on a single dielectric boundary**

Let $\vec{E}_i = E_i \exp\left[i(\omega t - \vec{k}_i \cdot \vec{r})\right]$ be an electric field of an incident plane wave with frequency $\omega$ and wave propagation vector $\vec{k}_i$. The reflected and transmitted plane-wave fields are designated as

$$\vec{E}_r = E_r \exp\left[i(\omega t - \vec{k}_r \cdot \vec{r})\right] \tag{2.2-13}$$

$$\vec{E}_t = E_t \exp\left[i(\omega t - \vec{k}_t \cdot \vec{r})\right] \tag{2.2-14}$$

Here, $\vec{k}_r$ and $\vec{k}_t$ are the corresponding propagation vectors. Any boundary conditions that relates these three field amplitudes at the plane interface $z = 0$ will require that the spatial variation of all fields be the same. From Fig. 2-2, we see immediately that all three waves

propagation vectors $\vec{k}_i$, $\vec{k}_r$ and $\vec{k}_t$ must lie in one plane. This plane is known as the *plane of incidence*. Furthermore the tangential components of all three wave vectors must be equal. If $\theta_i$, $\theta_r$ and $\theta_t$ are the incident, reflected, and transmitted angles, respectively, of the wave vectors with respect to the normal of the plane interface, the following relation must hold:

$$n_1 \sin\theta_i = n_1 \sin\theta_r = n_2 \sin\theta_t \qquad (2.2\text{-}15)$$

This implies the angle of reflection must equal the angle of incidence ($\theta_i = \theta_r$) as well as Snell's law:

$$\frac{\sin\theta_i}{\sin\theta_t} = \frac{n_2}{n_1} \qquad (2.2\text{-}16)$$

### 2.2.2.1 Reflection and Transmission of s-polarized light (TE wave)

We denote waves in the direction of incidence by the symbol + (that is, positive going) and waves in the opposite direction by − (that is, negative going). The s-polarized light is also known as a TE electromagnetic wave because the electric field vector $\vec{E}$ is transverse to the plane of incidence. Referring to Fig. 2-3, we consider the reflection and transmission of the TE wave. All electric field vectors are perpendicular to the plane of incidence, and the magnetic field vectors are chosen to give a positive energy flow in the direction of the wave vectors.

Imposing the continuity of the tangential E and H fields at the interface z =0 leads to

$$E_{1s}^+ + E_{1s}^- = E_{2s}^+ + E_{2s}^- \qquad (2.2\text{-}17)$$

$$\sqrt{\frac{\varepsilon_1}{\mu_1}}(E_{1s}^+ - E_{1s}^-)\cos\theta_i = \sqrt{\frac{\varepsilon_2}{\mu_2}}(E_{2s}^+ - E_{2s}^-)\cos\theta_t \qquad (2.2\text{-}18)$$
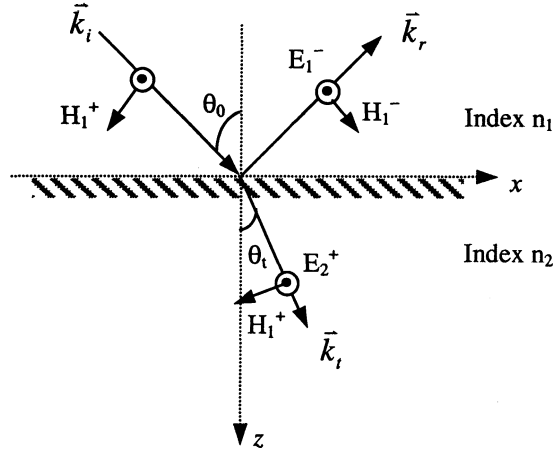
**Fig. 2-3 Convention defining the positive directions of the electric and magnetic vectors for s-polarized light (TE waves)**

Since we assume the light is incident from medium 1 to medium 2, the reflection and transmission coefficients for a single interface are given as

$$r_s = \left( \frac{E_{1s}^-}{E_{1s}^+} \right)_{E_{2s}^-=0} = \frac{n_1 \cos\theta_i - n_2 \cos\theta_t}{n_1 \cos\theta_i + n_2 \cos\theta_t} \tag{2.2-19}$$

$$t_s = \left( \frac{E_{2s}^+}{E_{1s}^+} \right)_{E_{2s}^-=0} = \frac{2n_1 \cos\theta_i}{n_1 \cos\theta_i + n_2 \cos\theta_t} \tag{2.2-20}$$

where we assume $\mu_1 = \mu_2$, which is generally true for most materials at optical frequencies. The refractive indices of media 1 and 2 are $n_1$ and $n_2$, respectively. The suffix $s$ has been used in the above expressions to denote $s$-polarization.

$$R_s = |r_s|^2 = \left( \frac{n_1 \cos\theta_i - n_2 \cos\theta_t}{n_1 \cos\theta_i + n_2 \cos\theta_t} \right)^2 \tag{2.2-21}$$

$$T_s = \frac{n_2 \cos\theta_t |t_s|^2}{n_1 \cos\theta_i} = \frac{4n_1 n_2 \cos\theta_i \cos\theta_t}{\left( n_1 \cos\theta_i + n_2 \cos\theta_t \right)^2} \tag{2.2-22}$$

It should be noted eqn. (2.2-22) is only valid for pure dielectric media with real $n_1$ and

$n_2$, and $\theta_i$ and $\theta_t$. It can be shown that eqns. (2.2-21)-(2.2-22) are in agreement with the law of

conservation of energy, that is $(R + T) = 1$.

### 2.2.2.2 Reflection and Transmission of p-polarized light (TM wave)

The p-polarized light is also known as a TM electromagnetic wave because the magnetic

field vector $\vec{H}$ is perpendicular to the plane of incidence.
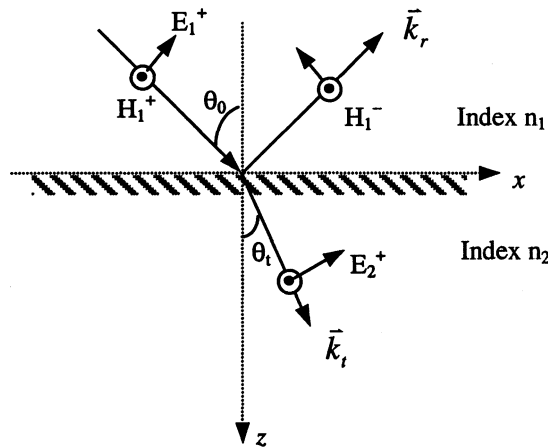
**Fig. 2-4 Convention defining the positive direction of the electric and magnetic vectors for p-polarized light (TM waves).**

Referring to Fig. 2-4, we consider the reflection and transmission of the TM wave.

Similar to the above analysis to TE wave, by imposing the boundary conditions, the following

two relations hold:

$$(E_{1p}^+ + E_{1p}^-)\cos\theta_i = (E_{2p}^+ + E_{2p}^-)\cos\theta_t \qquad (2.2\text{-}23)$$

$$\sqrt{\frac{\varepsilon_1}{\mu_1}}(E_{1p}^+ - E_{1p}^-) = \sqrt{\frac{\varepsilon_2}{\mu_2}}(E_{2p}^+ - E_{2p}^-) \qquad (2.2\text{-}24)$$

When we assume the light is incident from medium 1 to medium 2, the reflection and transmission coefficients for a single interface are given as

$$r_p = \left(\frac{E_{1p}^-}{E_{1p}^+}\right)_{E_{2p}^-=0} = \frac{n_1 \cos\theta_t - n_2 \cos\theta_i}{n_1 \cos\theta_t + n_2 \cos\theta_i} \qquad (2.2\text{-}25)$$

$$t_p = \left(\frac{E_{2p}^+}{E_{1p}^+}\right)_{E_{2p}^-=0} = \frac{2n_1 \cos\theta_t}{n_1 \cos\theta_t + n_2 \cos\theta_i} \qquad (2.2\text{-}26)$$

The reflectance and transmittance are therefore obtained accordingly as

$$R_p = r_p^2 = \left(\frac{n_1 \cos\theta_t - n_2 \cos\theta_i}{n_1 \cos\theta_t + n_2 \cos\theta_i}\right)^2 \qquad (2.2\text{-}27)$$

$$T_p = \frac{n_2 \cos\theta_i |t_p|^2}{n_1 \cos\theta_t} = \frac{4n_1 n_2 \cos\theta_i \cos\theta_t}{(n_1 \cos\theta_t + n_2 \cos\theta_i)^2} \qquad (2.2\text{-}28)$$

The suffix $p$ has been used in the above expressions to denote $p$-polarization. Again, the law of energy conservation $(R + T) = 1$ holds at the boundary.

### 2.2.3 Reflection and transmission of a thin film

In many classical books dealing with thin film optics [6], [7], the optical admittance (instead of wave impedance to be discussed in the next section) is used extensively in order to calculate the reflectance with multilayer boundaries. The optical admittance in free space is defined as

$$y_0 = (\varepsilon_0/\mu_0)^{1/2} = 1/\eta_0 = 2.6544 \times 10^{-3} S \qquad (2.2\text{-}29)$$

The characteristic optical admittance of a medium with refractive index $n$ is written as

$$y = (\varepsilon_0 n^2/\mu_0)^{1/2} = ny_0 \qquad (2.2\text{-}30)$$

$y$ is also the optical admittance for normal incidence. The optical admittance for oblique

incidence are defined

$$Y_p = \frac{y}{\cos\theta_i} \tag{2.2-31}$$

$$Y_s = y\cos\theta_i \tag{2.2-32}$$

A simple extension of the above analysis for the single boundary occurs in the case of a

thin, plane parallel film of material covering the surface of a substrate. The presence of two (or

more) interfaces means that a number of beams will be produced by successive reflections and

the properties of the film will be determined by the summation of these beams.

*Incident plane*

$n_1$    Incident medium

*Physical thickness of film*    $n_2$    Film

$n_3$    Substrate

*Normal to film boundaries*
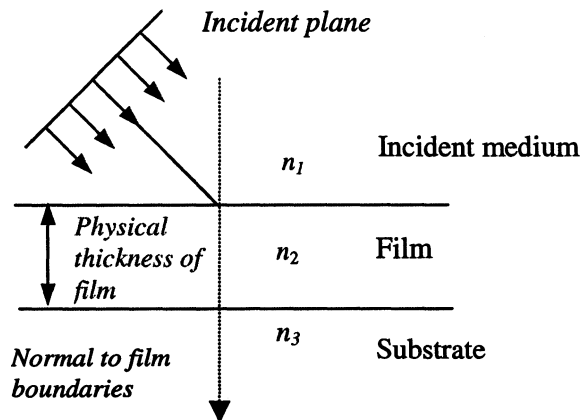
**Fig. 2-5 Plane wave incident on a thin film**

The schematic diagram of this thin film case is illustrated in Fig. 2-5. The interface

between the film and the substrate, denoted by the symbol b, can be treated in exactly the same

way as the simple boundary already discussed in 2.2.2. We consider the tangential components of

the fields. There is no negative-going wave in the substrate and the waves in the film can be

summed into one resultant positive-going wave and one resultant negative going wave. Due to

the limited space, here it only lists the resultant characteristic matrix. The detailed derivation can

be obtained from [6],[7]

$$\begin{bmatrix} \vec{E}_a \\ \vec{H}_a \end{bmatrix} = \begin{bmatrix} \cos\delta & j\sin\delta/y_1 \\ jy_1\sin\delta & \cos\delta \end{bmatrix} \begin{bmatrix} \vec{E}_b \\ \vec{H}_b \end{bmatrix}$$
(2.2-33)

where $\delta$ is defined as

$$\delta = 2\pi n_1 d\cos\theta_i/\lambda$$
(2.2-34)

Equation (2.2-33) can be written as

$$E_a\begin{bmatrix} 1 \\ Y \end{bmatrix} = \begin{bmatrix} \cos\delta & j\sin\delta/y_1 \\ jy_1\sin\delta & \cos\delta \end{bmatrix} \begin{bmatrix} 1 \\ y_2 \end{bmatrix} E_b$$
(2.2-35)

where Y is the input admittance of the assembly defined by

$$Y = H_a/E_a$$
(2.2-36)

and Y can be obtained as

$$Y = \frac{y_1\cos\delta + jy_1\sin\delta}{\cos\delta + j(y_2/y_1)\sin\delta}$$
(2.2-37)

Normally, $Y$ is the parameter which is of interest and the matrix product on the right hand side of

eq. (2.2-35) gives sufficient information for calculating it:

$$\begin{bmatrix} B \\ C \end{bmatrix} = \begin{bmatrix} \cos\delta & j\sin\delta/y_1 \\ jy_1\sin\delta & \cos\delta \end{bmatrix} \begin{bmatrix} 1 \\ y_2 \end{bmatrix}$$
(2.2-38)

where

$\begin{bmatrix} B \\ C \end{bmatrix}$ is defined as the transmission matrix (or characteristic matrix) of the assembly. Clearly,

$Y = C/B$, the reflectance of this single film is then calculated by

$$R = \left(\frac{y_0 - Y}{y_0 + Y}\right)^2 \qquad\qquad (2.2\text{-}39)$$

Note that for the above equations, the subscript s or p are both omitted, which implies these equations apply to both cases.

## 2.2.4 Reflection and transmission of an assembly of thin films

Let more films be added to the single film of the previous section 2.2.3, so that the results obtained in (2.26) can be extended to the general case of an assembly of $q$ layers, when the characteristic matrix is simply the product of the individual matrices taken in the correct order, i.e.

$$\begin{bmatrix} B \\ C \end{bmatrix} = \left(\prod_{r=1}^{q} \begin{bmatrix} \cos\delta_r & j\sin\delta_r/y_r \\ jy_r\sin\delta_r & \cos\delta_r \end{bmatrix}\right)\begin{bmatrix} 1 \\ y_m \end{bmatrix} \qquad (2.2\text{-}40)$$

where

$$\delta_r = 2\pi n_r d_r \cos\theta_r / \lambda$$

$$y_r = y_0 n_r \cos\theta_r, \text{ for s-polarized wave (TE)}$$

$$y_r = y_0 n_r / \cos\theta_r, \text{ for p-polarized wave (TM)}$$

If $\theta_0$, the angle of incidence is given, the values of $\theta_r$ can be found from Snell's law, i.e.

$$n_0 \sin\theta_0 = n_r \sin\theta_r = n_m \sin\theta_m \qquad\qquad (2.2\text{-}41)$$

Equation (2.2-40) is of prime importance in optical thin-film optics analysis and forms the basis of almost all calculations in this area [6].

A useful property of the transmission matrix (characteristic matrix) of a thin film is that the determinant is unity. This means that the determinant of the product of any number of these

matrices is also unity.
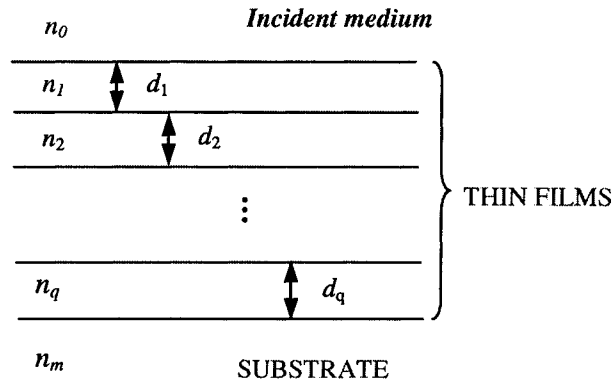


**Fig. 2-6 Schematic diagram for q layer of films on a substrate**

## 2.3  FINITE DIFFERENCE TIME DOMAIN METHOD

### 2.3.1  Basic Formulations

For the linear, isotropic, non-dispersive, time invariant medium, the two Maxwell's curl equations can be rewritten as:

$$\nabla \times \vec{E} = -\mu \frac{\partial \vec{H}}{\partial t} \tag{2.3-1}$$

$$\nabla \times \vec{H} = \varepsilon \frac{\partial \vec{E}}{\partial t} \tag{2.3-2}$$

The decomposed scalar expressions are

$$\frac{\partial H_z}{\partial t} = \frac{1}{\mu}(\frac{\partial E_x}{\partial y} - \frac{\partial E_y}{\partial x} - \rho' H_z) \tag{2.3-3}$$

$$\frac{\partial E_z}{\partial t} = \frac{1}{\varepsilon}(\frac{\partial H_y}{\partial x} - \frac{\partial H_x}{\partial y} - \sigma E_z) \tag{2.3-4}$$

where $\rho'$ is an equivalent magnetic resistivity in ohms per meter and $\sigma$ is the electric conductivity in siemens per meter. For $H_x$, $H_y$, $E_x$ and $E_y$ we have similar equations. We denote a space point in a uniform rectangular lattice as

$$(i, j, k) = (i\Delta x, j\Delta y, k\Delta z) \tag{2.3-5}$$

where $\Delta x$, $\Delta y$ and $\Delta z$ are, respectively, the lattice space increments in the $x$, $y$, and $z$ coordinate directions, and $i, j,$ and $k$ are integers. Further, we denote any function $u$ of space and time evaluated at a discrete point in the grid and at a discrete point in time as

$$u^n(i, j, k) = u(i\Delta x, j\Delta y, k\Delta z, n\Delta t) \tag{2.3-6}$$
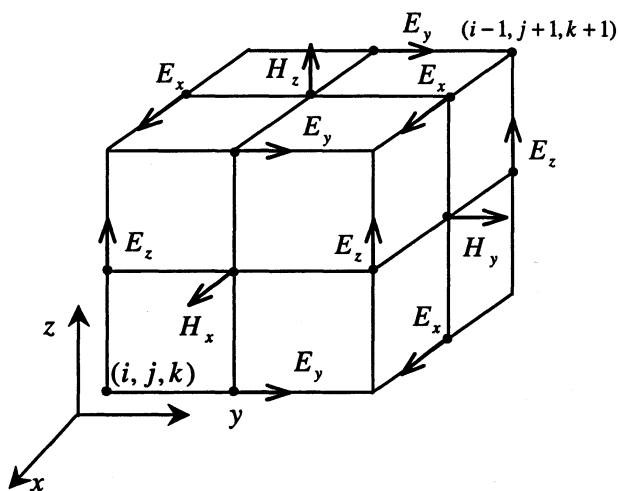
**Fig. 2-7 Position of the electric and magnetic field vector components around a cubic unit cell of the Yee space lattice**

Yee used centered finite-difference (central-difference) expressions for the space and time derivatives that are both simply programmed and second-order accurate in the space and time increments [10]. The expressions are as follows

$$\frac{\partial u^n(i, j, k)}{\partial x} = \frac{u^n(i+\frac{1}{2}, j, k) - u^n(i-\frac{1}{2}, j, k)}{\Delta x} + O(\Delta x^2) \qquad \text{(2.3-7)}$$

$$\frac{\partial u^n(i, j, k)}{\partial t} = \frac{u^{n+\frac{1}{2}}(i, j, k) - u^{n-\frac{1}{2}}(i, j, k)}{\Delta t} + O(\Delta t^2) \qquad \text{(2.3-8)}$$

Substituting (2.3-7), (2.3-8) into (2.3-3)The other components may be obtained in the same way. They form the Yee algorithm, which is the basic relation in FDTD.

$$H_z^{n+\frac{1}{2}} = \frac{1 - (\rho'\Delta t/2\mu)}{1 + (\rho'\Delta t/2\mu)} H_z^{n-\frac{1}{2}} + \frac{\Delta t}{\mu} \frac{1}{1 + (\rho'\Delta t/2\mu)} \left[ \frac{E_x^n(i+\frac{1}{2}, j+1, k) - E_x^n(i+\frac{1}{2}, j, k)}{\Delta y} \right.$$

$$\left. + \frac{E_y^n(i, j+\frac{1}{2}, k) - E_y^n(i+1, j+\frac{1}{2}, k)}{\Delta x} \right] \qquad \text{(2.3-9)}$$

### 2.3.2 Semi-vectorial Wave Equations

The wave equation representations of FDTD method has been proved to save the computer storage memory as well as the CPU time, when the problem to be analyzed can be treated as a two dimensional case [11]-[21]. This assumption is valid for most of the stripe waveguide structure. The following time domain wave equations will be based on this semi-vectorial assumption. The coordinates and an example of structure are shown in Fig. 2-8.
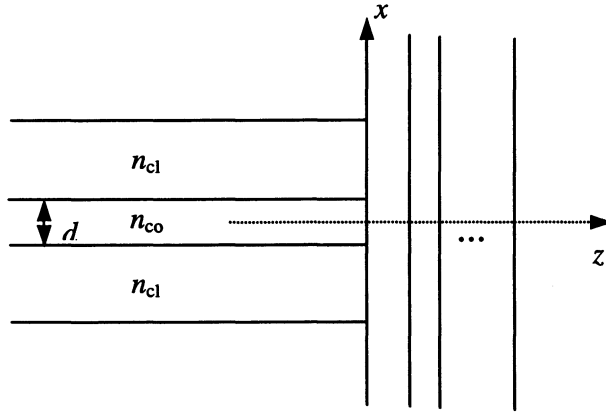
**Fig. 2-8 Two-dimensional model for the analysis of a multilayer coated laser diode in the full wave FDTD analysis.**

### 2.3.2.1    TE Wave

The assumption made here is y-invariant field distribution. For TE-polarized light (Ey, Hx, and Hz), the Maxwell's equations can be written as

$$\frac{\partial E_y(x,z)}{\partial t} = \frac{1}{n^2(x,z)}\left[\frac{\partial H_y(x,z)}{\partial z} - \frac{\partial H_z(x,z)}{\partial x}\right] \qquad (2.3\text{-}10)$$

$$\frac{\partial H_z(x,z)}{\partial t} = -\frac{1}{\mu}\frac{\partial E_y(x,z)}{\partial x} \qquad (2.3\text{-}11)$$

$$\frac{\partial H_x(x,z)}{\partial t} = -\frac{1}{\varepsilon}\frac{\partial E_y(x,z)}{\partial z} \qquad (2.3\text{-}12)$$

In the semi-vectorial approximation, the optical signal is assumed to be linearly polarized, and hence the coupling terms can be eliminated[11], [14]. The resulting 2D semi-vectorial wave equations (SVWEs) are

$$\frac{\partial^2 E_y}{\partial x^2} + \frac{\partial^2 E_y}{\partial z^2} - \frac{n^2}{c^2}\frac{\partial^2 E_y}{\partial t^2} = 0 \qquad (2.3\text{-}13)$$

$$\frac{\partial^2 H_x}{\partial x^2} + n^2 \frac{\partial}{\partial z}\left(\frac{1}{n^2}\frac{\partial H_x}{\partial z}\right) - \frac{n^2}{c^2}\frac{\partial^2 H_x}{\partial t^2} = 0 \qquad (2.3\text{-}14)$$

where $n^2 = \varepsilon / \varepsilon_0$

Following the standard finite difference time domain scheme, the central difference is implemented for both the spatial ($x$ and $z$) and time dimensions.

The following gives the time marching iteration formula for the user-defined computation region.

$$E_{y_{i,k}}^{n+1} = -E_{y_{i,k}}^{n-1} + 2\left(1 - \frac{\delta_x^2}{n^2} - \frac{\delta_z^2}{n^2}\right)E_{y_{i,k}}^{n} + \frac{\delta_x^2}{n^2}(E_{y_{i+1,k}}^{n} + E_{y_{i-1,k}}^{n}) + \frac{\delta_z^2}{n^2}(E_{y_{i,k+1}}^{n} + E_{y_{i,k-1}}^{n}) \quad (2.3\text{-}15)$$

where

$$\delta_x = \frac{c \cdot \Delta t}{\Delta x}, \qquad \delta_z = \frac{c \cdot \Delta t}{\Delta z}$$

In order to truncate the infinite space to be finite computation region, absorbing boundary condition is needed in order to simulate the finite space by using finite calculation window.

### 2.3.2.2    TM Wave

For TM-polarized light (Hy, Ex, and Ez), the Maxwell's equations can be written as

$$\frac{\partial H_y(x,z)}{\partial t} = -\frac{1}{\mu}\left[\frac{\partial E_x(x,z)}{\partial z} - \frac{\partial E_z(x,z)}{\partial x}\right] \qquad (2.3\text{-}16)$$

$$\frac{\partial E_x(y,z)}{\partial t} = -\frac{1}{n^2(x,z)}\frac{\partial H_y(y,z)}{\partial z} \qquad (2.3\text{-}17)$$

$$\frac{\partial E_z(y,z)}{\partial t} = \frac{1}{n^2(x,z)}\frac{\partial H_y(y,z)}{\partial x} \qquad (2.3\text{-}18)$$

Similarly, the resulting 2D semi-vectorial wave equations (SVWEs) for the TM wave case are

$$\frac{\partial}{\partial x}\left(\frac{1}{n^2}\frac{\partial H_y}{\partial x}\right)+\frac{\partial}{\partial z}\left(\frac{1}{n^2}\frac{\partial H_y}{\partial z}\right)-\frac{1}{c^2}\frac{\partial^2 H_y}{\partial t^2}=0 \qquad (2.3\text{-}19)$$

$$\frac{\partial}{\partial x}\left(\frac{1}{n^2}\frac{\partial E_x}{\partial x}\right)+\frac{\partial^2 E_x}{\partial z^2}-\frac{c^2}{n^2}\frac{\partial^2 E_x}{\partial t^2}=0 \qquad (2.3\text{-}20)$$

### 2.3.3  Numerical stability

The Numerical algorithms for Maxwell's curl equations defined by the finite-difference systems require that the time increment $\Delta t$ have a specific bound relative to the lattice space increments $\Delta x$, $\Delta y$, and $\Delta z$. This bound is necessary to avoid numerical instability, an undesirable possibility with explicit differential equation solvers that can cause the computed results to spuriously increase without limit as time-marching continues. To reveal the physic insight, we take the one dimensional wave propagation as an example, for space step $\Delta s_1 = \Delta x$, the time step $\Delta t$ should be less than

$$\nabla t < \Delta x/v_{\text{max}} \qquad (2.3\text{-}21)$$

where $v_{\text{max}}$ is the maximum possible phase velocity of waves. Only in this way, one may keep tracing the information from time to time continuously.

The extension to the 3-D case is straightforward with the stability criteria as

$$\Delta t \leq \frac{\Delta s_3}{v_{\text{max}}}=\frac{\left[\left(\frac{1}{\Delta x}\right)^2+\left(\frac{1}{\Delta y}\right)^2+\left(\frac{1}{\Delta z}\right)^2\right]^{-\frac{1}{2}}}{v_{\text{max}}} \qquad (2.3\text{-}22)$$

### 2.3.4  Numerical dispersion

Dispersion is defined as the variation of a propagating wave's wavelength $\lambda$ with frequency $f$. For the physical insight of the numerical dispersion

Consider the 1-D case

$$\frac{\partial H_x}{\partial t} = -\frac{1}{\mu}\frac{\partial E_z}{\partial y} \tag{2.3-23}$$

$$\frac{\partial E_z}{\partial t} = -\frac{1}{\varepsilon}\frac{\partial H_x}{\partial y} \tag{2.3-24}$$

from (2.3-7), (2.3-8) we may have

$$\left.\begin{array}{c} -\dfrac{1}{\varepsilon}\dfrac{H_x^{n+\frac{1}{2}}(j+\frac{1}{2}) - H_x^{n+\frac{1}{2}}(j-\frac{1}{2})}{\Delta y} = \dfrac{E_z^{n+1}(j) - E_z^{n}(j)}{\Delta t} \\[4mm] -\dfrac{1}{\mu}\dfrac{E_z^{n}(j+1) - E_z^{n}(j)}{\Delta y} = \dfrac{H_x^{n+\frac{1}{2}}(j+\frac{1}{2}) - H_z^{n-\frac{1}{2}}(j+\frac{1}{2})}{\Delta t} \end{array}\right\} \tag{2.3-25}$$

Let $H_x^{n} = H_x e^{j(k_y j\Delta y - \omega n\Delta t)}$, $E_z^{n} = E_z e^{j(k_y j\Delta y - \omega n\Delta t)}$, and substitute them into (2.3-25) we have

$$\frac{H_x}{\varepsilon\Delta y}\sin\frac{k_y\Delta y}{2} = \frac{E_z}{\Delta t}\sin\frac{\omega\Delta t}{2} \tag{2.3-26}$$

$$\frac{E_z}{\mu\Delta y}\sin\frac{k_y\Delta y}{2} = \frac{H_x}{\Delta t}\sin\frac{\omega\Delta t}{2} \tag{2.3-27}$$

The combination of (2.3-26) and (2.3-27) yields

$$\left(\frac{1}{c\Delta t}\right)^2 \sin^2\left(\frac{\omega\Delta t}{2}\right) = \frac{1}{(\Delta y)^2}\sin^2(\frac{k_y\Delta y}{2}) \qquad (2.3\text{-}28)$$
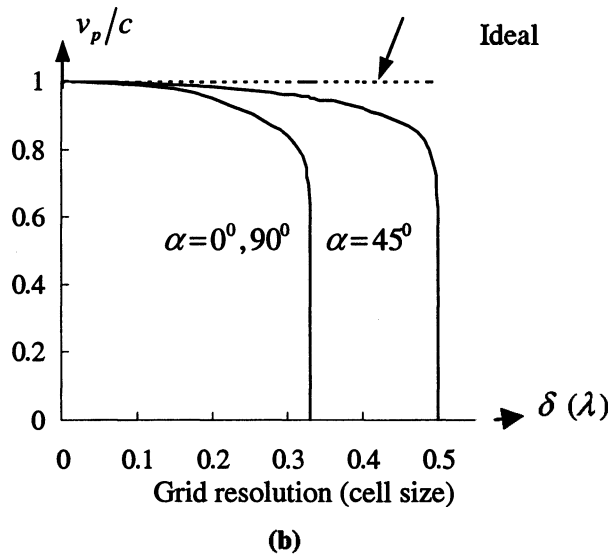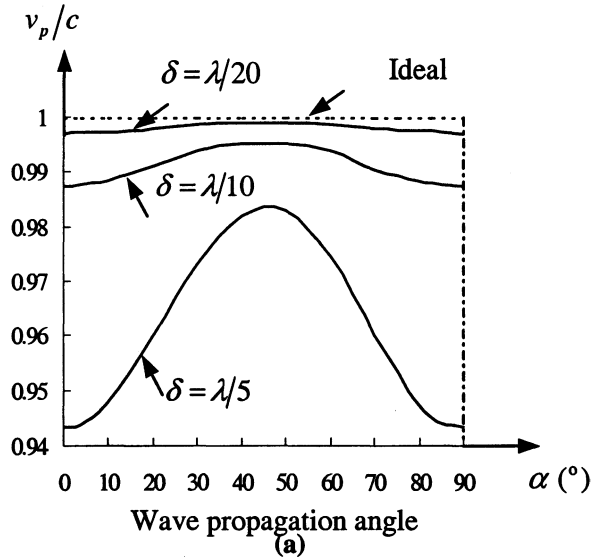


**Fig. 2-9 Variation of FDTD numerical wave phase velocity (dispersion). (a) with wave propagation angle in the grid for three different grid discretization; (b) with grid resolution for three different wave propagation angles**

The extension of (2.3-28) into 3-D case leads to

$$\left(\frac{1}{c\Delta t}\right)^2 \sin^2\left(\frac{\omega\Delta t}{2}\right) = \frac{1}{(\Delta x)^2}\sin^2(\frac{k_x\Delta x}{2}) + \frac{1}{(\Delta y)^2}\sin^2(\frac{k_y\Delta y}{2}) + \frac{1}{(\Delta z)^2}\sin^2(\frac{k_z\Delta z}{2}) \quad (2.3\text{-}29)$$

### 2.3.5   Perfectly Matched Layer Absorbing Boundary Conditions

The truncation of the computation region should simulate the infinite space, that is, the wave is transparent without reflection. The boundary condition introduced on the truncated boundary is called the absorbing boundary condition, or ABC in short. The frequency domain information is quite sensitive to the accuracy in time domain analysis, therefore, the low reflection of the ABC is important. Usually, the reflection should be at least less than 1%~5% at the absorbing boundary which is 10~20 meshes away from the interacting structure.

Existing analytical ABC's such as *Mur*, provide effective reflection coefficients in the order of −35 to −45 dB for most FDTD simulations. To attain a larger dynamic range, more accurate ABC's are needed than currently exist analytical ones. Such an advance may be realized with the appearance of PML. In 2-D, it is reported that reflection coefficients for PML as low as 1/3000th those of standard second and third order analytical ABC's such as Mur. PML involves creation of a non-physical absorber adjacent to the outer grid boundary that has wave impedance independent of the angle of incidence and frequency of outgoing scattered waves.

On the boundary between PML and the usual medium, the tangential wavenumbers should be equal and the normal wavenumber $k_z$ within PML should be complex in order to have a decay factor. Therefore, PML should be anisotropic.

For the simplicity of illustration, consider 2-D $TE_z$ case, namely $k_z = 0$, $E_z = 0$, $H_x = H_y = 0$, the interface between PML and free space is *xoz* plane shown in Fig. 4.9. If $\sigma$

and $\sigma^*$ denote electric conductivity and magnetic loss assigned to PML to absorb outgoing waves

respectively, it is well known that

$$\sigma / \varepsilon_0 = \sigma^* / \mu_0 \qquad\qquad\qquad (2.3\text{-}30)$$

provides for reflectionless transmission of a plane wave propagating normally across the

interface between free space and the outer boundary layer. However, the absorption is thought at

best to be in the order of the analytical ABC's because of increasing reflection at oblique incident

angles.
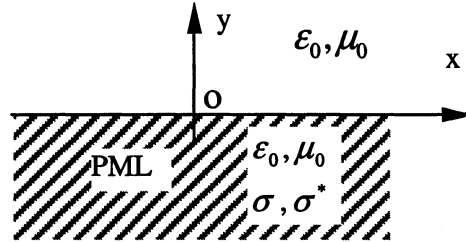


**Fig. 2-10 Boundary between PML and free Space**

The PML technique introduces a new degree of freedom in specifying loss. In the same time,

the anisotropy may be realized by defining different $\sigma$ and $\sigma^*$ along $x$ and $y$ direction.

## 2.3.5.1    Implementation of PML in wave equations

According to the stretched coordinate approach [19], [21], the PML for the semi-vector

wave equation (SVWE) for 2D TE case can be modified as

$$\nabla_s^2 E_y - \frac{n^2}{c^2}\frac{\partial^2}{\partial t^2} E_y = 0, \ \nabla_s = \hat{x}\frac{1}{s_x}\frac{\partial}{\partial x} + \hat{z}\frac{1}{s_z}\frac{\partial}{\partial z} \qquad\qquad (2.3\text{-}31)$$

where $s_x$, $s_z$ are the stretched coefficients in $X$- and $Z$-directions respectively.

First we only consider PML in $z$-direction, and PML in other directions can be considered the same way. $s_z = a_z + \dfrac{\sigma_z}{j\omega\varepsilon_0 n^2}$ and $s_x = 1$.

In frequency domain, the wave equation we discussed in the previous part eq. (2.3-31) becomes

$$\frac{\partial^2}{\partial x^2}E_y + \frac{\partial}{s_z\partial z}\left(\frac{\partial}{s_z\partial z}E_y\right) - \frac{n^2}{c^2}(j\omega)^2 E_y = 0 \qquad (2.3\text{-}32)$$

By introduce two auxiliary variables [19],[21] as follows:

$$j\omega D_{z1} = \frac{1}{s_z}\frac{\partial}{\partial z}E_y \qquad (2.3\text{-}33)$$

$$j\omega D_{z2} = \frac{1}{s_z}\frac{\partial}{\partial z}(j\omega D_{z1}) \qquad (2.3\text{-}34)$$

Then in frequency domain eq. (2.3-31) becomes

$$\frac{n^2}{c^2}(j\omega)^2 E_y = \frac{\partial^2 E_y}{\partial x^2} + j\omega D_{2z} \qquad (2.3\text{-}35)$$

From eq.(2.3-33)-(2.3-35), we can easily write the wave equations in PML region in time domain by replacing $j\omega$ with $\frac{\partial}{\partial t}$ :

$$a_z\frac{\partial D_{z1}}{\partial t} + \frac{\sigma_z}{n^2}D_{z1} = \frac{\partial E_y}{\partial z} \qquad (2.3\text{-}36)$$

$$a_z\frac{\partial D_{z2}}{\partial t} + \frac{\sigma_z}{n^2}D_{z2} = \frac{\partial^2 D_{z1}}{\partial t\partial z} \qquad (2.3\text{-}37)$$

$$\frac{n^2}{c^2}\frac{\partial^2 E_y}{\partial t^2} = \frac{\partial^2 E_y}{\partial x^2} + \frac{\partial D_{z2}}{\partial t} \qquad (2.3\text{-}38)$$

The FDTD time marching iteration equations in the PML region becomes:

$$D_{z1i,k+1/2}^{n+1/2} = \frac{a_z - \sigma_z \Delta t / 2\varepsilon_0 n_{i,k+1/2}^2}{a_z + \sigma_z \Delta t / 2\varepsilon_0 n_{i,k+1/2}^2} D_{z1i,k+1/2}^{n-1/2}$$

$$+ \frac{1}{a_z + \sigma_z \Delta t / 2\varepsilon_0 n_{i,k+1/2}^2} (E_{y i,k+1}^n - E_{y i,k}^n) \qquad (2.3\text{-}39)$$

$$D_{z2i,k}^{n+1/2} = \frac{a_z - \sigma_z \Delta t / 2\varepsilon_0 n_{i,k}^2}{a_z + \sigma_z \Delta t / 2\varepsilon_0 n_{i,k}^2} D_{z2i,k}^{n-1/2} + \frac{1}{a_z + \sigma_z \Delta t / 2\varepsilon_0 n_{i,k}^2}$$

$$(D_{z1i,k+1/2}^{n+1/2} - D_{z1i,k-1/2}^{n+1/2} - D_{z1i,k+1/2}^{n-1/2} + D_{z1i,k-1/2}^{n-1/2}) \qquad (2.3\text{-}40)$$

$$E_{y i,k}^{n+1} = -E_{y i,k}^{n-1} + 2\left(1 - \frac{\delta_x^2}{n_{i,k}^2} - \frac{\delta_y^2}{n_{i,k}^2}\right) E_{y i,j,k}^n + \frac{\delta_x^2}{n_{i,j,k}^2}(E_{y i+1,k}^n + E_{y i-1,k}^n)$$

$$+ \frac{\delta_z^2}{n_{i,k}^2}(D_{z2i,k}^{n+1/2} - D_{z2i,k}^{n-1/2}) \qquad (2.3\text{-}41)$$

where $\delta_x = c\Delta t / \Delta x$, $\delta_z = c\Delta t / \Delta z$. $D_{z2}$ locates at the same position of $E_y$ and $D_{z1}$ is half of

a grid away from $E_y$ both in Z-directions.

As discussed previously, PML is a non-physical absorber, and its equivalent conductivity

in z-direction (for simplicity) is defined [16]- [21]as

$$\sigma_z(z) = \left(\frac{z}{d}\right)^m \sigma_{z\max} = -\left(\frac{z}{d}\right)^m \frac{n^2 \varepsilon_0 c (m+1)\ln(R_0)}{2d} \qquad (2.3\text{-}42)$$

where $d$ is the depth of PML along z direction, $m$ is the order, and $R_0$ is the initially defined

reflection from PML at normal incidence. It is to be noted that the best absorption efficient of

PML absorber is obtained by choosing special parameters, which results in a specific $\sigma$. This

choices of parameters could be different for different structures to be analyzed. In our

antireflection coating design presented in Chapter 3 and 5, the parameters used in PML are tested before they are employed to analyze a waveguide structure.

### 2.3.6    Source Excitation and connecting boundary

The computation region can be separated into two sub regions, the total field region and the reflected field region. The plane separating these regions is called the incident plane. In the total field region, structures of interest such as a junction or more complicated structures are defined. The interaction between the incident wave the waveguide geometry will take place in this region so that its field quantities must retain the information of both incident and scattered waves. In the reflected field region, there are no junctions or discontinuities and the field quantities in this region are the reflections from the total field region. Since there are no discontinuities in this region, these signals will not be reflected back into the total field region. The excitation scheme of a +z propagating incident waveform consists of a total field region and a reflected field region that are located at $z \geq 0$ and $z \leq 0$, respectively. The incident wave can be generated by specifying the exact field distribution on the incident plane at each time interval. Although the excitation can be of the form of a point source or a plane wave, the incident wave in most optical waveguide problems generally has the form of a guided mode. A poor excitation scheme will generate unwanted transient and backward propagating parasitic waves, which can create noise problems. If the excitation scheme is perfect, there should not be any light detected by an observer located in the reflected region, unless there are some obstacles such as discontinuities in the total field region which would generate the reflection.

As shown in Fig. 2-11, the connecting condition between total fields and scattering field should be properly treated. On this boundary, when calculating the total field on the boundary of

total field region, according to the difference approximation, it requires the total field in the

reflected field region. For a reflected field, the situation is the same. The 1–D free space case is

chosen as an example to show how to solve this problem. Consider the wave propagates along $z$

axis with the incident field components $E_{x,i}$, $H_{y,i}$ as shown in Fig. 2-11, we may write the

following expression for incident wave

$$E_{x,i}^{n+1}(k) = E_{x,i}^{n}(k) + \frac{\Delta t}{\varepsilon \Delta z}\left[ H_{y,i}^{n+\frac{1}{2}}(k-\frac{1}{2}) - H_{y,i}^{n+\frac{1}{2}}(k+\frac{1}{2}) \right] \qquad (2.3\text{-}43)$$

$$H_{y,i}^{n+\frac{1}{2}}(k+\frac{1}{2}) = H_{y,i}^{n-\frac{1}{2}}(k+\frac{1}{2}) + \frac{\Delta t}{\mu \Delta z}\left[ E_{x,i}^{n}(k) - E_{x,i}^{n}(k+1) \right] \qquad (2.3\text{-}44)$$

At the source point

$$E_{x,i}^{n+1}(k'-1) = E_{source} \qquad (2.3\text{-}45)$$

At the connecting boundary shown in Fig. 2-11, for certain space step $k'$ related to connecting

boundary, when $k \le k'-1$ or $k > k'$, the original FDTD equations remains unchanged. For

$k = k'-1/2$ or $k = k'$, they should be modified. When $k = k'$, we have

$$E_{x,t}^{n+1}(k') = E_{x,t}^{n}(k') + \frac{\Delta t}{\varepsilon \Delta z}\left[ H_{y,t}^{n+\frac{1}{2}}(k'-\frac{1}{2}) - H_{y,t}^{n+\frac{1}{2}}(k'+\frac{1}{2}) \right] \qquad (2.3\text{-}46)$$

$$H_{y,t}^{n+\frac{1}{2}}(k'-\frac{1}{2}) = H_{y,s}^{n+\frac{1}{2}}(k'-\frac{1}{2}) + H_{y,i}^{n+\frac{1}{2}}(k'-\frac{1}{2}) \qquad (2.3\text{-}47)$$

where subscripts $i$, $r$, $t$ denote incident, reflected and total fields respectively. In (4.7-4), the total

field in reflected field region $H_{y,t}^{n+1/2}(k'-1/2)$ is required which is not recorded in this region.

However, it may be obtained by the superposition of reflected and incident fields as shown in

(2.3-47). From (2.3-46), (2.3-47), the modified expression for $E_{x,t}^{n+1}(k')$ in total field region at

$k = k'$ is obtained as

$$E_{x,t}^{n+1}(k') = E_{x,t}^{n}(k') + \frac{\Delta t}{\varepsilon \Delta z}\left[H_{y,s}^{n+1/2}(k'-1/2) + H_{y,i}^{n+1/2}(k'-1/2) - H_{y,t}^{n+1/2}(k'+1/2)\right] \text{ (2.3-48)}$$

Similar to (2.3-48), we may have the modified expression for $H_{y,s}^{n+1/2}(k'-1/2)$ in

scattering field region at $k = k'-1/2$

$$H_{y,s}^{n+1/2}(k'-1/2) = H_{y,s}^{n-1/2}(k'-1/2) + \frac{\Delta t}{\mu \Delta z}\left[E_{x,s}^{n}(k'-1) - E_{x,t}^{n}(k') + E_{x,i}^{n}(k')\right] \qquad \text{(2.3-49)}$$
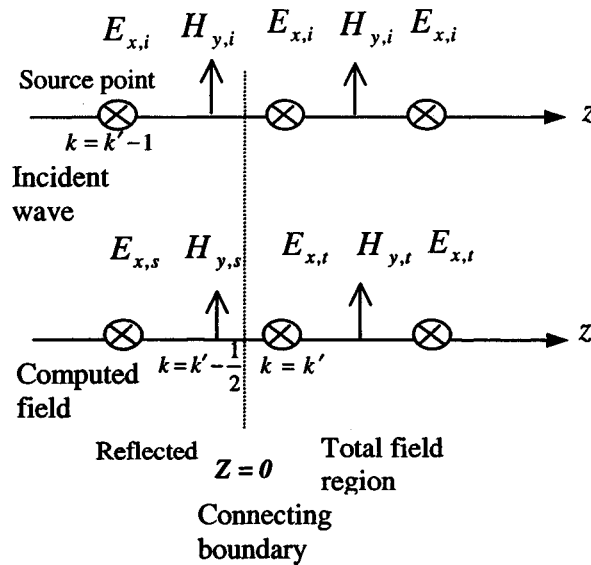
**Fig. 2-11 Illustration of the connecting boundary.**

## 2.4  MODE CALCULATION AND EFFECTIVE INDEX METHOD

### 2.4.1  One-dimensional Slab Waveguide Mode

Mode analysis involves solving the propagation constant $\beta$ or the effective index $n_{eff}$

of a slab waveguide. For a simplest three-layer symmetric slab waveguide shown as Fig. 2-12 (a),

the mode can be obtained by the approximated analytical formula provided in [24] as

$$E_y(x) = \begin{cases} A\cos(dh_a/2)\exp[h_c(d/2 - x)], & d/2 \leq x \\ A\cos(h_a x), & -d/2 \leq x \leq d/2 \\ A\cos(dh_a/2)\exp[h_c(d/2 + x)], & -d/2 \geq x \end{cases} \qquad (2.4\text{-}1)$$

where

$$h_c^2 = \beta^2 - k_c^2 \qquad (2.4\text{-}2)$$

$$h_a^2 = k_a^2 - \beta^2 \qquad (2.4\text{-}3)$$

which satisfy

$$h_c \cos(dh_a/2) = h_a \sin(dh_a/2) \qquad (2.4\text{-}4)$$

$k_{a,c} = 2\pi n_{a,c}/\lambda$ are the phase constant or wave numbers in the active and cladding region,

respectively, and A is an arbitrary constant. For the symmetric three-layer slab waveguide, this

analytical solution can provide a Gaussian-like mode profile as illustrated in Fig. 2-12 (a), which

is highly accurate compared to a more general numerical approach to be discussed next.

For the more complex waveguide structure with mutiple layers, especially like quantum

well structure, the above eq. (2.4-1) can not be applied and a more general numerical tool such as

finite difference (FD) method has to be employed, in order to calculate the modal propagation

constant of a slab waveguide with arbitrary index distributions. We will only highlight a few

important steps for this general approach, and the interested readers can refer to some literatures,

which talked about this topic in a more detail [25], [26]. The discussions on FD in the next part is

for the general 2D planar waveguide. The 1D mode can be simply obtained by setting $\dfrac{\partial F}{\partial y} = 0$.
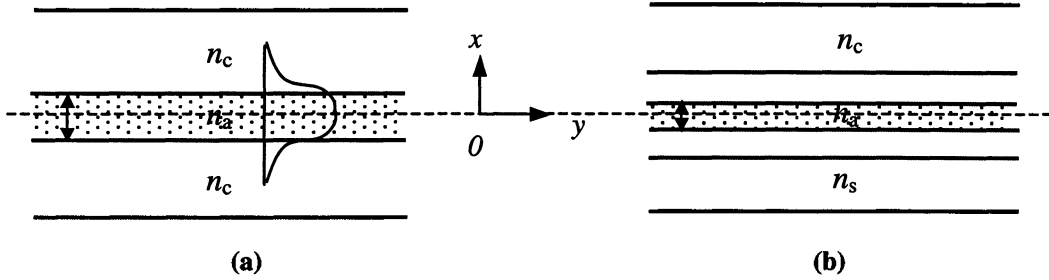


**Fig. 2-12 One dimensional Slab waveguide. (a) three layer symmetric slab waveguide; (b) Multilayer slab waveguide.**

### 2.4.2  Finite Difference Analysis

The scalar Helmholtz equations can be summarized in the form

$$\nabla_T^2 F + k^2 F = \beta^2 F \qquad\qquad (2.4\text{-}5)$$

For scalar mode, the eigenfunction $F(x, y)$ and its gradients $(\partial F/\partial x)$, $(\partial F/\partial y)$ are continuous

throughout the modelled waveguide structure. In the case of semi-vectorial polarized modes,

$F(x, y)$ represents one of the principal transverse $\vec{E}$ - field or $\vec{H}$ - field amplitude components

which are required to satisfy appropriate continuity and discontinuity conditions across each cell

boundary. The finite difference schemes ([25], [26]) will convert eq. (2.4-5) into the matrix

eigenvalue problem as

$$A\vec{F} = \beta^2 \vec{F} \qquad\qquad (2.4\text{-}6)$$

where $\beta$ is the modal propagation eigen value and $\vec{F}$ is the corresponding normalized eigen

vector, representing the appropriate modal field profile $F(x, y)$. $A$ is a real band matrix (called

the *finite difference matrix*) which is symmetric for scalar modes but non-symmetric for semi-

vectorial polarized modes.

The finite difference grid is enclosed by an outer rectangular box boundary along which

it is usual to impose either a closed boundary condition with zero values for the field profile

$F(x, y)$ at all points provided the box is sufficient large (called perfectly electric conductor, PEC

boundary), or an open boundary condition with exponential decay of the field (like perfectly

matched layer, PML discussed previously).

The matrix eigenvalue problem eq. (2.4-6) may be solved by means of the shifted inverse

power iteration method [26],[27] as

$$\vec{F}^{(m+1)} = \left(A - p^2 I\right)^{-1} \vec{F}^{(m)} \qquad\qquad (2.4\text{-}7)$$

used in the form

$$\left(A - p^2 I\right)\vec{F}^{(m+1)} = \vec{F}^{(m)}/\eta_m \qquad\qquad (2.4\text{-}8)$$

where $p^2$ is an initial estimate of $\beta^2$, $I$ is the unit matrix, and $m = (0,1,2,3,...)$ is the iteration

counter. $\eta_m$ is chosen to normalize each $\vec{F}^{(m)}$ so that the latter's element of largest magnitude is

equal to unity. The iteration processes in (2.4-8) converges to the eigenvalue $\beta^2$ of $A$ (together

with its corresponding eigenvalue of this matrix. Thus, any required propagation mode (i.e.,

propagation constant plus related field profile) of a waveguide structure may be determined by

choosing a suitable initial value of $p^2$.

### 2.4.3   Effective Index Method

The typical buried planar structure, namely the buried channel and buried rib waveguides shown in Fig. 2-13 (a) can be fabricated in II-V semiconductor compounds, which might form part of a number of active devices in Optoelectronics. The internal refractive index of the structures fabricated from III-V compounds may be assumed to be of low contrast, or termed as the weak guidance approximation.
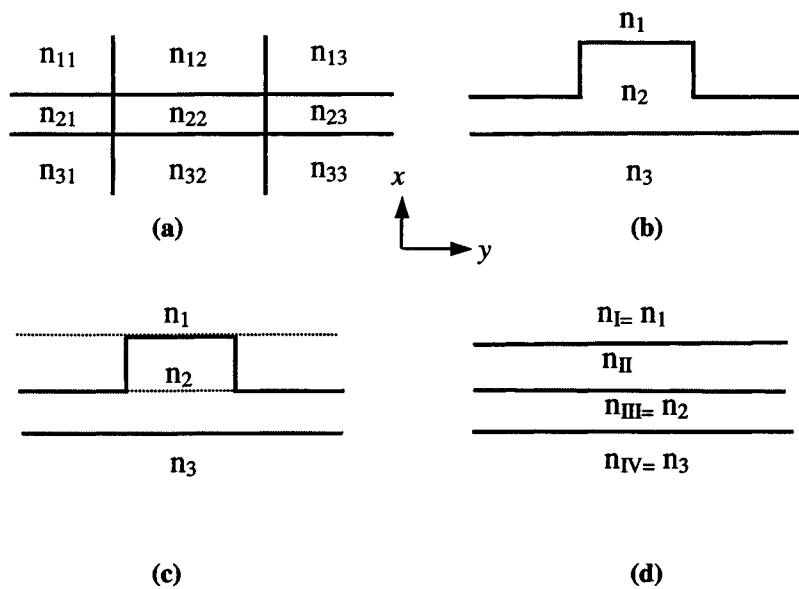


**Fig. 2-13 (a) A buried channel waveguide; (b) A buried rib waveguide. (c) The divisions of the buried rib waveguide from x direction. (d) The four uniform regions equivalent to (c)**

The effective index method (EIM) is a variational method in principal [33]. For a simplified explanation, we use the simple case of the rib waveguide shown in Fig. 2-13 (b). After finding the propagation constants $\beta_{II}$, which is a three layer symmetric waveguide we discussed

previously, the rib layer in Fig. 2-13 (c) is replaced by a homogenous region II. Therefore a new 4 layer homogenous slab waveguide is shown in Fig. 2-13 (d). Finding the propagation constant for a two-dimensional rib waveguide becomes solving the propagation for an equivalent 1D slab waveguide. In our full wave analysis for the 2-D ridge waveguide in Chapter 5 and 6, we use this EIM to decrease the dimension from 2 to 1, and combined with 2D FDTD and simulate the wave propagation within the deep-etched multi-boundary structure. The information from the finite etched ridge in y direction is involved by this EIM.

## REFERENCE

[1]   H. Haus, *Waves and Fields in Optoelectronics*. Englewood Cliffs, Nf: Prentice-Hall, 1984.

[2]   Z. Knittl. *Optics of Thin Films*, John Wiley, New York, 1976.

[3]   P. Yeh, *Optical Waves in Layered Media*, John Wiley, New York, 1988.

[4]   Larry A Coldren, Scott W. Corzine, Chap. 3 and 6 of the book *Diode lasers and photonic integrated circuits*, John Wiley & Sons, Inc., 1995.

[5]   S. Ramo, J. R. Whinnery, and T. van Duzer, *Fields and Waves in Communication Electronics*, John Wiley, New York, 1984.

[6]   H. A. Macleod, Thin-Film Optical Filters, 2$^{nd}$ ed. McGraw-Hill, New York, 1989, pp.80, 118-119.

[7]   Alfred Thelen, Design of optical interference coatings, 1989.

[8]   J. A. Dobrowolski, Coatings and filters, in *Handbook of Optics*, W. G. Driscoll, eds., McGraw-Hill, New York, 1978.

[9]   S. A. Furman and A. V. Tikhonravov, *Basics of Optics of Multilayer Systems* (Editions Frontieres, Gif-sur-Yette, France, 1992).

[10] K. S. Yee, "Numerical solution of initial boundary value problem involving Maxwell's equations," *IEEE Trans. Antenna Propagat.*, vol. AP-14, pp.302-307, 1966.

[11] S. T. Chu and S. K. Chaudhuri, "A finite difference time-domain method for the design and analysis of guide-wave optical structures," *J. Lightwave Technol.*, vol.7, pp.2033-2038, 1989.

[12] R. Y. Chan and J. M. Liu, "Time-domain wave propagation in optical structures," *IEEE Photon. Technol. Lett.*, vol. 18, pp. 1001–1003, 1994.

[13] A. Taflove, Computational Electrodynamics: The Finite-Difference Time-Domain Method. Norwood, MA: Artech House, 1995.

[14] W. P. Huang, S. T. Chu and S. K. Chaudhuri, "A semivectorial finite-difference time-domain method," *IEEE Photon. Technol. Lett.*, vol. 3, pp. 803-806, Sept. 1991.

[15] W. P. Huang, C. L. Xu, S. K. Chaundhuri, "A finite difference vector beam propagation method for three dimensional waveguide structures", *IEEE Photon. Technol. Lett.*, 4, pp.148-151, 1992.

[16] D. G. Fang, "Finite difference time domain method" in *Computational electromagnetics, Lecture Notes* in Millimeter-wave Technique Lab, Nanjing University of Sci. & Tech. Nanjing, China, Ch. 4, 2000.

[17] J. P. Berenger, "A perfectly matched layer for the absorption of electromagnetic waves," *J. Comput. Phys.*, vol.114, pp.185-200, 1994.

[18] B. Chen, D. G. Fang and B. H. Zhou, "Modified Berenger PML absorbing boundary condition for FD-TD meshes," *IEEE Microwave and Guided Wave Lett.*, vol. 5, pp. 399-401, Nov., 1995.

[19] W. C. Chew and W. H. Weedon, "A 3-D perfectly matched medium from modified Maxell's equations with stretched coordinates," *Microwave and Optical Tech. Lett.*, vol. 7, pp. 599-604, Sept. 1994.

[20] N. Georgieva and E. Yamashita, "Time-domain vector-potential analysis of transmission line problems," *IEEE Trans. on Microwave Theory and Techniques*, vol. 46, No 4, pp. 404-410, April 1998.

[21] D. Zhou, W. -P. Huang, C. -L. Xu, D.G. Fang,, B. Chen, "The perfectly matched layer boundary condition for scalar finite-difference time-domain method", *IEEE Photon. Technol. Lett.*, pp. 454-456, May. 2001.

[22] E. A. J. Marcatili, "Dielectric rectangular waveguide and directional coupler for integrated optics," *Bell Syst. Tech. J.*, vol.48, no.7, pp.2071-2102, 1969.

[23] R. Ulrich, and R. J. Martin, "Geometrical optics in thin film lightguides," *Applied Optics*, vol.10, pp.2077-2085, 1971.

[24] A. Yariv, Quantum Electronics, 2$^{nd}$ ed. New York: Wiley, 1975, pp.512.

[25] M. S. Stern, "Semivectorial polarized finite difference method for optical waveguides with arbitrary index profiles," *IEE Proc. J.* 135, pp.56-63, 1988.

[26] M. S. Stern, "Finite difference analysis of planar optical waveguides," *Progress in Electromagnetics Research*, PIER 10, pp. 123-186, ed. W.-P. Huang, 1995.

[27] L. W. Johnson, and R. D. Riess, *Numerical Analysis*, Addison-Wesley, Reading, Massachusetts, 1977.

[28] V. Ramaswamy, "Strip-loaded film waveguide," *Bell Syst. Tech. J.*, vol.53, pp.697-704, 1974.

[29] J. Buus, "The effective index method and its application to semiconductor lasers," *IEEE J. Quantum Electron.*, QE-18, pp.1279-1286, 1982.

[30] A. Hardy, "Formulation of two-dimensional reflectivity calculations based on the effective-index method", *J. Opt. Soc. Am.* Part A, vol.1, no.5, pp. 550-555, May 1984.

[31] K. S. Chiang, "Dual effective index method for the analysis of rectangular dielectric waveguides," *Applied Optics*, vol.25, pp.2169-2174, 1986.

[32] E. A. J. Marcatili, and A. A. Hardy, "The azimuthal effective index method," *IEEE J. Quantum Electron.*, QE-24, pp.766-774,1988.

[33] P. C. Kendall, "Layered theory of the rib waveguide", in *Rib waveguide theory by the spectral index method*, Optoelectronics Series, eds P. N. Robson and P.C. Kendall, Research Studies Press and Wiley, ch. 2, pp.9-34, 1990.

[34] D. Marcuse, *Theory of dielectric optical waveguide*, 2nd ed., Academic Press, San Diego, 1991,pp.307-318.

# 3 Antireflection Coatings

This chapter presents one of most important application for thin film interference coatings, the antireflection (AR) coatings. Two major AR applications are discussed, which include AR coating for conventional bulk optics glass substrate, and for semiconductor laser and travelling wave amplifiers (TWA). The two numerical methods discussed in the previous chapter, the transmission matrix method (TMM) and finite difference time domain (FDTD) methods, are both employed for the analysis in this chapter. Comparisons and some improvements are made, based on the published literatures data.

## 3.1 INTRODUCTION

Of all the possible thin film coating applications, antireflection (AR) coatings have had the greatest impact on technical optics, and exceed all other types of coatings. In some applications, AR coatings are simply required for the reduction of surface reflection. In others, not only must surface reflection be reduced, but the transmittance must also be increased (optical bandpass filters) [1]- [5].

The antireflection coating depends for its operation on more or less complete cancellation of the light reflected at the upper and lower of the two surfaces of the thin film. The following will give a brief explanation of the AR coating.

It is known that when an electromagnetic radiation reaches a dielectric boundary between two media of different refractive indices, $n_1$ and $n_2$, respectively, Fresnel reflection occurs. The reflection is a result of the dielectric discontinuity and can be reduced or even eliminated by the proper coating of thin dielectric layers.

From the theory we discussed in chapter 2, at normal incidence case, the intensity of reflected electromagnetic wave at a boundary between two dielectric media is expressed by the reflectance

$$R = \frac{(n_2 - n_1)^2}{(n_2 + n_1)^2} \qquad\qquad\qquad (-3.1-1)$$

For the case of a glass-air interface, which has a refractive index contrast of 1.52/1.0, this reflectance is approximately 4% in the visible spectrum regime. This reflectance is much higher in the case of infrared materials, which can have very much higher refractive indices.

Antireflection (AR) coated lasers are of great interest for applications such as external cavity lasers and optical amplifiers. In both cases, it is desirable to reduce as much as possible he modal reflectance, in the former case so as to avoid resonance due to the semiconductor chip cavity, and in the latter case, the low reflectance results in the so-called travelling wave amplifiers (TWA). Two issues are important for fabricating a high performance AR coating for laser structure. One is the accurate control of the coating refractive index as well as the thickness during the deposition process; the other is the accurate theoretical prediction for the coating parameters.

This chapter begins with the study on AR coatings for the glass substrate, which is widely used in conventional bulk optics. Based on the transmission matrix method (TMM) introduced in Chapter 2, for both the single and double layer AR coatings, the optimum design

solutions (optimum index and quarter wavelength optical thickness QWOT rule) are given. Supporting numerical examples show the necessity of AR coatings for eliminating the residual reflection. AR coatings for a semiconductor optical amplifier waveguide facet have been studied extensively by various numerical strategies [6]-[19]. In the second part of this chapter, numerous examples of AR-coated TWA were analyzed based on simulation with FDTD. The emphasis is given to the study of the optimum AR conditions, specifically compared to the one with AR coating on glass substrate. Studies show that the optimum index and QWOT requirement obtained with AR coatings on homogenous substrate cannot be applied directly in the case of AR coating at waveguide end. A higher coating index than the square root of the effective index of the waveguide and a larger thickness than QWOT are required, especially when the waveguide has large index contrast between core and cladding and the active layer is thin. With this case, the contribution from radiation mode cannot be neglected. The double-layer AR coating, according to its advantages of broadening the bandwidth and more flexible in choosing material, is very attractive and also widely used.

The research on AR coating in this chapter is a foundation to the study of our proposed integration compatible structure, the deep-etched antireflective waveguide gratings in the next chapter, in the sense of achieving a low reflectivity within certain wavelength range. The more important feature is its potential of reducing fabrication cost.

## 3.2  AR COATINGS ON GLASS SUBSTRATE

### 3.2.1  Single-layer AR Coating

#### 3.2.1.1    Basic Theory

The single homogeneous layer AR coating is the first and simplest dielectric structure to achieve this goal and is still widely used. Such AR coating consists of a single homogeneous layer a quarter-wavelength in optical thickness, that is,

$$d = \frac{\lambda_0}{4n}$$

(3.2-1)

where $n_1$ and $d$ are refractive index and thickness of the coating layer, respectively. The reflectance of this single film has already been evaluated by TMM in Chapter 2. The solution to achieve zero reflectance at the desired wavelength $\lambda_0$, requires the refractive index must satisfy

$$n = \sqrt{n_0 n_s}$$

(3.2-2)

In practice, materials with such a refractive index may not exist. Nevertheless, using available materials with refractive index close to that given in (3.2-2), a great reduction in reflectance is obtained. According to the theory we discussed in Chapter 2, the residual reflectance at the desired wavelength is given by

$$R = \frac{\left(n_s n_0 - n_1^2\right)^2}{\left(n_s n_0 + n_1^2\right)^2}$$

(3.2-3)

Note that residual reflectance is of the second order of the deviation in the index. We also notice that by using materials with an index of refraction between $n_s$ and $n_0$, a single-layer coating as shown in Fig. 3-1, will reduce reflectance regardless of the layer thickness. Thus, the

reflectance of a coated surface is always lower than that of an uncoated one, provided that the

refractive index of this coating layer is between that of the two media. In some sense, the coating

layer smoothes the sharp dielectric discontinuity between two media.
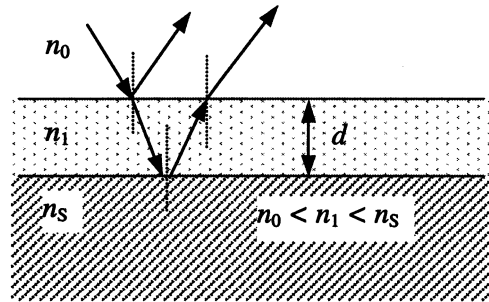


**Fig. 3-1 Schematic diagram of a single layer antireflection coating on a homogenous substrate.**

### 3.2.1.2    Numerical Examples by TMM

According to eq.(3.2-2), the choosing of the film refractive index is crucial to achieve the

antireflection purpose. In Fig. 3-2, it shows the reflectance of single-layer AR coated substrate,

simulated by TMM, with three different choices of film refractive index $n_L$ and substrate

refractive index $n_S$. The physical thickness $d$ in all three cases is fixed with satisfying QWOT at

centre wavelength $\lambda_0$. The refractive index 1.38 refers to MgF$_2$, which is the coating material

with smallest refractive index available in practice. From the three curves, it can be clearly seen

only the second curve approaches antireflection requirement and film refractive index (1.38) is

close to its ideal value $\sqrt{1.75} = 1.322$. From this example, it can be clearly observed that for the

single layer AR coating, coating material index is required to be as close to the square root of its

substrate as possible. Once this optimum material is fixed, the physical thickness $d$ is therefore

determined according to the QWOT rule. The achievable bandwidth with this single layer AR

coating is around 30nm for a reflectivity less than $10^{-4}$ theoretically and numerically.
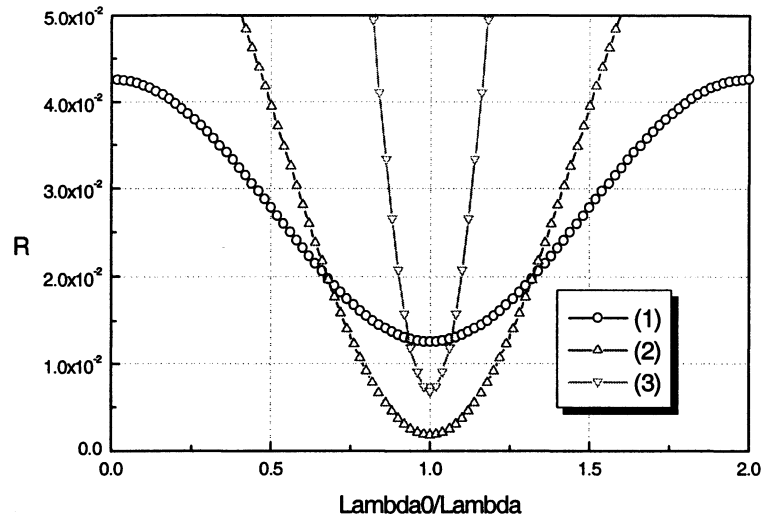


**Fig. 3-2 Reflectance of single-layer antireflection coatings simulated by TMM. 1.0|L|$n_S$ with $n_{L1}$=1.38 and $n_{S1}$ = 1.52 (open circle), $n_{L2}$=1.38 and $n_{S2}$ = 1.75 (up triangle), $n_{L3}$=2.2 and $n_{S3}$ = 4.1(down triangle).**

## 3.2.2   Double-layer AR coating

### 3.2.2.1   Basic Theory

It is possible to achieve antireflection by using more than one layer. Generally speaking, the addition of layers offers the possibility of achieving zero reflectance at the desired wavelength using available materials, and the possibility of achieving low reflectance over a broader spectral region [1]-[3].

The disadvantage of the single-layer coating, as far as the antireflection design is concerned, is the limited number of the adjustable parameters, or the degree of freedom. The

refractive index or optical admittance, of the layer is uniquely determined as $n_1 = (n_s n_0)^{1/2}$.

There is thus no room for manoeuvre in the design of a single-layer coating. In practice, the

refractive index is not a parameter, which can be varied at will. Materials suitable for use as thin

films are limited in number and the designer has to use what is available. A more rewarding

approach, therefore, is to use more layers, specifying obtainable refractive indices for all layers at

the start, and to achieve zero reflectance by varying the thickness. Then, too, there is the

limitation that the single-layer coating can give zero reflectance at one wavelength only and low

reflectance over a narrow region. A wider region of high performance demands additional layers.

The problem of ensuring zero reflectance at a single wavelength by using two layers of

coatings will be first investigated through TMM theory and then the attempt is given to achieve a

broader bandwidth by manipulating the two refractive indices. Compared with single layer AR

coating, one more degree of freedom is obtained and therefore a broader bandwidth is expected

to be achievable.
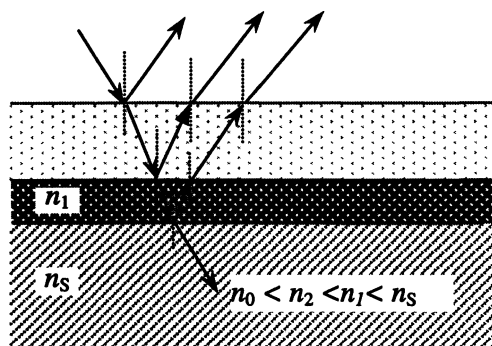


**Fig.3-3 Schematic diagram of double-layer AR coatings on a homogeneous substrate.**

The transmission matrix method (TMM) is employed in calculating the reflectance from the two

layer coating as shown in Fig.3-3 with the refractive index as $n_1$ and $n_2$, respectively. The

solution of the zero reflectance requirement can be summarized in a useful diagram shown in Fig.

3-4, known as Schuster diagram after one of the originators [2] and the shaded areas are those in

which real solutions for $n_1$ and $n_2$, satisfying zero reflectance at single wavelength.

(1) Zero reflectance at single wavelength
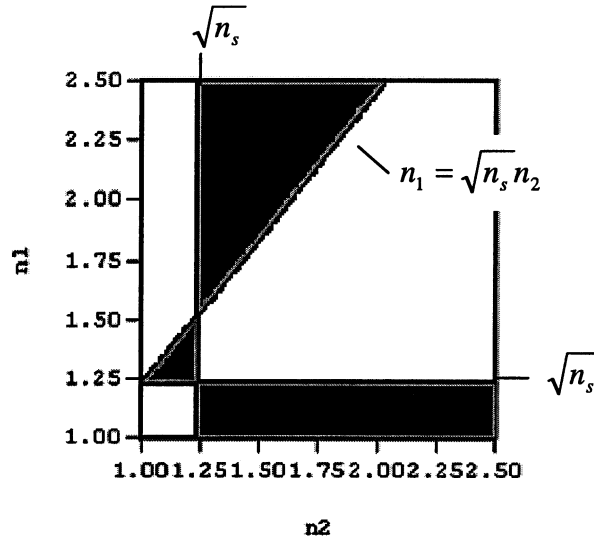


**Fig. 3-4 A Schuster diagram for two-layer coatings on glass substrate for the possible coating indices $n_1$ and $n_2$ ($n_s$=1.52, n$_0$=1.0).**

(2) Broadband antireflection design

Among all the possible solutions in Fig. 3-4, the solutions which satisfy

$$n_1 = n_2 \sqrt{n_s} \qquad (3.2\text{-}4)$$

are widely used and in this case, each layer still satisfy the quarter wavelength optical thickness

(QWOT) rule, or $n_1 d_1 = 1/4 \lambda_0$, $n_2 d_2 = 1/4 \lambda_0$ is satisfied.

It has been proved analytically that among all the solutions, the one which provides the

low reflectivity over broadest bandwidth is given by [3], [4]

$$n_1 = n_s^{3/4}, \quad n_2 = n_s^{1/4} \qquad (3.2\text{-}5)$$

### 3.2.2.2 Example by plane wave TMM

The reflectance of double layer AR coating with two different material coating combinations are calculated by TMM and shown in Fig. 3-5. For both curve 1 and curve 2, the relationship given in (3.2-4) is satisfied, therefore both cases, QWOT are required for the thickness. It is shown in the figure that with different choices of $n_1$ and $n_2$, the bandwidth is also not the same. Curve 1 gives a broader bandwidth than curve 2 simply because the combination of $n_1$ and $n_2$ in this case is closer to the broadband AR optimum solution given in (3.2-5).
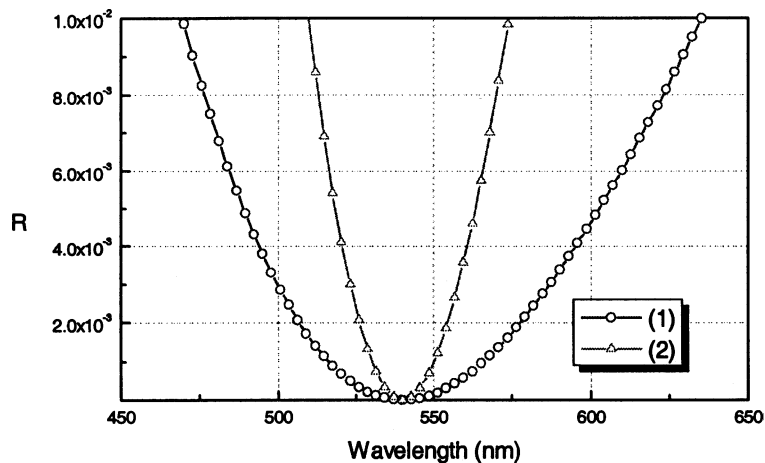


Fig. 3-5 Reflectance as a function of wavelength for double layer AR coating on a glass substrate. Simulated by TMM, 1.0|L|H|1.52 with $n_{L1}$=1.38 and $n_{H1}$ = 1.7 (open circle, curve 1), $n_{L2}$=1.86 and $n_{H2}$ = 2.3 (up triangle, curve 2).

## 3.3 AR COATINGS FOR SEMICONDUCTOR WAVEGUIDE FACET

As we have discussed in Chapter 1, AR coating is a crucial component for fabricating the semiconductor optical amplifier (SOA). What is different from AR coating in the previous part is that the media is optical waveguide with dielectric boundaries, instead of a uniform, homogenous

substrate. The incident wave is a fundamental mode profile as shown in Fig. 3-6, instead of a single plane wave, which occurs at the previous part. Therefore, although the design concepts can be borrowed from AR on glass substrate, the specific design results will not be the same. The simulation tool has also been updated from 1D TMM to 2D FDTD, which simulates the wave propagation within the structure in a more accurate way.

### 3.3.1   Single Layer AR Coating

#### 3.3.1.1   Basic Theory

In order to simulate a waveguide structure with reflection boundaries, the first step is to obtain the mode which propagates in the waveguide without boundaries. This mode analysis has already been introduced in the third part of Chapter 2. Then use this mode as the excitation which incidents from a plane within the waveguide (incident plane), and then starts FDTD time marching scheme to simulate its propagation along z direction. Since the excitation is a continuous wave (CW), it will finally reach a steady state distribution for a given wavelength. By calculating the overlap integral of the reflected field with the incident mode distribution along x-direction, the modal reflectivity is obtained. The reflectance is obtained as the square of its amplitude.
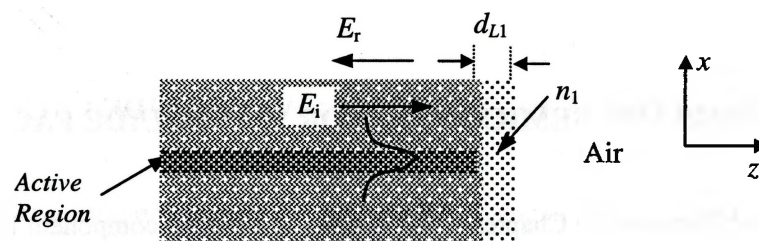
**Fig. 3-6 Schematic diagram of single-layer antireflection coatings for waveguide facet**

### 3.3.1.2    Example by full wave FDTD

#### 3.3.1.2.1    Numerical test for absorbing boundary condition

The FDTD method and PML absorbing boundary conditions (ABC) have been introduced in Chapter 1. It should be noted that the performance of the absorbing boundary condition (ABC) used with FDTD method determines the dynamic range of the numerical simulation. Widening the dynamic range is crucial to the evaluation of low power reflectivities, particularly for a multilayer AR coating. It has been studied with comparisons among different ABCs (like *Mur* second order ABC) that PML is necessary and sufficiently accurate for evaluating low reflectivities from the endface of optical waveguides with an AR coating [17].

Before we move on to calculate the reflectivity for structures with single and double-layer AR coatings, it is necessary to test the parasitic or non-physical reflection generated with our FDTD-PML computer program. This is also meaningful in the sense that PML's perfomance depends on choices of absorbing parameters. For a stringent requirement like AR coating, the parasitic reflectivity from PML has to be as small as possible, in order to guarantee obtaining a reliable design solution. The testing example we choose is a two-dimensional three-layer optical waveguide without any dielectric discontinuity, which ideally will result in zero reflectivity. A three-layer symmetric slab waveguide without any discontinuity along z direction is simulated by FDTD with PML absorbing boundary conditions. The incident plane is chosen at the half of the structure. The fundamental mode of this slab waveguide is calculated in advance analytically or numerically which is shown in Fig. 3-7 (b). The steady state field distribution is obtained as shown in Fig. 3-7 (a). The calculated power modal reflectivity is $2 \times 10^{-7}$ and is sufficiently low.

**(a)**                                        **(b)**
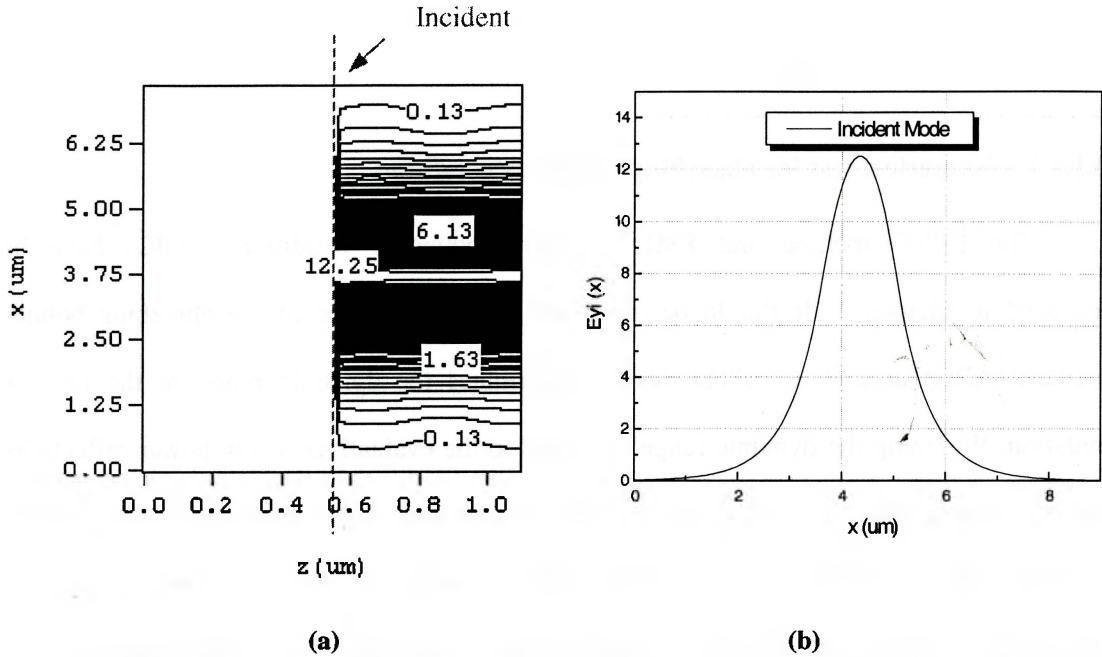
**Fig. 3-7 Numerical pre-testing for PML ABC; (a) Steady state field distribution for a straight waveguide, (b) the according incident fundamental mode.**

### 3.3.1.3    Simulation Examples for Single layer AR Coating

Once we have done enough numerical tests for the absorbing boundary conditions, the same program can be used for AR coating analysis. Similar to [17], we first analyze the reflection for a single-layer AR coating. The configuration to be investigated is a two-dimensional symmetric waveguide whose end facet is coated with an AR layer of refractive index $n_1$ and thickness $d_1$ respectively, as shown in Fig. 3-8 (a). The refractive indices of the core and cladding are chosen to be $n_{co} = 3.6$ and $n_{cl} = 3.564$, respectively. A wavelength $\lambda_0 = 1.55\mu$m is used and the normalized frequency is taken to be V=1.5, which corresponds to the active layer thickness as 2d = 2×0.73=1.46μm for this analysis.   The coating index for the simulation is chosen as

$$N_{AC} = \sqrt{N_{eff}} = 1.8938 \text{, and the coating thickness is chosen as } d_1 = 0.206 \mu m = \lambda_0 / 4n_1 \text{.}$$
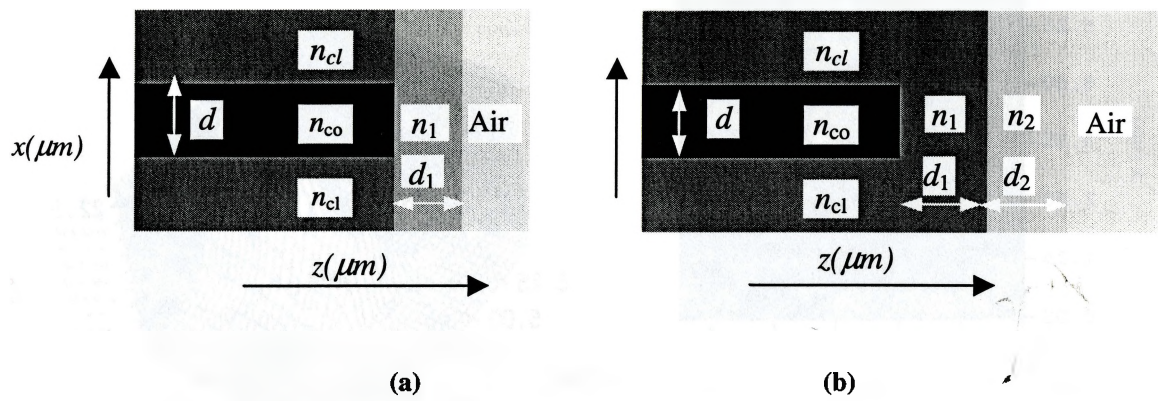
**Fig. 3-8 Configuration of (a) Single-layer AR coating and (b) double-layer AR coating.**
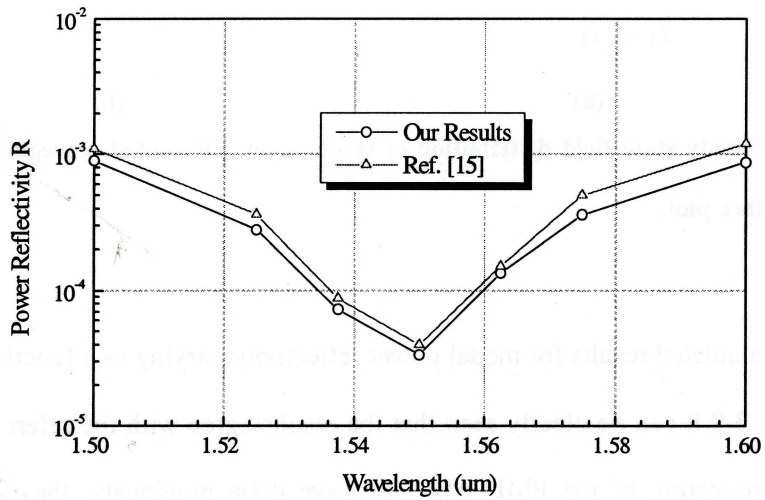


**Fig. 3-9 Modal Reflectance as a function of wavelength for single-layer AR coating**

**(a)**                                                                            **(b)**
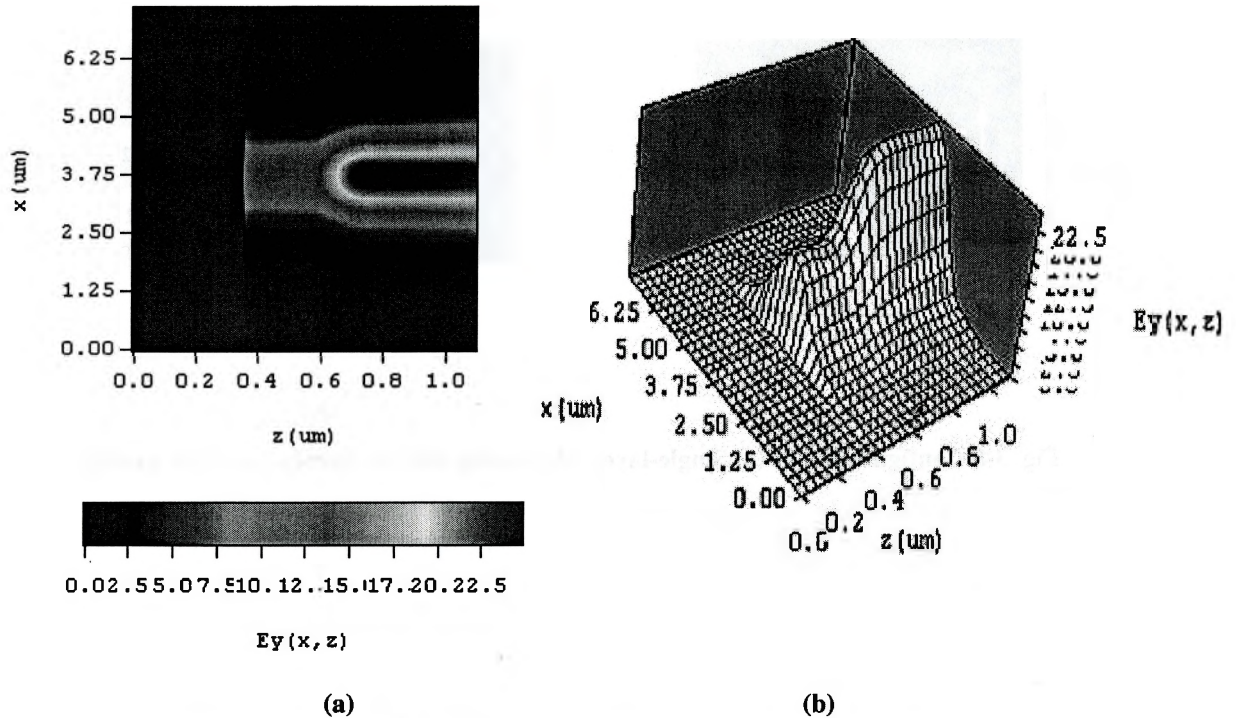
**Fig. 3-10 Steady state field distribution of single layer AR coated waveguide, (a) color shaded image; (b) surface plot.**

The calculated results for modal power reflectivity varying as a function of wavelength is shown in Fig. 3-9.It can be clearly seen that the results agree with the reference [17] very well. Due to the pre-testing of the PML ABC we have done previously, the reflectivity we have calculated shows a little lower than the results from [17]. In Fig. 3-10, the calculated steady state $E_y$ field distribution shows that for the chosen parameters (refractive index of the coating layer and the quarter wave optical thickness), the reflection has been cancelled almost completely. This solution accords with the cases of single layer AR coating on a glass substrate as we discussed previously. However, from the more examples we studied afterwards, this coincidence only occurs for certain waveguide structure.

### 3.3.1.4   Further investigations on optimum n1 and t with different examples

The waveguide structure we have chosen for the previous example has two features: (1) very

small refractive index difference between the core and cladding layer, which is 3.6/3.564. (2) the

active layer thickness is large (1.46μm). The single-layer antireflection solution obtained for this

structure, which are $n_f = \sqrt{n_{eff}}$ and $n_f d_f = \lambda_0/4$ coincides with the one for glass substrate

coatings. Then the question we are asking is: will this condition be valid for any structure?

Therefore, further investigation on the optimum AR design condition for different waveguide

structures is necessary. The next example is channel stripe waveguide as shown in Fig. 3-11 (a).

The cross section shows the active region is rectangular with thickness (x-direction dimension)

much smaller than width (y-direction dimension). The same structure has been analyzed by

integral equation method based on Fourier decomposition in [9]-[10] which predicted a different

optimum condition for AR coatings at laser diode end facet, with different active layer thickness

$d$. For an equivalent 2D structure, that slab waveguide with $n_{co}$=3.524, $n_{cl}$=3.17, is shown in Fig.

3-11 (b). The core layer thickness can vary from 0.11 μm to around 1.0μm. It is expected that the

analysis done by FDTD here should provide similar solutions.

The effective index of this slab waveguide $N_{eff}$ as a function of active layer thickness $d$

is calculated and shown in Fig. 3-12. As $d$ increases from around 0.1 μm to 1.0 μm, $N_{eff}$ varies

monotonically from 3.18 ($\sim n_{cl}$) to 3.50 ($\sim n_{co}$). If we assume that the optimum refractive index

of the single layer AR coating always satisfy the optimum condition $n_1 = \sqrt{n_{eff}}$, as what

occurred in the last example we calculated or from [17], then the optimum coating index should

have the same profile, or specifically for any $d$, coating index $n_1$ should never go beyond $\sqrt{n_{co}}$ for a single layer AR coating.



**(a)**



**(b)**
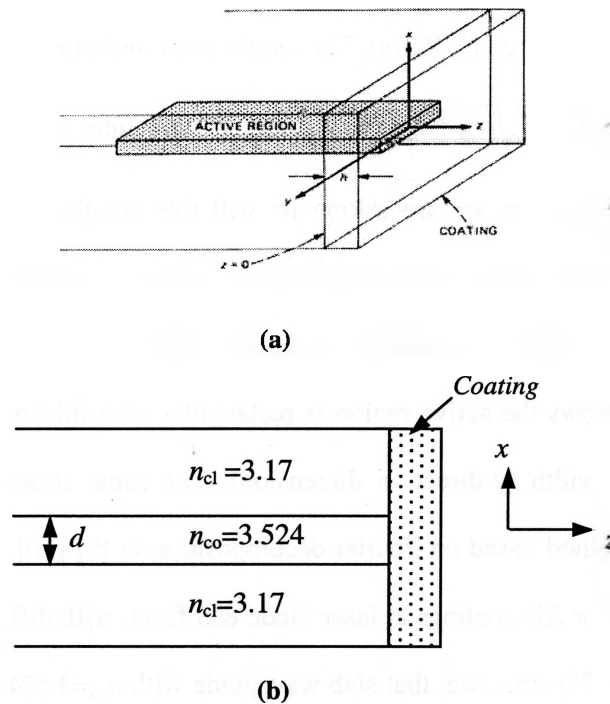
**Fig. 3-11 Schematic diagram of a strip waveguide and sideview of its structure with a single layer AR coating (a) 3D view [7]; (b) 2D view.**

From Fig. 3-13 to Fig. 3-15, we have done some simulations for this waveguide structure with different choices of active layer thickness $d$. In Fig. 3-13, we calculated the modal reflectivity varied as a function of coating thickness $d_1$ with two choices of coating index $n_1$. The waveguide structure for our FDTD simulation is chosen as $n_{co}$=3.524, $n_{cl}$=3.17, and $d = 0.5\mu m$. The curve with open circle symbol provided the results for a coating index of 1.92, it reached a very low reflectivity of $6.2 \times 10^{-6}$ at $d_1 = 0.23 \mu m$. It is to be noted that in this case,

$n_1^2 = 1.92^2 = 3.686 > n_{co} = 3.524 > n_{eff} = 3.3856$, and $n_1 d_1 = 0.276\lambda_0 > 0.25\lambda_0$, with the

center wavelength $\lambda_0$ chosen as 1.55μm. In other words, we've obtained an antireflection in the

case that none of the optimum conditions satisfied. Then we can take a look at the second curve

with the up-triangle symbol. The coating index for this case is chosen as $n_1 = \sqrt{n_{eff}} = 1.84$. For

a coating thickness, which satisfy QWOT ($d_1 = 0.21\mu m$), the modal reflectivity is only around

$1 \times 10^{-2}$, which is far from the AR coating requirement for SOA facet. The lowest reflectivity

with this coating index is obtained as $1.2 \times 10^{-3}$, by varying the coating thickness to be larger, as

shown in Fig. 3-13. From this example, we can conclude the assumption about same optimum

condition is invalid. Although the results we calculated with the first example and from the

reference [17] are correct, the AR solutions cannot be applied to arbitrary waveguide structures.
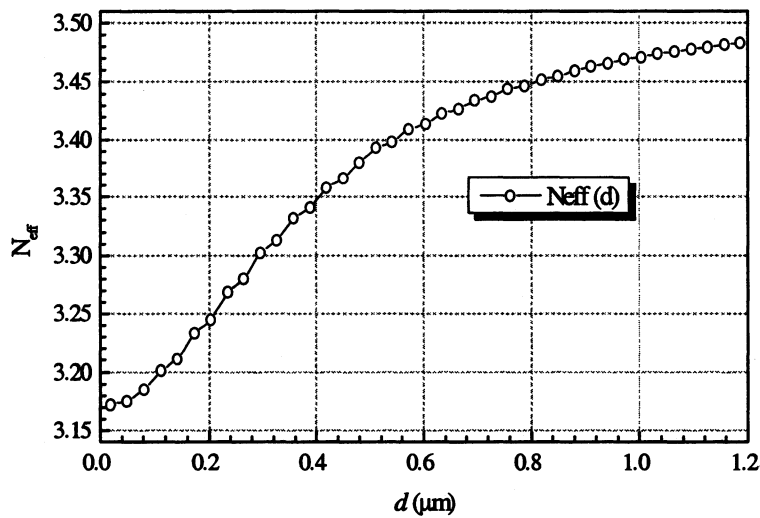


**Fig. 3-12 Effective index vary as a function of the active layer thickness $d$.**
**Parameter chosen as $n_{co}$=3.524, $n_{cl}$=3.17, wavelength=1.55μm.**
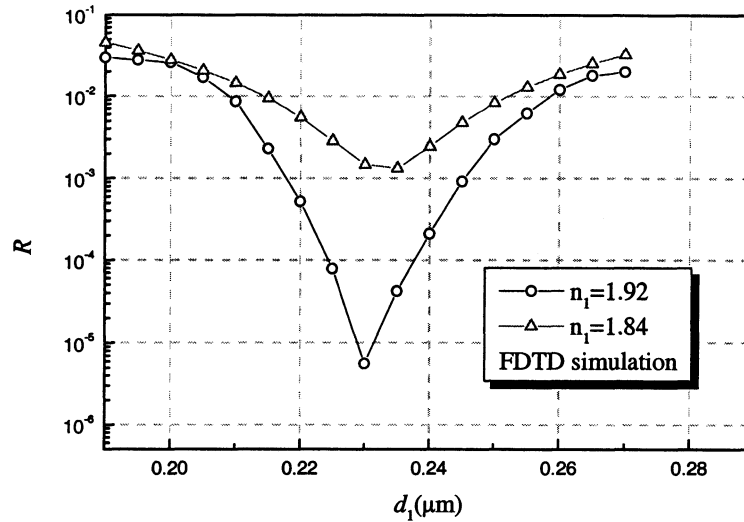
**Fig. 3-13 Modal reflectivity as a function of the film thickness $d_1$, for the film refractive indices $n_1$ =1.92 and $n_1$=1.84= $(N_{eff})^{1/2}$ as a function of film thickness when $n_{co}$ = 3.524, $n_{cl}$ = 3.17, active layer thickness is 0.5$\mu$m, the operating wavelength is 1.55$\mu$m.**

We provided two more examples for the effect of waveguide structure on the optimum coating index in Fig. 3-14 and Fig. 3-15.

CASE 1: Structure with very thin active layer thickness $d$ (<0.2$\mu$m)

Fig. 3-14 presents the $E_y$ field distribution for the single layer AR-coated waveguide structure with very thin active layer thickness ($d$=0.11$\mu$m), simulated by FDTD. The coating parameter is given as $n_1$=1.81, $d_1$=0.222$\mu$m. The according modal reflectivity is $R$= 6.4$\times$10$^{-6}$.

CASE 2: Structure with relatively wide active layer thickness $d$ (>1.0$\mu$m)

Fig. 3-15 presents the $E_y$ field distribution with relatively thick active layer thickness $d$=1.5$\mu$m. In this case, the coating index is $n_1$=1.87 = $\sqrt{N_{eff}}$ , ($N_{eff}$= 3.496). $n_1 d_1$ = 0.277$\lambda_0$. The reflectivity calculated is around $R$=4.0$\times$10$^{-4}$.
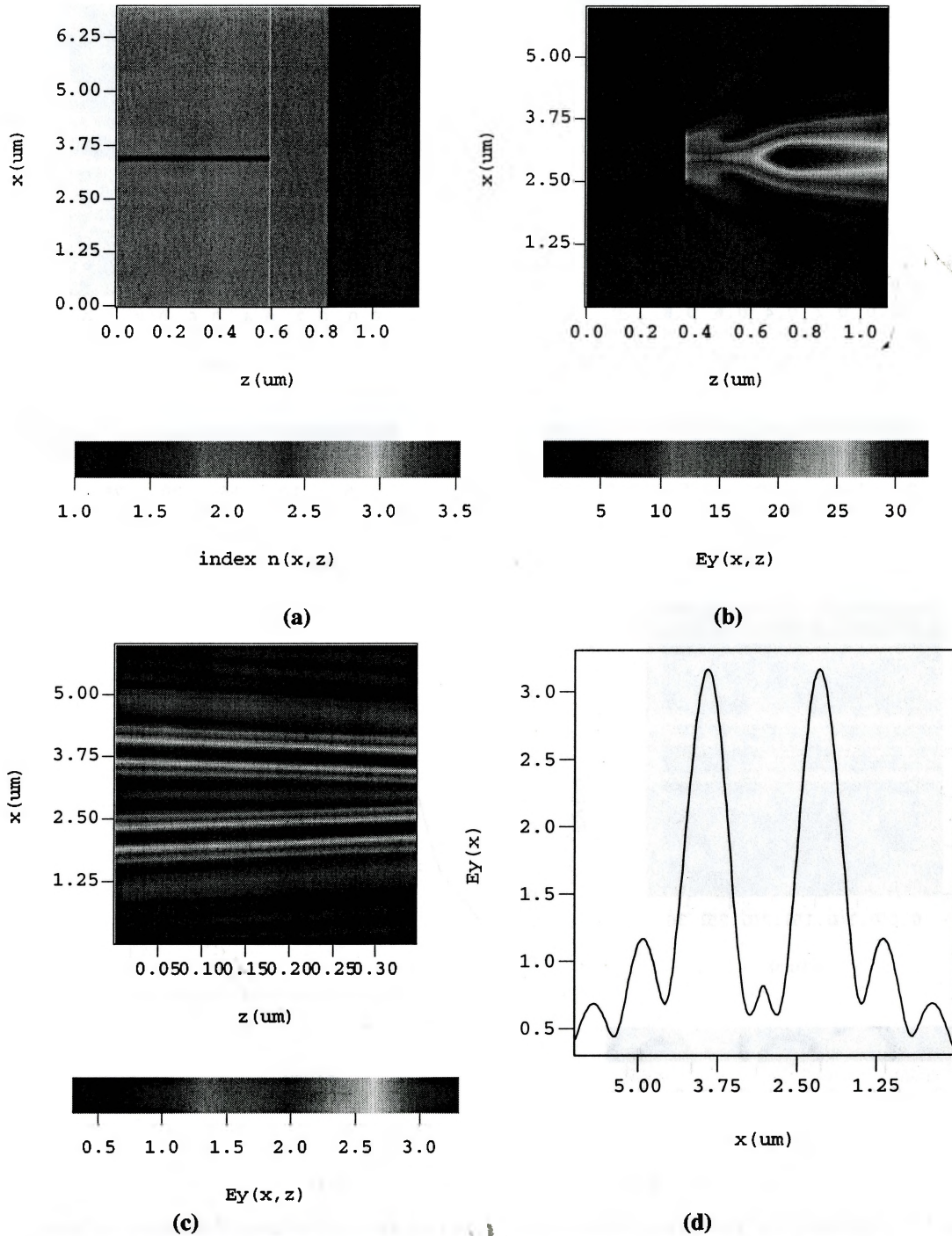
**Fig. 3-14 Reflection for the waveguide structure with very thin active layer thickness d=0.11μm, simulated by FDTD. (a) Index distribution; (b) steady state field distribution in the total computation region; (c) steady state field distribution in the reflected region; (d) A z-slice view of the reflected field.**
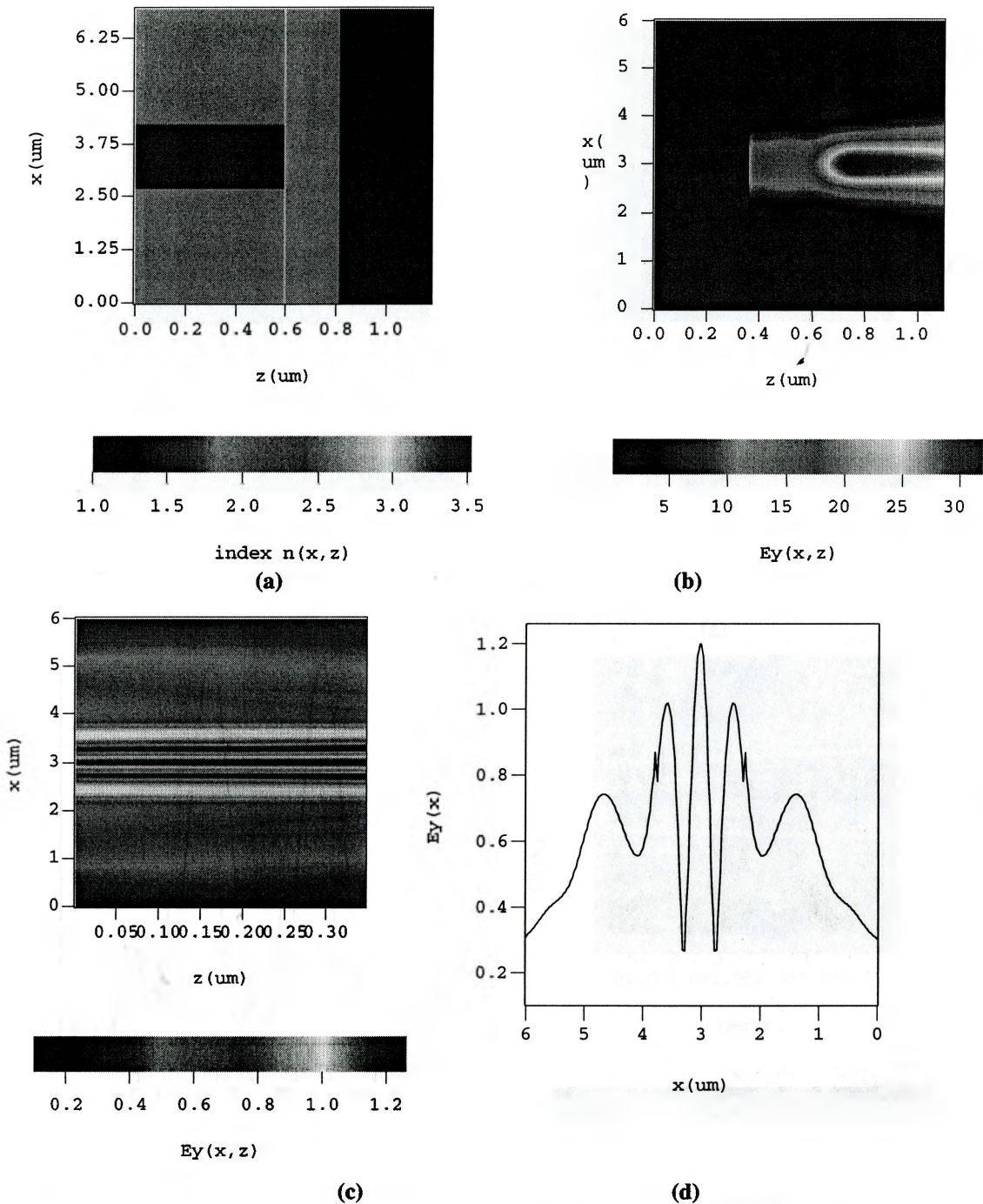
**Fig. 3-15 Reflection for the waveguide structure with very thin active layer thickness *d*=1.5μm, simulated by FDTD. (a) Index distribution; (b) steady state field distribution in the total computation region; (c) steady state field distribution in the reflected region; (d) A z-slice view of the reflected field.**

### 3.3.2  Double-Layer AR Coating

As we discussed in 3.2.2, the double-layer of AR can be expected to provide a broader bandwidth, which provide one more degree of freedom, smoothen the discontinuity from 3.2 (waveguide) to 1.0 (air) in a further and more continuous way. The two layer of coatings deposited at waveguide facet are shown schematically in Fig. 3-16 Normally the first layer is a higher index coating (such as TiO2), followed by a coating layer with lower index (like $SiO_2$). The two coating thickness will vary according to the choices of $n_H$ and $n_L$.
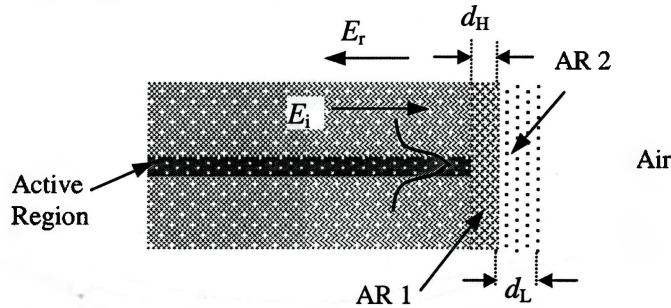


**Fig. 3-16 Schematic diagram of a double-layer AR coatings for semiconductor amplifier facet.**

#### 3.3.2.1  Results for the double-layer AR Coating

The first example we chose for simulation is the same as [17], with the configuration already shown in Fig. 3-8 (b). Parameters for the two coating layers are chosen as $n_2$=1.46, $n_1 = n_2(N_{eff})^{(1/2)}$ =2.76494, $d_1$= $\lambda_0/(4n_1)$ =0.138 μm, $d_2$= $\lambda_0/(4n_2)$ =0.266μm, and $\lambda_0$=1.55μm is the center wavelength. The calculated modal Reflectivity as a function of wavelength for double-layer AR coating structure is shown in Fig. 3-17. As we expected, both our results and reference predict the same optimum condition, which again accords with the condition of double-layer AR coating for glass substrate. Based on the knowledge from single-layer AR coating previously, this optimum condition will also be valid only for specific waveguide and is not a general solution.

For single-layer AR coating, it requires a higher coating index than the square root of the waveguide effective index as well as a larger thickness than QWOT. Similar conclusions have been obtained with different simulation tools or observed through practical experiments [9]- [13]. For double-layer AR coatings, the requirements on the coating index are not as critical as what is required for single-layer AR coating. However, a non-QWOT thickness for both layers is expected.
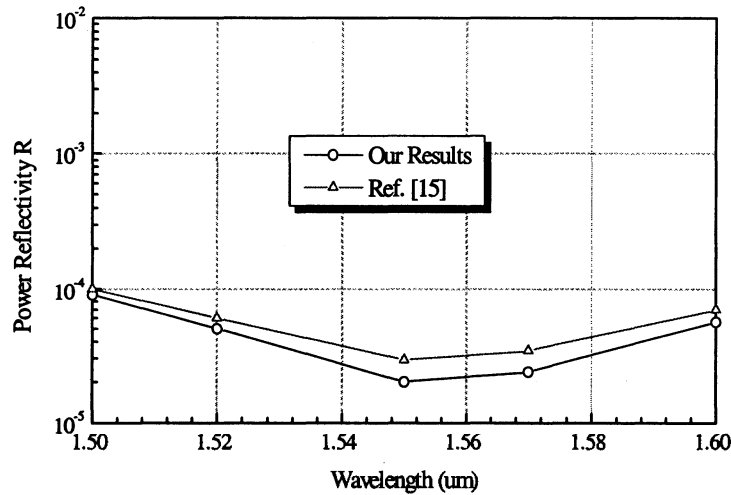


**Fig. 3-17 Modal Reflectivity as a function of wavelength for double-layer AR coating structure shown in Fig. 3-8 (b). Parameters used in the calculation: $n_{co}$=3.6, $n_{cl}$ = 3.564, $n_2$=1.46, $n_1$=$n_2$N$_{eff}^{1/2}$=2.76494, $d_1$= $\lambda_0$/($4n_1$)=0.138 $\mu$m, $d_2$= $\lambda_0$/($4n_2$)=0.266$\mu$m, $\lambda_0$=1.55$\mu$m is the centre wavelength.**

The field distributions for both the total region and reflected region are shown in Fig. 3-18. It is seen that the reflected fields are successfully suppressed due to the double-layer AR coatings. From a detailed view of the reflected field distribution in (c), the dominant component in the reflected field is still the fundamental mode, with the largest value occurring at the core region. The contributions from other component (higher order guided mode and radiation mode) are relatively small. This could work as the main reason why the AR solution obtained with this structure is so close to the solution obtained by plane wave model.

(a)



(b)



(c)



(d)
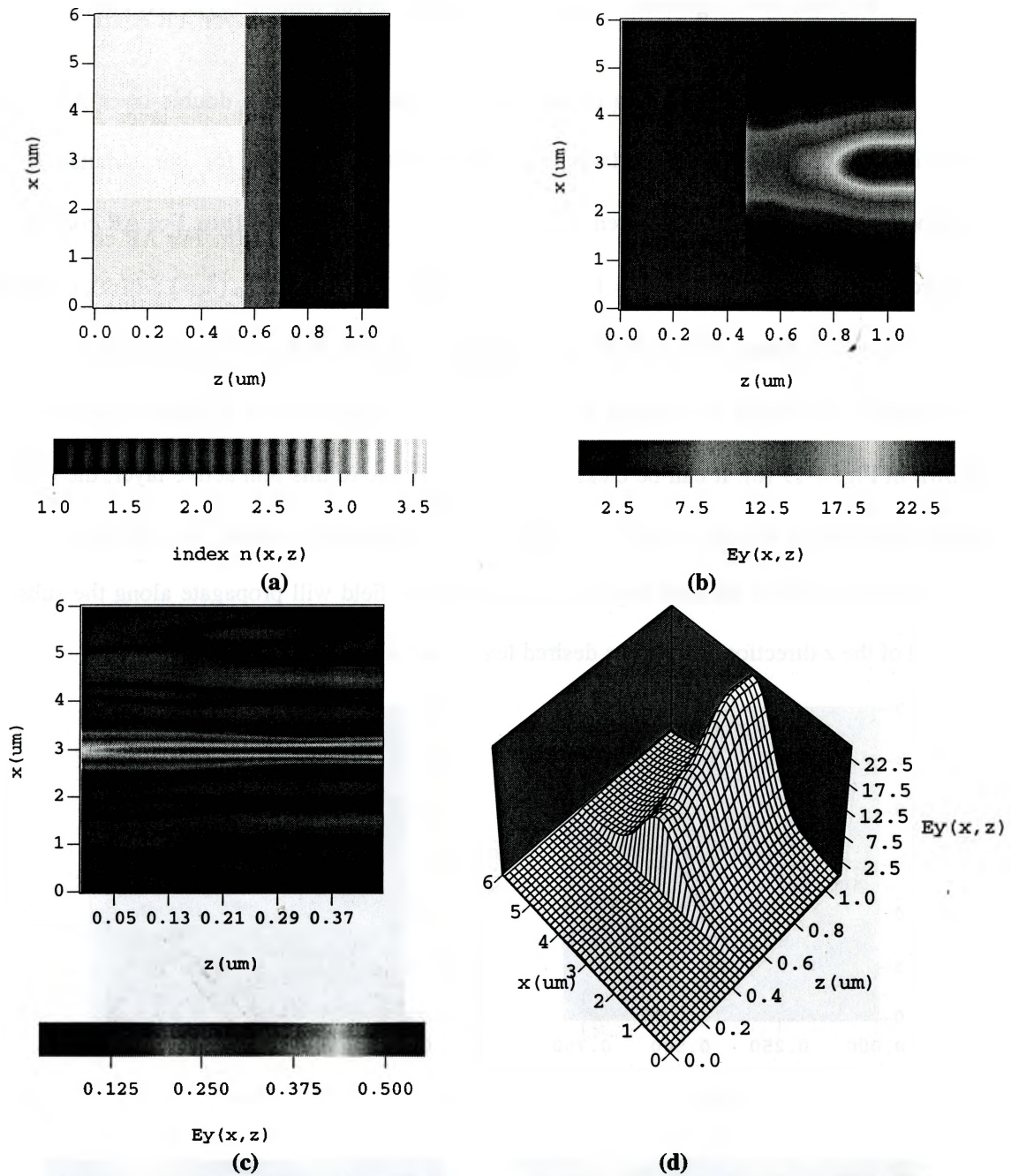
**Fig. 3-18 FDTD simulation results for double layer AR coatings for the semiconductor waveguide facet. (a) index distributions; (b) steady state field distributions in color plot; (c) steady state reflected field distribution in color plot. (d) steady state field distributions in surface plot.**

### 3.3.2.2    Further investigations on optimum conditions for double-layer AR coatings

For a further investigation of the optimum conditions with a double-layer AR coating deposited at optical waveguide facet, we chose another example for our simulation. The parameters for waveguide are chosen as $n_{co}$ = 3.524, $n_{cl}$ = 3.17, $d$ = 0.11μm. For AR coatings, the first coating layer is chosen as $n_1$ = 1.82, $d_1$ = 0.1815μm, $n_1 d_1$ = 0.215$\lambda_0$ ($\lambda_0$=1.54μm), the second coating layer are chosen as $n_1$ = 1.65, $d_2$ = 0.052μm, $n_2 d_2$ = 0.056$\lambda_0$. For the wavelength 1.54μm, we obtained the modal reflectivity as R=6.24×10$^{-5}$. The steady state $E_y$ field distributions are shown in Fig. 3-19 (e). It can be clearly observed that due to this thin active layer, the radiation mode contribution become significant compared to fundamental mode. This results in the fact that both the fields in the total region and the reflected field will propagate along the substrate, instead of the z-direction, which is a desired feature for AR design.



(a)



(b)

**(c)**

**(d)**



**(e)**
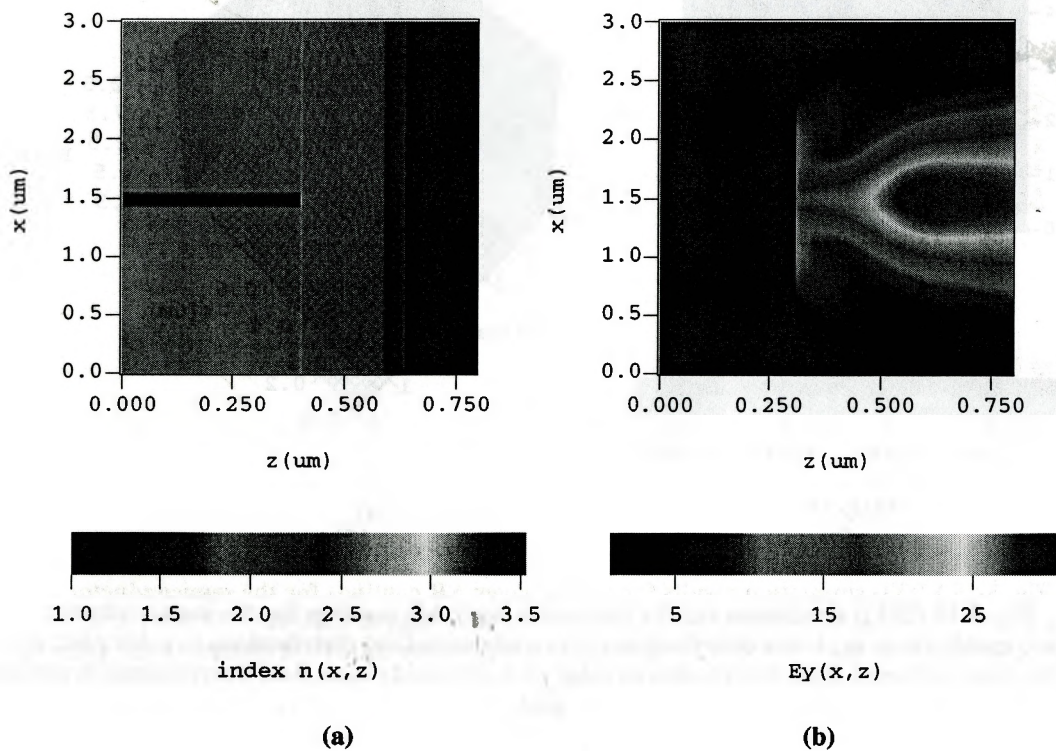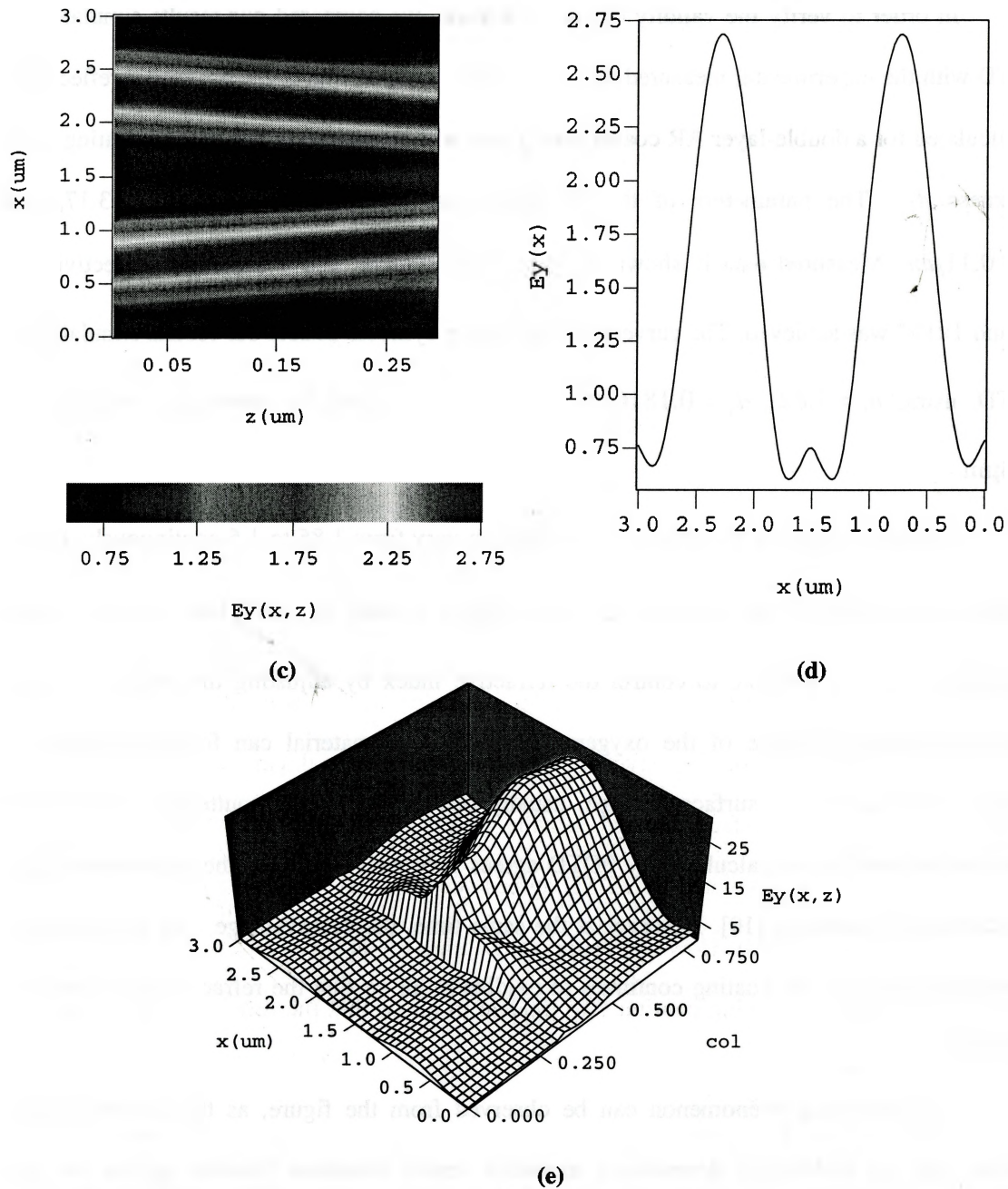
**Fig. 3-19 FDTD simulation results for double layer AR coatings deposited at the semiconductor waveguide facet with a different waveguide structure. (a) refractive index distributions; (b) steady state field distributions in the total region; (c) steady state reflected field distribution in color plot. (d) Reflected field distribution with z-slice. (e) surface plot of the steady state field distributions in the total region.**

### 3.3.3  Comparison with Experimental Data

In order to verify the validity of our simulation, we compared our results simulated by FDTD with the experimental measured data provided in [10]. In Fig. 3-20, the modal reflectivity is calculated for a double-layer AR coated waveguide with variations of the second coating layer thickness $d_2$. The parameters of the waveguide are chosen as $n_{co}$=3.524, $n_{cl}$=3.17, and $d = 0.11\mu m$. Measured data is shown in open circle symbol, and a minimum reflectivity of around $1\times10^{-4}$ was achieved. The curve with up-triangle symbols denote our results simulated by FDTD, using $n_1 = 1.82$, $d_1 = 0.1816\mu m$, and $n_2 = 1.65$, and the operating wavelength is 1.54μm.

Refractive index of evaporated $SiO_x$ film can vary from 1.85 to 1.5 continuously, by the control of pressure of the oxygen [10]. AR coating formed by $SiO_x$ film has two major advantages: 1) It is possible to control the refractive index by adjusting the evaporation rate and/or the partial pressure of the oxygen. Therefore, one material can form two layers of coatings. 2) There is no surface damage, usually observed with the sputtering method. The optimum value of $d_2$ we calculated by FDTD agrees very well with both the experimental data and theoretical results in [10]. However at the same time, the disadvantage with this pressure-controlled coating is the coating continues to oxidize in air so that the refractive index reduces with time.

An interesting phenomenon can be observed from the figure, as the authors in [10] pointed out, the reflectivity dependence measured seems somehow broader against the film thickness than the theoretical predictions.
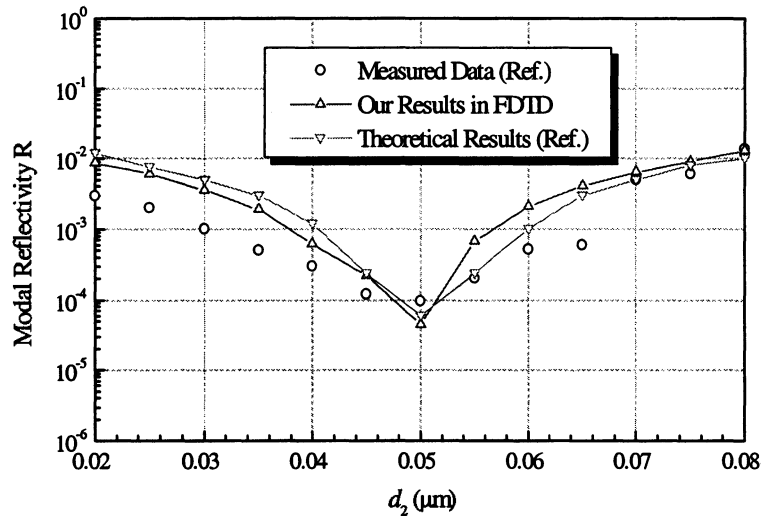
**Fig. 3-20 Facet reflectivity of double-layer AR coated BH laser structure as a function of a second-layer coating thickness for $n_1$=1.82, $d_1$=0.1815μm, $n_2$=1.65, and wavelength at 1.54μm. The open circle symbol and the curve with up-triangle represent the experimental values and our theoretical results, respectively.**

## REFERENCE

[1] J. A. Dobrowolski, *Coatings and filters*, in *Handbook of Optics*, W. G. Driscoll, eds., McGraw-Hill, New York, 1978.

[2] H. A. Macleod, *Thin-Film Optical Filters*, 2nd ed. McGraw-Hill, New York, 1989, pp.80, 118-119.

[3] A. Thelen, Design of optical interference coatings, in McGraw-Hill Optical and Electro-optical engineering series, McGraw-Hill, 1989.

[4] R. E. Collin, Theory and design of wide-band multisection quarter-wave transformers, *Proc. IRE*, vol.43, pp.179-185, 1955.

[5] Sh. A. Furman and A. V. Tikhonravov, *Basics of Optics of Multilayer Systems* (Editions Frontieres, Gif-sur-Yette, France, 1992).

[6] R. H. Clarke, "Theoretical performance of an anti-reflection coating for a diode laser amplifier, " *Int. J. Electron.,* vol.53, no. 5, pp.495-499, 1982.

[7] G. Eisenstein, "Theoretical design of single layer antireflection coatings, " *Bell Syst. Tech. J.,* vol. 63, no.2, pp.357-364, 1984.

[8] D. R. Kaplan, and P. P. Delmel, "Exact calculation of the reflection coefficient for coated optical waveguide devices," *AT&T Bell Laboratories Technical Journal,* vol.63, no.6, pp.857-877, July-Aug. 1984.

[9] C. Vassalo, "Rigorous and approximate calculations of antireflection layer parameters for travelling-wave diode laser amplifiers", *Electronics Lett.,* vol.21, no.8, Apr. 1985.

[10] T. Sitoh, T. Mukai, and O. Mikami, "Theoretical analysis and fabrication of antireflection coatings on laser-diode facets," *IEEE J. Lightwave Technol.,* vol. LT-3, pp.288-293, 1985.

[11] D. M. Braun, and R. L. Jungerman, "Broadband multiplayer antireflection coating for semiconductor laser facets," *Opt. Lett.,* vol.20, no.10, pp.1154-1156, 1995.

[12] L. I. Maissel and R. Glang, *Handbook of Thin Film Technology,* McGraw-Hill, New York, 1970, pp.11-48.

[13] D. J. Gallant, M. L. Tilton, D. J. Bossert, J. D. Barrie, and G. C. Dente, "Optimized single-layer antireflection coatings for semiconductor lasers", *IEEE Photon. Technol. Lett.,* vol.9, pp.300-302, Mar. 1997.

[14] J. Lee, T. Tanaka, S. Uchiyama, et. al, "Broadband double-layer antireflection coatings for semiconductor laser amplifiers", *Japan J. Appl. Phys.,* vol.36, pp.L52-L54, Jan.1997.

[15] J. Lee, T. Tanaka, S. Sasaki, S. Uchiyama, "Novel design procedure of broadband multilayer antireflection coatings for optical and optoelectronic devices", *IEEE J. Lightwave Technol.*, vol. LT-16, no.5, pp.884-891, 1998.

[16] J. Lee, T. Kamiya, "Improved characterization of multilayer antireflection coatings for broad-band semiconductor optical amplifiers", *IEEE J. Lightwave Technol.*, vol. LT-18, pp.2158-2166, 2000.

[17] J. Yamauchi, M. Mita, S. Aoki, and H. Nakano, "Analysis of antireflection coatings using the FD-TD method with the PML absorbing boundary condition," *IEEE Photon. Technol. Lett.*, vol.8, pp.239-241, 1996.

[18] J. Yamauchi, H. Kanbara, and H. Nakano, "Analysis of optical waveguides with high-reflection coatings using the FD-TD method," *IEEE Photon. Technol. Lett.*, vol.10, pp.11-13, 1998.

[19] P. Sewell, M. Reed, T. M. Benson, and P.C. Kendall, "Full vector analysis of two-dimensional angled and coated optical waveguide facets," *IEEE J. Quantum Electron.*, vol.33, pp.2311-2318, Dec. 1997.

[20] A.G. Sveshnikov, A.V. Tikhonravov, and M. Trubetskov, "Modern methods for synthesizing multiplayer optical coatings", *J. of Communications Technology and Electronics*, v. 45, No Suppl. 2, pp. S151-S159, 2000.

[21] J. A. Dobrowolski, D. Poitras, et al, "Towards 'perfect' antireflection coatings", in *Optical Interference Coatings*, OSA Technical Digest (Optical Society of America), pp. TuA2-1–TuA2-3, July 15-20, 2001.

# 4 High-Reflection Coatings

This chapter presents another important thin film coating applications, high-reflection (HR) optical coatings. Both TMM and finite difference time domain (FDTD) methods are employed to analyze a semiconductor laser facet reflector. The results show significant difference between FDTD and TMM, especially for TM wave incidence.

## 4.1 INTRODUCTION

High reflectors are coatings, which maximize the reflectance of an optical surface in a specified wavelength region. The optical performance outside the specified region is generally of no interest. In Chapter 1, it was mentioned that a high reflection (HR) coating can be obtained from a stack of quarter-wave dielectric layers of alternate high an low index. This is because the beams reflected from all the interfaces in the assembly are of equal phase when they reach the front surface, where they combine constructively.

These multilayer dielectric HR coatings are very useful in many applications, since mirrors made of metallic films often cause severe heating problems and large absorption loss. For conventional HR coating, the transmission matrix method (TMM) [2], [4] has been widely used to design an HR coating. However, TMM assumes a homogenous medium in the transverse direction, so that the estimated results do not necessarily agree with the experimental results.

Since the HR coating for a homogenous substrate is trivial, by alternating quarter wave optical thickness layers with low and high index will result in perfect 100% reflection. Therefore, in this chapter, we will only deal with the HR coating for a laser facet end, which makes FDTD analysis inevitable. This Chapter first based on one of the published literature [7], by using the same method and same parameters, trying to produce the same results. After that, we extend the analysis and discussions with applications on 1.55μm, since the original work only dealt with 0.8 μm application. The study with effect of core width on the reflectivity is done, both for TE and TM wave. The calculated wavelength dependence showed existence of the field propagating along the coating layers, resulting in the deterioration of reflectivity, especially for TM wave. Increasing the core layer width can increase the reflectivity with TM wave.

## 4.2  HIGH-REFLECTION COATINGS AT LASER FACET
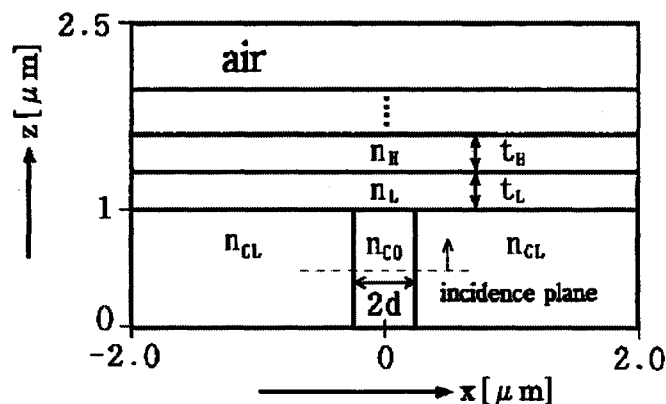
**Fig. 4-1 Configuration of an HR-coated waveguide [7].**

The structure we use for HR coating study is the same as in [7]. As shown in Fig. 4-1, a two-dimensional waveguide whose facet is coated with alternating dielectric layers. The low-index dielectric is chosen as $Al_2O_3$, which is adjacent to the facet, and Si as the high-index dielectric material, i.e. $n_L=1.7$, and $n_H=3.5$. The refractive indices of the core and cladding are chosen as $n_{co}=3.6$, $n_{cl}=3.24$, respectively.

### 4.2.1   Reflection for TE and TM mode

This part, we will re-calculate the results provided by [7]. When it has proved to have good agreement, we can move to obtain some new results.

In the Fig. 4-2 and Fig. 4-3 we calculated the steady-state field distribution for both TE and TM polarizations. The results are for a six-layer stack with parameters chosen as $2d = 0.487$ μm. For $TE_0$ mode incidence, the modal reflectance calculated is R=0.97. For TM0 mode incidence, the modal reflectance calculated is $R=0.88$, both for the wavelength of 0.8μm. The results we calculated agree perfectly with what provided from [7]. By looking at the field distributions, it can be found that there exists some power propagating along the coating layers, especially for TM wave, which results in a decreased reflectance for this polarization. It should be noted that the alternating dielectric layers on a waveguide facet could be regarded as a leaky wave structure [7], [8].
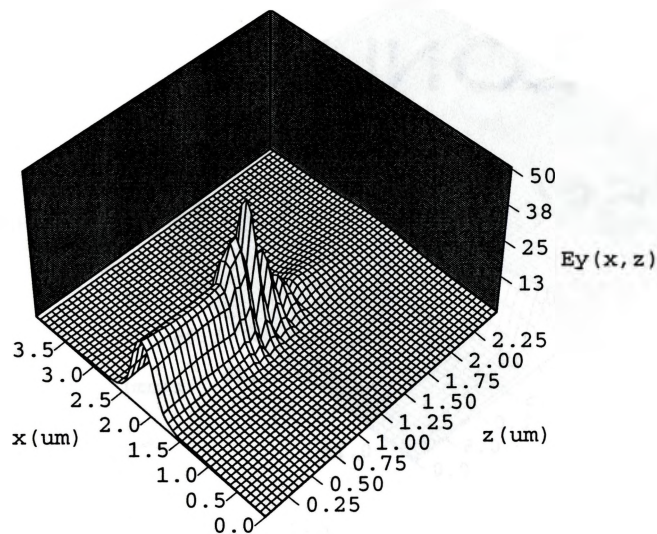
(a)
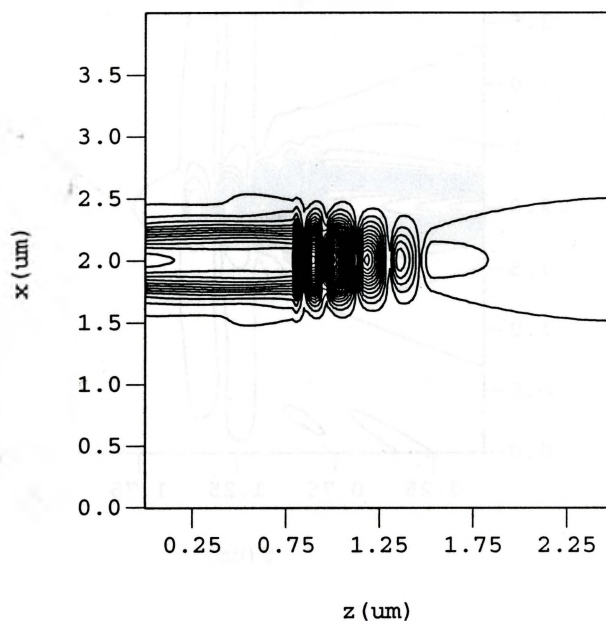


(b)

**Fig. 4-2 Steady state Ey field distributions for TE mode incidence. (a) surface plot; (b) contour view.**
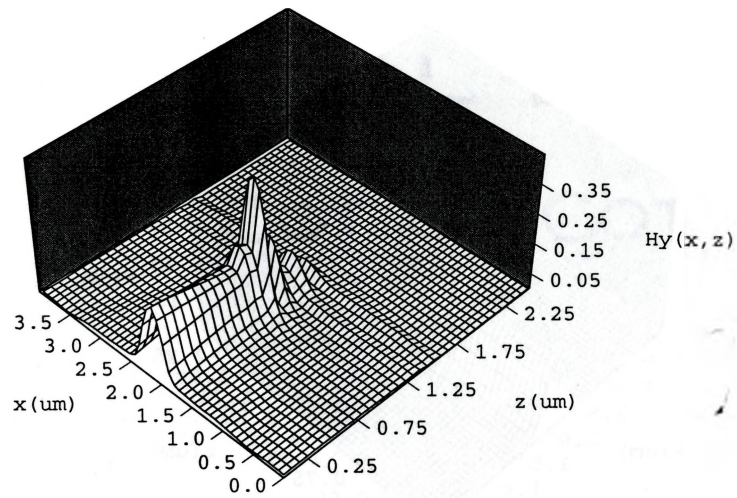
(a)
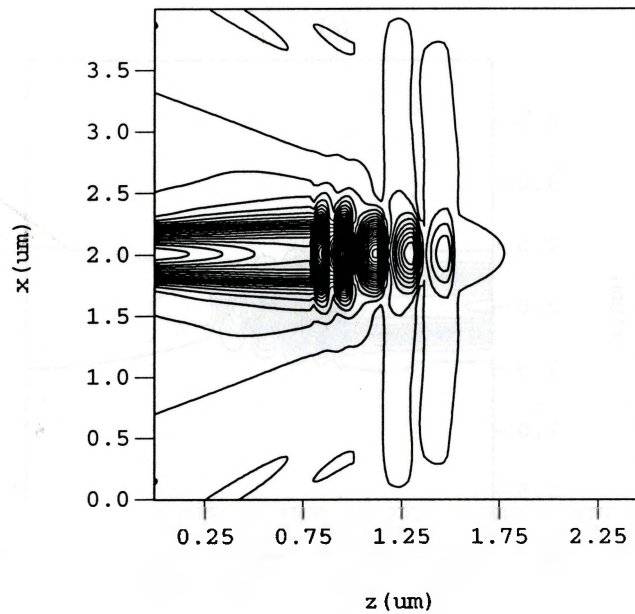


(b)

**Fig. 4-3 Steady state Hy field distributions for TM mode incidence. (a) surface plot; (b) contour view.**

### 4.2.2 Numerical Results for 1.55μm Applications

All the results calculated in [7] have chosen the operating wavelength as 0.8μm. However, in optical communication, we are more interested in the performance of the devices working at 1.55μm. The following results Fig. 4-4 to Fig. 4-6, were obtained based on a 1.55μm design, simulated by FDTD method. For a 3-groove structure, each layer is chosen to satisfy QWOT. The waveguide structure has been varied, by changing the core layer width from the original value 0.487μm to a thinner value 0.30μm and a wider value 1.2μm. Field distributions are depicted in Fig. 4-4 and Fig. 4-5.



(a)                                                      (b)
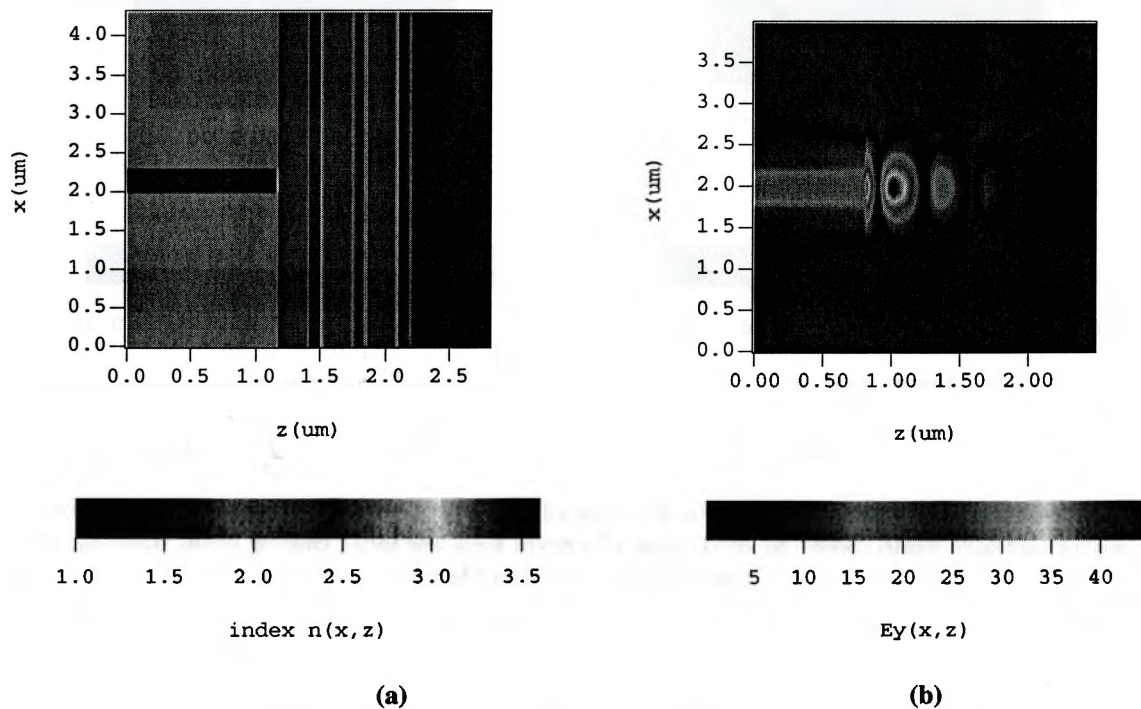
**Fig. 4-4  (a) Refractive index distribution (b) steady state Ey field distribution of the structure, waveguide core width chosen as *2d*=0.3μm, 6 layers of high-low index coating films, *R*=0.925, TE wave, *N*ₑ𝒻𝒻 = 3.40, λ=1.55μm.**

For the first case in Fig. 4-4, the reflectivity is only 0.925 with TE mode polarization. The scheme of thin active layer waveguide will decrease the reflectivity can be understood with the aid of antireflection (AR) coating design in the previous Chapter, where the radiation mode component becomes larger for this waveguide structure.
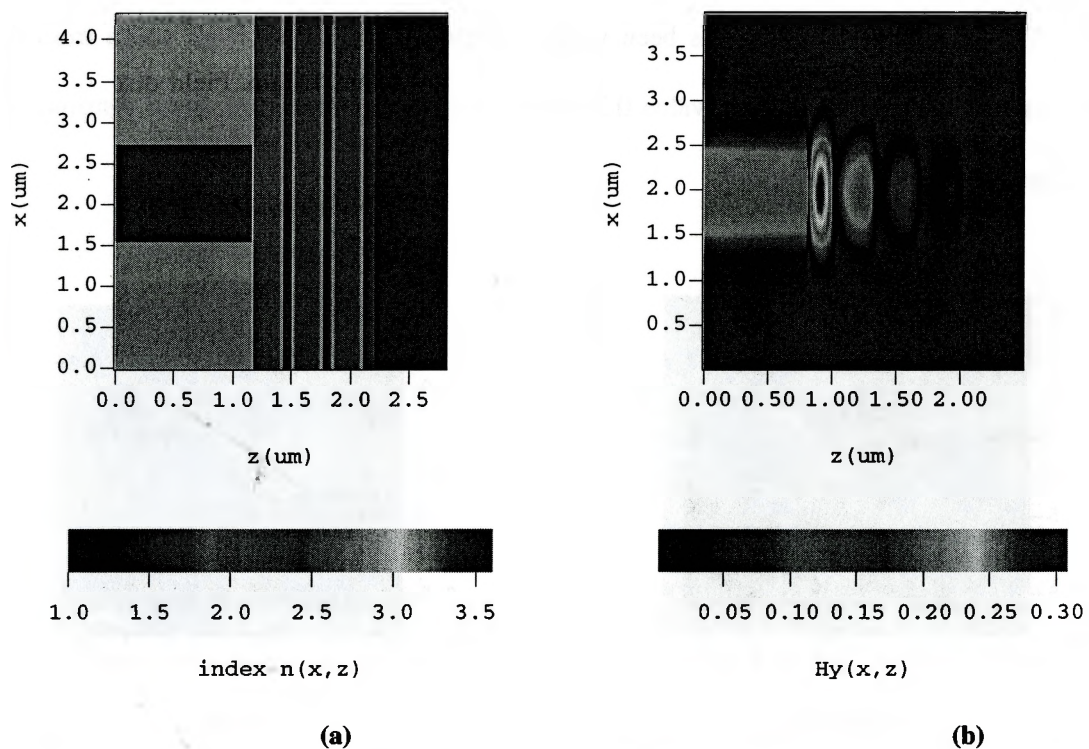


**Fig. 4-5 (a) Refractive index distribution (b) steady state Hy field distribution of the structure , waveguide core width chosen as 2d=1.2μm, 6 layers of high-low index coating films, R=0.936, TM wave, $N_{eff}$ = 3.56, λ=1.55μm.**

For the second case in the reflectivity with TM mode is increased from 0.88 to 0.936 by increasing the core width from 0.487μm to 1.2μm. It has been proved that with the increasing of

core layer width, both TE and TM results will converge with TMM results and approaches to 1.0

for HR design [7] Here, we observed the same phenomena with the 1.55μm operation.

Final consideration is given to the wavelength dependence of reflectivity. Fig. 4-6 shows

the results for a six-layer stack with 2d=0.487μm. Each coating thickness is fixed to be a QWOT

at λ=1.55μm. The TE wave exhibits high reflectivities over a wide spectral range from 0.7 to 1.0

μm, showing good agreement with the TMM results. It should be noted that the alternating

dielectric layers on a waveguide facet can be regarded as a leaky wave structure [8], so that the

field propagating along the coating layers tends to decay as it propagates. Furthermore, the

reflected field from the coating involves radiation modes, particularly for the TM waves. The low

reflectivity in the TM waves can be explained by these observations.
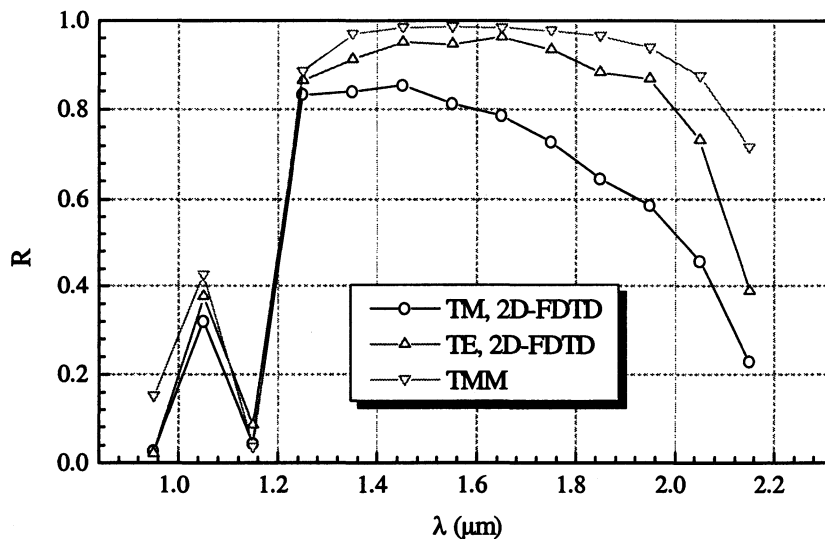


**Fig. 4-6 Modal reflectance wavelength dependence for a 3 LH stack, (6 layer) structures.**

**REFERENCE**

[1]    S. Ramo, J. R. Whinnery, and T. van Duzer, *Fields and Waves in Communication Electronics*, John Wiley, New York, 1984.

[2]    H. A. Macleod, *Thin-Film Optical Filters*, 1st ed. (1982), 2nd ed. (1985), 3rd ed. (2001), Chap. 1-4, McGraw-Hill, New York.

[3]    A. Thelen, *Design of Optical Interference Coatings*, McGraw-Hill Optical and Electro-Optical Engineering Series, Chap. 1-5, McGraw-Hill, 1989.

[4]    P. Yeh, *Optical Waves in Layered Media*, John Wiley, New York, 1988.

[5]    S. T. Chu and S. K. Chaudhuri, "A finite difference time-domain method for the design and analysis of guide-wave optical structures," *IEEE J. Lightwave Technol.*, vol.7, pp.2033-2038, 1989.

[6]    J. P. Berenger, "A perfectly matched layer for the absorption of electromagnetic waves," *J. Comput. Phys.*, vol.114, pp.185-200, 1994.

[7]    J. Yamauchi, H. Kanbara, and H. Nakano, "Analysis of optical waveguides with high-reflection coatings using the FD-TD method," *IEEE Photon. Technol. Lett.*, vol.10, pp.11-13, 1998.

[8]    M. Miyagi, *Introduction to Optical Fiber Transmission*. Tokyo, Japan; Shokodo,1991.

# 5  Deep-etched Antireflective Waveguide Gratings

## 5.1 INTRODUCTION

The term optoelectronic integrated circuit (OEIC) refers to the integration of optoelectronics devices, such as sources and detectors, which electronic devices such as transistors are also included. Photonic integrated circuits (PICs) are a subset of OEICs focusing on the single-substrate or monolithic integration of *optically interconnected* guided-wave optoelectronic devices [1]-[4],[70].

The driving force for PICs is the expected complexity of next-generation optical communication links, networking architectures, and even possibly switching systems. The wavelength division multiplexing (WDM) scheme [5], as well as high-speed time division multiplexing (TDM), involve a great variety of optically cascaded sources, modulators, filters, amplifiers, switches, detectors, etc. A large component of the cost of such architectures is due to the single-mode optical connections between the guided-wave components. Such devices normally provide optimized performance with tightly confined waveguides, resulting in difficult submicrometer alignment tolerances when coupling to single-mode optical fibers [3]. By replacing such individually aligned connections with lithographically produced waveguides, PICs offer the promise of cost reduction, dramatically reduced size, and increased robustness [3], [70].

The replacing of conventional coating at the semiconductor laser waveguide end to form a distributed Bragg reflector (DBR) instead of a high-reflection (HR) coating has been proven to be successful, although this research has only started for a few years [74]- [79]. The advantage of large semiconductor/air refractive index contrast has been utilized to achieve a high-reflection mirror with much fewer grating period and significant cost reduction. This deep-etched waveguide grating structure in the application of semiconductor/air Bragg reflector (SABAR) provides a solution of manufacturing arrays of lasers on-chip based on a full-wafer technology.

As we have discussed in Chapter 1 and 3, another important coating application, anti-reflection coating is always considered as a crucial component for building semiconductor travelling wave amplifiers (TWA). Large amount of research work have been dedicated to accurate analysis and design of antireflection coating for a laser diode structure [29]-[29]. Fabricating high-performance antireflection (AR) requires *in-situ* monitoring and enough practical experiences [5], [17]. The charm of PICs has enlightened a lot of researchers to come up with new structures that are easy for monolithic integration. Successful theoretical design and manufacture of SABAR is a good example.

In this chapter, we are attempting to analyze the feasibility of designing a deep-etched waveguide grating structure for AR application, by varying groove widths or the overall etching profile. The theoretical design results shown in this chapter can prove preliminarily that this idea is feasible and has the hope of being employed by PICs in the future [80].

This chapter first tried to obtain an equivalent 1D homogenous structure in order to use what has been available in thin film dielectric antireflection (AR) coating simulation and design. The plane wave transmission matrix method (TMM) has been employed to simulate semiconductor/air-grating structure. The design strategies have also been applied to obtain maximally flat and low reflection spectrum. The design procedure started from one etching groove structure and then extend to structures with more etching grooves for the purpose of widening the bandwidth. After certain

numerical refinement, for a 3-groove structure, the results obtained by TMM show a 60 nm and 90

nm bandwidth with the reflection less than $1 \times 10^{-3}$ for a 2-groove structure and 3-groove structure, are

achieved accordingly. The further full wave verification is done by 2D finite difference time domain

(FDTD) method [23]-[27] , together with the effective index method (EIM)[21],[22] in order to

consider the 2D-cross-section of the waveguide, as well as decreasing one dimension of computation

effort). Results show that 40nm is achieved for 2-groove etching structure, with the reflectivity less

than $10^{-3}$.


## 5.2 SOA STRUCTURE WITH DEEP-ETCHED WAVEGUIDE GRATING

The structure chosen for our analysis is depicted in Fig. 5-1. The semiconductor optical

amplifier (SOA) was fabricated from expitaxial material with an $In_{1-x}Ga_xAs_{1-y}P_y$-InP waveguide,

and InGaAsP as an active layer. The physical and geometric parameters are listed in Table 1. An

N doped InP buffer layer is grown on the InP substrate in (8). The active layer (5) is sandwiched

between an upper and bottom layer shown as (4) and (6). In order to obtain polarization

insensitive gain media, a tensile stress has been applied to the middle layer. The InP cladding

layer on above is etched as shown in (2). The ridge structure which is symbolized with W, has

the typical dimension of 2~3 μm. In the following calculations, this parameter is chosen as 2μm.

The semiconductor optical amplifier with deep-etched waveguide grating as antireflection

element is schematically shown in Fig. 5-2. By etching the waveguide with a depth of $H$, the

semiconductor/air grating is formed. The groove width is depicted as $d_L$ and the semiconductor layer

is $d_H$. Similar structure has been employed in fabricating a distributed Bragg reflector (DBR) with the

laser resonator[74]-[79]. When this structure was used as a reflector, the dimensions for $d_L$ and $d_H$ are

normally required as odd number of quarter wave optical thickness (QWOT), such as $\lambda_0/4$ for the

air groove layer, and $3\lambda_0/4$ or $5\lambda_0/4$ for the semiconductor layer [78], [79]. By using a few

number of grating periods, (typically around 3, [79]), the reflection over 90% is achieved. For our

problem in this Chapter, the parameters that we can vary limited to $d_L$, $d_H$ and grating numbers Np. It

has to be noted that $d_L$ and $d_H$ are not fully independent. Based on the knowledge we have gained

from antireflection coating design in Chapter 3, when the coating indices are not chosen as optimum

(from Schuster diagram, here $n_1$ and $n_2$ are chosen as 1.0 and $N_{eff}$, typically 3.2), the QWOT rule will

not apply to the optimum $d_L$ and $d_H$. Meanwhile, we are expecting to see a narrower bandwidth for

our structure compared with optimized double-layer AR coating, according to our discussions on

optimum coating indices for broadband AR coatings in Chapter 3. However, one fact that has to be

kept in mind is that the huge cost-effective benefit is gained through this integration-compatible deep-

etching technology. As long as the low reflectivity ($<10^{-4}$) is achieved at single wavelength, the

bandwidth is expected to be broadened by increasing the grating period, similar to what happened in

antireflection coating design with increasing coating layers. It has to be noted that increasing the

number of etching grooves will not increase fabrication cost, which is another important feature

compared to thin film dielectric multilayer coatings, where the case is that the cost is increased

significantly with the number of coating layers.
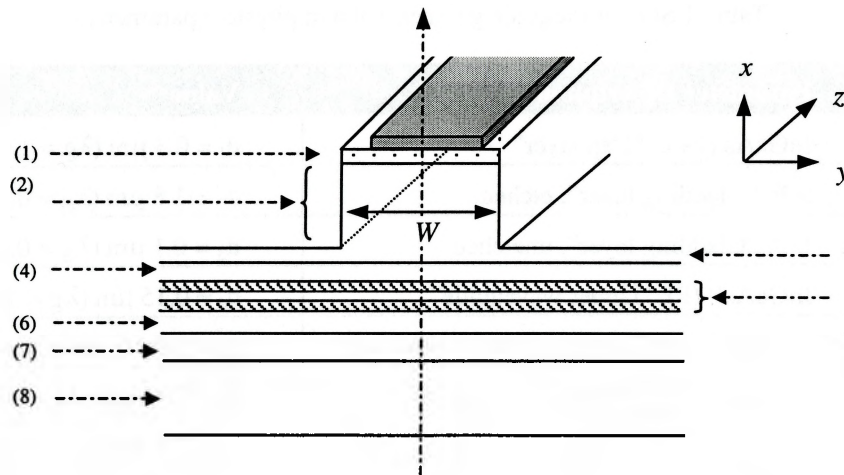
**Fig. 5-1 Cross-section schematic diagram of a semiconductor optical amplifier waveguide structure**
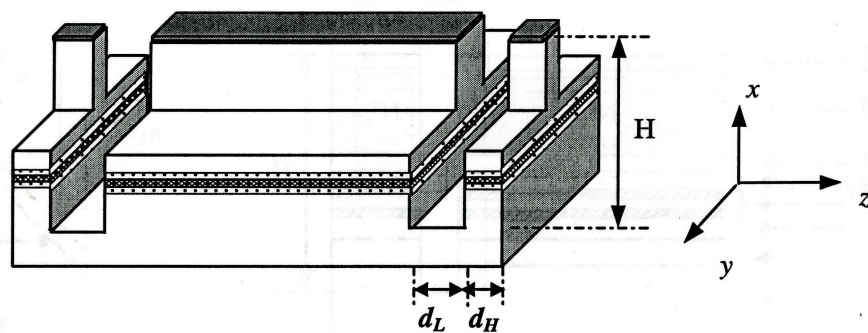


**Fig. 5-2 Three-dimensional schematic view of a semiconductor optical amplifier waveguide with deep-etched antireflective waveguide gratings**

Table 1 SOA waveguide geometrical and physical parameters

| | Parameter Description | Value |
|---|---|---|
| (1) | InGaAs (P+), "Cap layer" | $d_1 = 0.3$ μm ($\lambda g = 1.67$μm) |
| (2) | InP, "Cladding layer", etched | $d_2 = 1.8$ μm ($\lambda g = 0.9185$μm) |
| (3) | InP, "Cladding layer", unetched | $d_3 = 0.1$ μm ($\lambda g = 0.9185$μm) |
| (4) | InGaAsP (P), "Upper waveguide" | $d_4 = 0.15$ μm ($\lambda g = 1.24$ μm) |
| (5) | InGaAsP (tensile strained and unstrained) | $d_5 = 3 \times 0.05$ μm ($\lambda g = 1.55$ μm) |
| (6) | InGaAsP (N), "Bottom waveguide" | $d_6 = 0.15$ μm ($\lambda g = 1.24$ μm) |
| (7) | InP (N), "Buffer layer" | $d_7 = 2.0$ μm ($\lambda g = 0.9185$ μm) |
| (8) | InP (N), "Substrate layer" | $d_8 = 90.0$ μm |
| W | Ridge width | 2.0 μm |
| H | Antireflection Etching depth | 0~3.0μm |
| $d_L$ | Groove width | To be designed |
| $d_H$ | End waveguide width | To be designed |
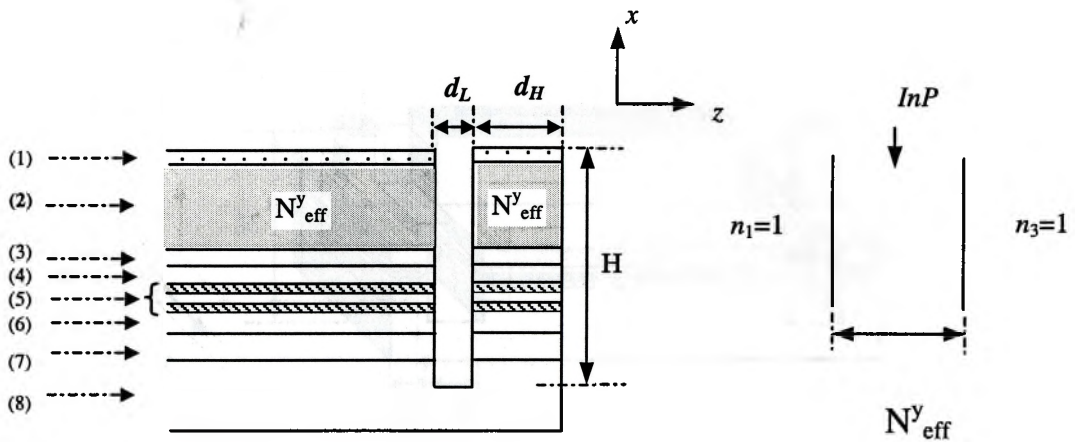


**Fig. 5-3 Equivalent Slab waveguide obtained by EIM. for the ridge waveguide structure shown in the previous figure.**

The refractive index for each material layer can be calculated through Henry's model [18].

Before we carry on any calculations of the SOA structure, the mode has to be determined in advance.

For the two-dimensional waveguide illustrated in Fig. 5-1, there are three ways of obtaining the effective index of the fundamental mode, which are 2-dimensional finite difference (FD) method [20], effective index method (EIM) [21][22] and 1-D sideview slab waveguide mode, as discussed in Chapter 2. For our 2-dimensional analysis, EIM is employed for obtaining the incident slab mode. Table 2 listed the comparisons of effective index obtained by these three ways, the results in the first column is obtained by 1D slab mode calculation [19][20], without considering any lateral ridge confinement. The results in the second column is obtained by using EIM in the lateral $y$ direction first to get an equivalent 1D slab waveguide (see Fig. 5-3), then use 1D mode solver to get the mode. This procedure can be viewed as a quasi-2D mode analysis. The last column is the results by 2D FD, which is considered the most accurate solution among these three. The comparison shows the EIM combined with 1D can approach the exact solution in a further way than the direct 1D mode analysis. The resulting 2D-FDTD is expected to achieve a better precision compared to 1D-slab mode combined with 2D FDTD, by partially considering the lateral confinement of the waveguide mode.

Table 2 List of the effective index calculated by different approaches

|  | 1D slab | EIM +1D | 2D xy-FD |
|---|---|---|---|
| $N_{eff1}$ (Quasi-TE$_{00}$, E$_y$) | 3.3118 | 3.3092 | 3.3046 |
| $N_{eff2}$ (Quasi-TM$_{00}$, H$_y$) | 3.2972 | 3.2934 | 3.2875 |

The equivalent slab waveguide has been illustrated in Fig. 5-3, notice that, after employing the EIM, the layer (2) (bold symbol) is no longer the refractive index of InP (3.17 at 1.55μm), but some modal effective index of a three layer slab waveguide (3.14 at 1.55). Therefore, the effect of the finite width ridge confinement can be considered to some extent. From Table 2, it can also be shown this effect can improve its accuracy of obtaining the effective index of the 2D cross-section waveguide illustrated in Fig. 5-1.

## 5.3 AR DESIGN BY TMM

Similarly to the AR coating design procedure we applied in Chapter 3, the simplest 1D plane wave Transmission matrix method (TMM) is employed first. Although TMM is not considered sufficiently accurate for analyzing the deep-etched waveguide structure, its analytical and computationally efficient nature has provided great convenience for AR design, especially for the case that no previous references could be found for our problem. The plane wave assumption requires us to get an equivalent 1D homogeneous layer stack for the 3D structure shown in Fig. 5-2, for the purpose of evaluating its reflectance by TMM. The substrate layer of this stack is chosen as the modal effective index of the 2D waveguide $N_{eff}$, which has been already obtained in Table 2. Same refractive index will also work as the high index layer, or mathematically, $n_s = n_H = N_{eff}$.

The refractive index of the low index layer (etching groove) can be calculated through the following equations by variational method shown in eq. (5.3-1), and the results are shown in Fig. 5-4. It can be seen that after the etching is deep enough to reach some threshold value $H_0$ (typically 3.4μm), the equivalent index of this etching groove layer will work the same way as an air gap, which mathematically means $n_L \approx 1.0$, when $H > H_0 \approx 3.4 \mu m$.

$$n_L^{TE} = \left( \frac{\int_0^\infty n^2(x,H)E_{y0}^2(x)dx}{\int_0^\infty E_y^2(x)dx} \right)^{1/2}, \qquad n_L^{TM} = \left( \frac{\int_0^\infty n^2(x,H)H_{y0}^2(x)dx}{\int_0^\infty H_y^2(x)dx} \right)^{1/2} \quad (5.3-1)$$

The following part will study several structures, starting from one etching groove structure, and then extended to structures with 2 or more etching grooves. The antireflection is obtained both by TMM and FDTD.
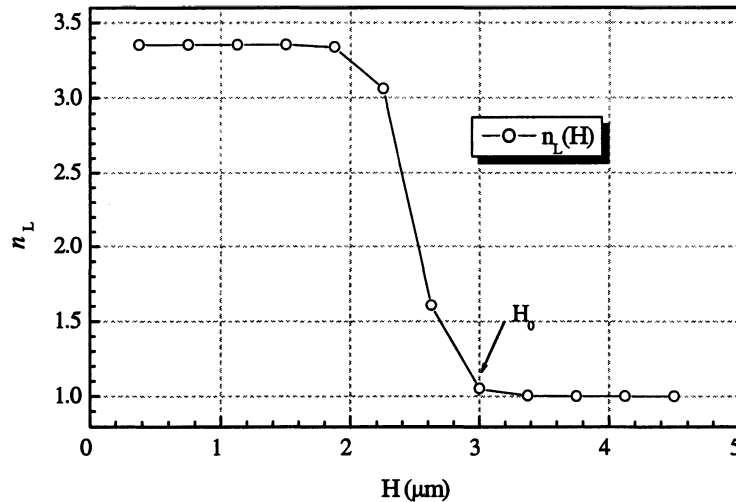


**Fig. 5-4 Equivalent index of the etching groove layer as a function of the etching depth H.**

## 5.3.1   One Etching Groove structure

### 5.3.1.1   Model illustration

The plane wave model for this 1-groove structure is illustrated in Fig. 5-5, it is easy to see that this structure is very similar to the double-layer thin film stack, therefore, the theory with double-layer AR coating can be employed in our analysis with this model directly. The important feature is the refractive index of the second "coating layer" is fixed as $n_H = N_{eff}$ in this case. The first "coating" layer can vary continuously with etching depth H as shown in Fig. 5-4. However, due to the large electromagnetic radiations from the air/semiconductor boundary, it can be understood that the plane wave model will not be valid for the middle range of etching. In other words, only the low end of Fig. 5-4 can be equivalent to a homogenous media. A more practical way of varying $n_L$ can be

implemented by filling stable materials into the deep-etched air groove. This situation has been

considered in the one-groove structure design.
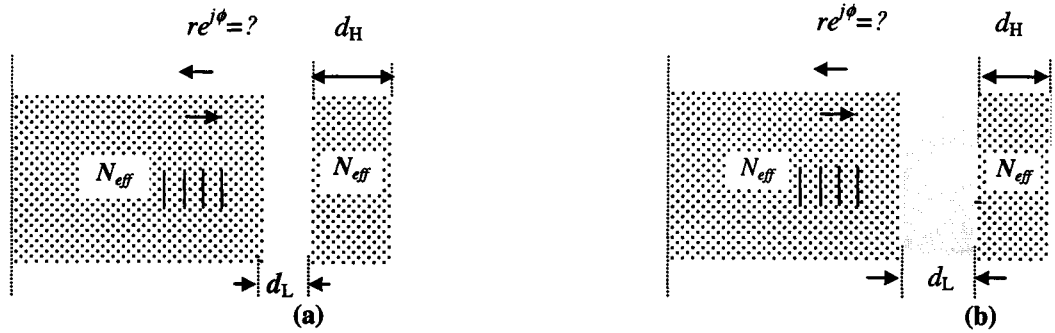


**Fig. 5-5 Illustration of equivalent 1D plane wave model with one etching groove structure; (a) completely etching the waveguide, similar to form a distributed Bragg reflector; (b) the model for the structure of filling materials after deep etching.**

### 5.3.1.2   Analytical solutions

By employing the 1D plane wave analytical TMM discussed in Chapter 2, and note the

fact that $n_2 = n_s = N_{eff}$, the transmittance of a substrate with two layer coating can be written as

$$T = 4n_0 n_s \left\{ 4n_0 n_s + \left[ (n_0 - n_s) \cos\phi_1 \cos\phi_2 - (n_0 n_1/n_s - n_s^2/n_1) \sin\phi_1 \sin\phi_2 \right]^2 + \left[ (n_s - n_0) \sin\phi_2 \cos\phi_1 + (n_1 - n_0 n_s/n_1) s \cos\phi_2 \sin\phi_1 \right]^2 \right\}^{-1}$$  (5.3-2)

In order to get $R(\lambda_0) = 0$, or $T(\lambda_0) = 1$, the solutions are

$$tg\phi_1 tg\phi_2 = \frac{n_0 - n_s}{n_0 n_1/n_s - n_s^2/n_1}, \text{ and } \frac{tg\phi_1}{tg\phi_2} = \frac{n_0 - n_s}{n_0 n_1/n_s - n_s^2/n_1}$$

where

$$\phi_1 = 2\pi n_1 d_L/\lambda_0, \text{ and } \phi_2 = 2\pi n_2 d_H/\lambda_0$$

and

$$n_s = N_{eff}, \text{ and } n_0 = 1.0$$  (5.3-3)

Finally we can solve $d_L$ and $d_H$ from the above equations. For the power reflectivity R

becomes zero at 1.55μm, $d_L$ and $d_H$ can be calculated analytically as 0.107μm and 0.286μm,

respectively. Fig. 5-6 gives the numerical solution for the optimum index for achieving AR. It

shows the minimum reflection $R_{min}$ at single wavelength (1.55μm) varying as a function of n1.

The results show that, in order to obtain small enough reflection ($<10^{-6}$) at one single wavelength,

the refractive index of this etching layer has to be chosen from 1.0 to $(n_s)^{1/2}$ or greater than $(n_s)^{3/2}$ .

One thing, which is worth mentioning, is that Fig. 5-6 is actually a one-dimension representation

of the Schuster diagram discussed in Chapter 3. It gives a special solution for the condition

that $n_2 = n_s = N_{eff}$ .
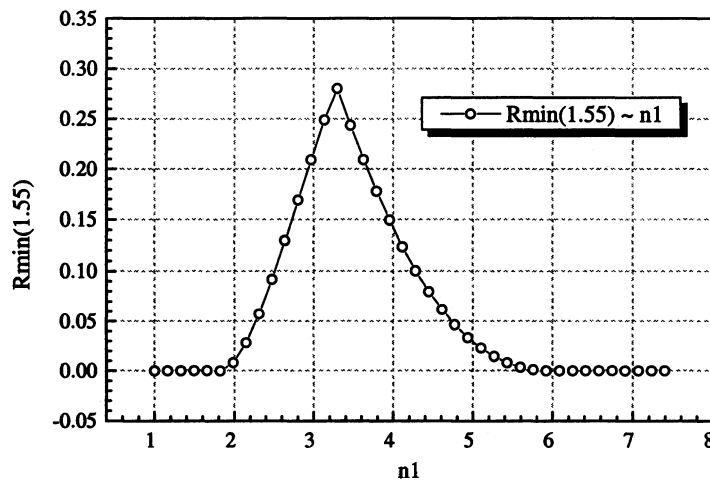


**Fig. 5-6 The minimum reflectivity as a function of optimum index of the etching layer.**

### 5.3.1.3    Design examples

Fig. 5-7 shows the design results for the one etching groove structure analyzed by the

above model, with different filling materials. The parameters $d_L$ and $d_H$ have been optimized in

advance both analytically and numerically. For the etching without filling material, the result is solved numerically as $d_{L1}$=0.107μm, $d_{H1}$=0.268μm ($n_{L1}$=1.0, open circle), or expressed in conventional thin film coating design representations as Ns|0.282L|0.211H|1.0, where $L$ and $H$ stand for the quarter wavelength optical thickness (QWOT) for the low (1.0) and high ($n_s$) index layers. This results accord with the ones we obtained previously by analytical method. For a $SiO_2$ filling structure, the design result are $d_{L2}$=0.129μm, $d_{H2}$=0.260μm ($n_{L2}$=1.46, up triangle), or similarly expressed as Ns|0.228L|0.204H|1.0, where L and H stand for the QWOT for the low (1.46) and high (Ns) index layers. As for the third example, the results are $d_{L3}$=0.169μm, $d_{H3}$=0.248μm ($n_{L3}$=1.75, down triangle), or represented in an alternative way as Ns|0.249L|0.195H|1.0. It is to be noted that although the three curves are obtained by different combinations of $d_L$ and $d_H$, the ultimate performance of wavelength dependence is almost the same, and can not be distinguished. The main reason is, for this one-groove structure, the degree of freedom is only one, there's no more room of manoeuvre. This situation is very similar to what we have experienced with the single layer antireflection coatings in Chapter 3, where the refractive index of this single film is the only parameter to be varied. The bandwidth with obtaining a zero reflectivity at centre wavelength is uniquely determined.

Therefore, the similar situation with bandwidth limitation enlightens us to investigate structures with more than one etching groove. We are expecting this multi-groove structure will also bring the same broadening benefit as what a double-layer AR coating does. Another worth-noticing fact is that the bandwidth for the reflectance lower than $10^{-3}$ is only around 20nm, it is much narrower compared to the single and double layer AR coating structures in Chapter 3. This result is reasonable due the fact that we lost the degree of freedom, which was gained double-layer AR coating, since the high-index is fixed as $N_{eff}$. And this makes the design away from the optimum design from the bandwidth point of view.
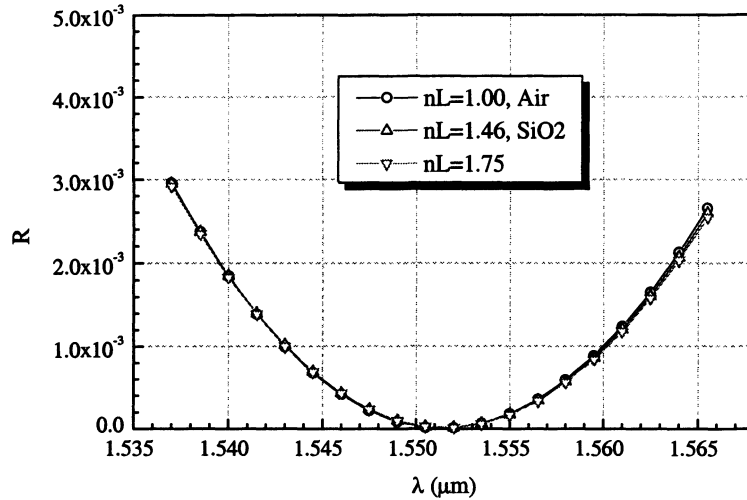
**Fig. 5-7 Wavelength dependence of the designed one etching groove structure with different choices of $n_L$, simulated by TMM, $R$ (1.55μm)=6.911×10$^{-7}$.**

## 5.3.2 Two-Groove Deeply Etching

### 5.3.2.1 Model illustration

The plane wave model for this two-groove structure is illustrated in Fig. 5-8, it has two etching grooves with the indices as $n_L$ and thickness as $d_{L1}$ and $d_{L2}$, respectively. For the high index layer, the refractive indices are both $N_{eff}$, the thicknesses are $d_{H1}$ and $d_{H2}$, respectively. Based on a homogenous layer assumption for the waveguide layers, this structure shown in Fig. 5-8 can therefore be analyzed the same as multiple layer of coatings by TMM. We give a few design examples for this two-groove structure with this plane wave model.

### 5.3.2.2 Design Examples

The structure is simulated in TMM, and the refining method is used in order to obtain an ideal design for antireflection application, based on manipulating all the adjustable parameters.
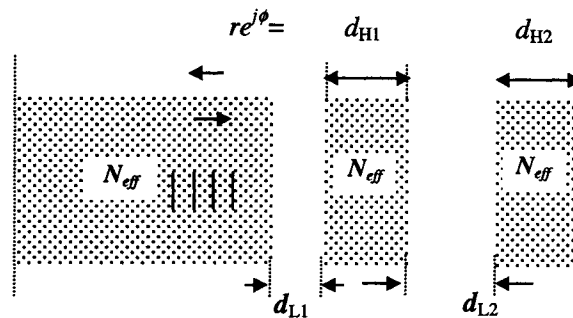
**Fig. 5-8 Illustration for two etching groove structure to be simulated by 1D TMM**

1)    CASE I: Single Wavelength R=0, Bandwidth (R<$10^{-3}$) = 25nm.
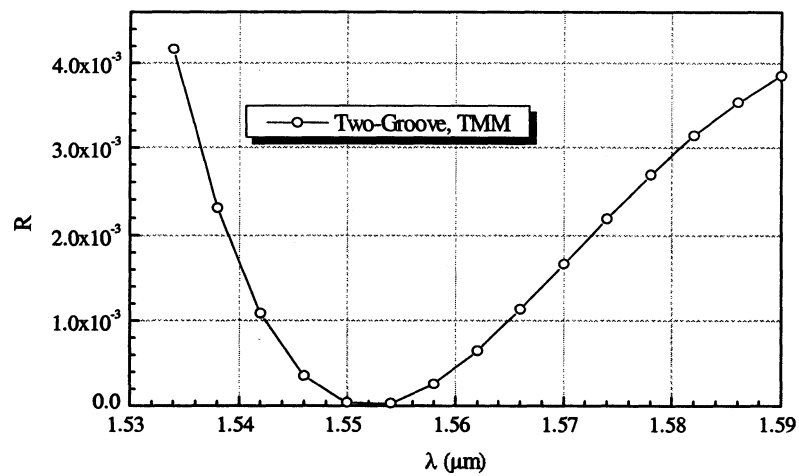


**Fig. 5-9 Reflectance of one design example after refining, $d_{L1}$=119.74nm, $d_{H1}$ = 271.20nm, $d_{L2}$ =419.31nm, $d_{H2}$ = 241.64nm, $R$ (1.55μm) = 7.2×$10^{-8}$.**

2)    CASE II: Bandwidth (R<$10^{-3}$) = 65 nm, flat, and 3.0 ×$10^{-4}$ at 1.55μm
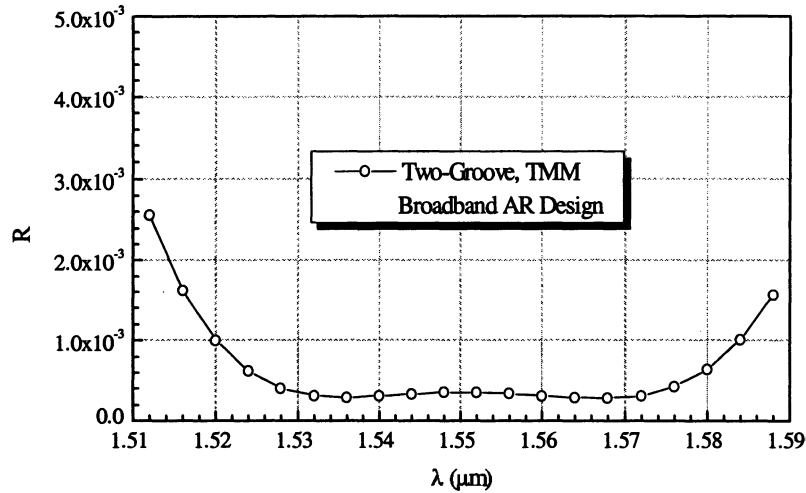
**Fig. 5-10 Reflectance wavelength dependence of one design example for the two etching groove structure with parameters chosen as $d_{L1}$=0.111µm, $d_{H1}$=0.267µm, $d_{L2}$=0.409µm, $d_{H2}$=0.235µm, the reflectivity at centre wavelength $R$ (1.55µm)=3.54×10$^{-4}$.**

Fig. 5-9 gives a design example after refining method is employed, for the case that the reflectance at single wavelength (1.55µm) is extremely low, which is in the order of 10$^{-8}$. However, the bandwidth for the reflectance lower than 10$^{-3}$ is only around 25nm, not much improvement compared to a single etching groove structure shown in Fig. 5-7.

What shows in Fig. 5-10 is another example for the case that the reflectance at single wavelength (1.55µm) is not zero, but the design can maintain a low reflectivity over a wider bandwidth (65nm for R<10$^{-3}$), for the broadband design requirement, this is a better design than the previous one. The design results obtained here in plane wave model combined with refining method will work as the initial design for our design in the second step by FDTD method.

### 5.3.3    Three-Groove Deeply Etching Structure

#### 5.3.3.1    Model Illustration

By adding one more grooves, we form the structure with three grooves as depicted in Fig. 5-11. One more degree of freedom is gained accordingly. The bandwidth is expected to be wider than what we have obtained for two-groove structure (65nm). Using the same refining design procedure, the design examples for different cased are shown in Fig. 5-12 - Fig. 5-13
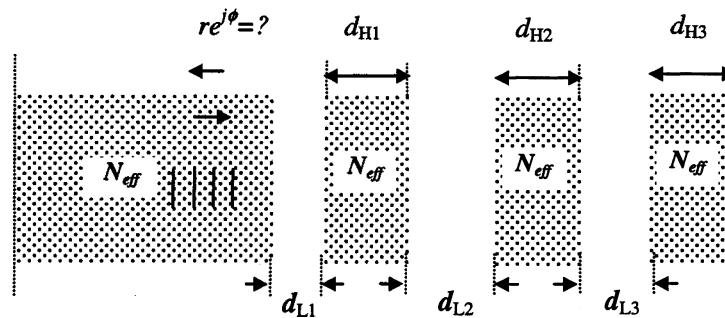


**Fig. 5-11 Model illustration for three etching groove structure to be simulated by TMM**

Fig. 5-12 gives a design example for the case that the reflectance at single wavelength (1.55μm) is almost zero, which is numerically obtained as $1.2 \times 10^{-8}$. However, the bandwidth for the reflectance lower than $10^{-3}$ is limited at only 12nm, which is an even worse situation compared to a single etching groove structure shown in Fig. 5-7 or two-etching groove structure in Fig. 5-9. This tells us if the design target is to ensure zero reflectivity of single wavelength, there's no need to use structures with more than one etching groove.

What shows in Fig. 5-13 is another example for the case that the reflectance at single wavelength (1.55μm) is not zero, but the design can maintain a low reflectivity over a much wider bandwidth (100nm for $R<10^{-3}$), for the broadband design requirement, this is a better design than the previous the last one. The improvement of the spectrum shape provided by

employing multiple etching layers can be understood similarly as what a multi-cavity can improve the spectrum shape of a thin film multilayer filter. Again more layers can form more resonance peaks (wells), by designing them to be aligned properly, the spectrum shape can vary at will. This is the basic idea of applying thin film synthesis.

1)    Case I: Single Wavelength Zero Reflection, $R \sim 1.2 \times 10^{-8}$ at 1.55μm, but bandwidth <15nm for the criteria of ($R < 10^{-3}$).
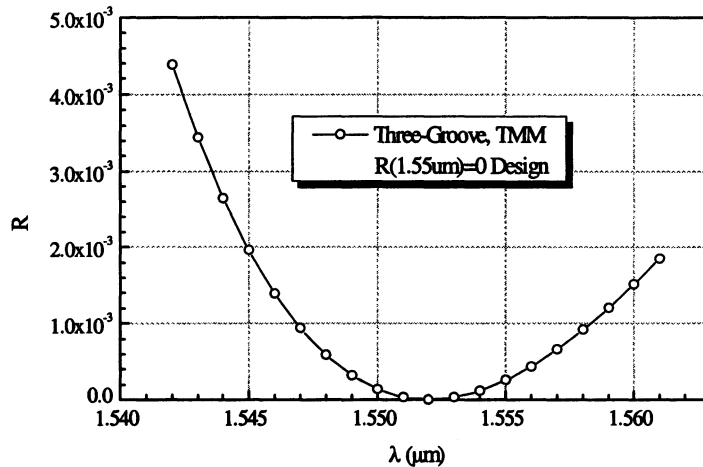


**Fig. 5-12 Reflectance wavelength dependence of one design example of the three etching groove structure with parameters chosen as ($d_{L1}$=0.108μm, $d_{H1}$ = 0.317μm, $d_{L2}$ =0.142μm, $d_{H2}$ = 0.336μm, $d_{L3}$=0.169μm, $d_{H3}$=0.276μm), the reflectance at centre wavelength R (1.55μm)= $1.2 \times 10^{-8}$.**

2)    CASE II: 100 nm Bandwidth ($1.0 \times 10^{-3}$), $R \sim 3.0 \times 10^{-4}$ at 1.55μm
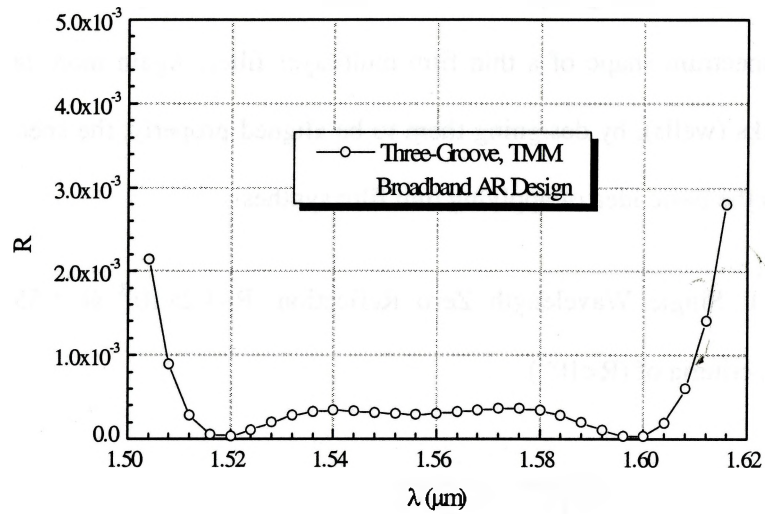
**Fig. 5-13 Reflectance wavelength dependence of one design example for the three etching groove structure with parameters chosen as** $(d_{L1}=0.110\mu m, d_{H1} = 0.267\mu m, d_{L2}=0.431\mu m, d_{H2} = 0.472\mu m,$ $d_{L3}=0.374\mu m, d_{H3}=0.238\mu m)$**, the reflectivity at centre wavelength R** $(1.55\mu m)= 3.2\times10^{-4}$**, the bandwidth for** $R<10^{-3}$ **is 100nm.**
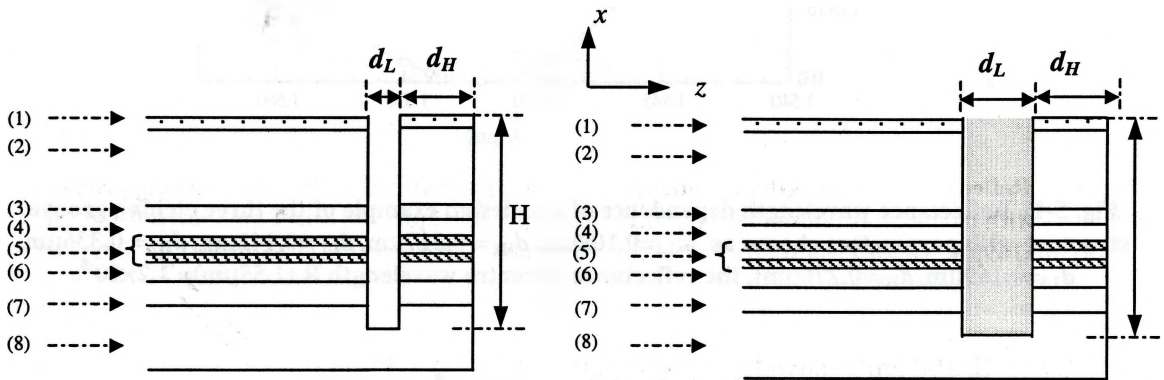


**Fig. 5-14 Schematic diagram of one groove structure simulated by FDTD method**

(a)



(b)



(c)
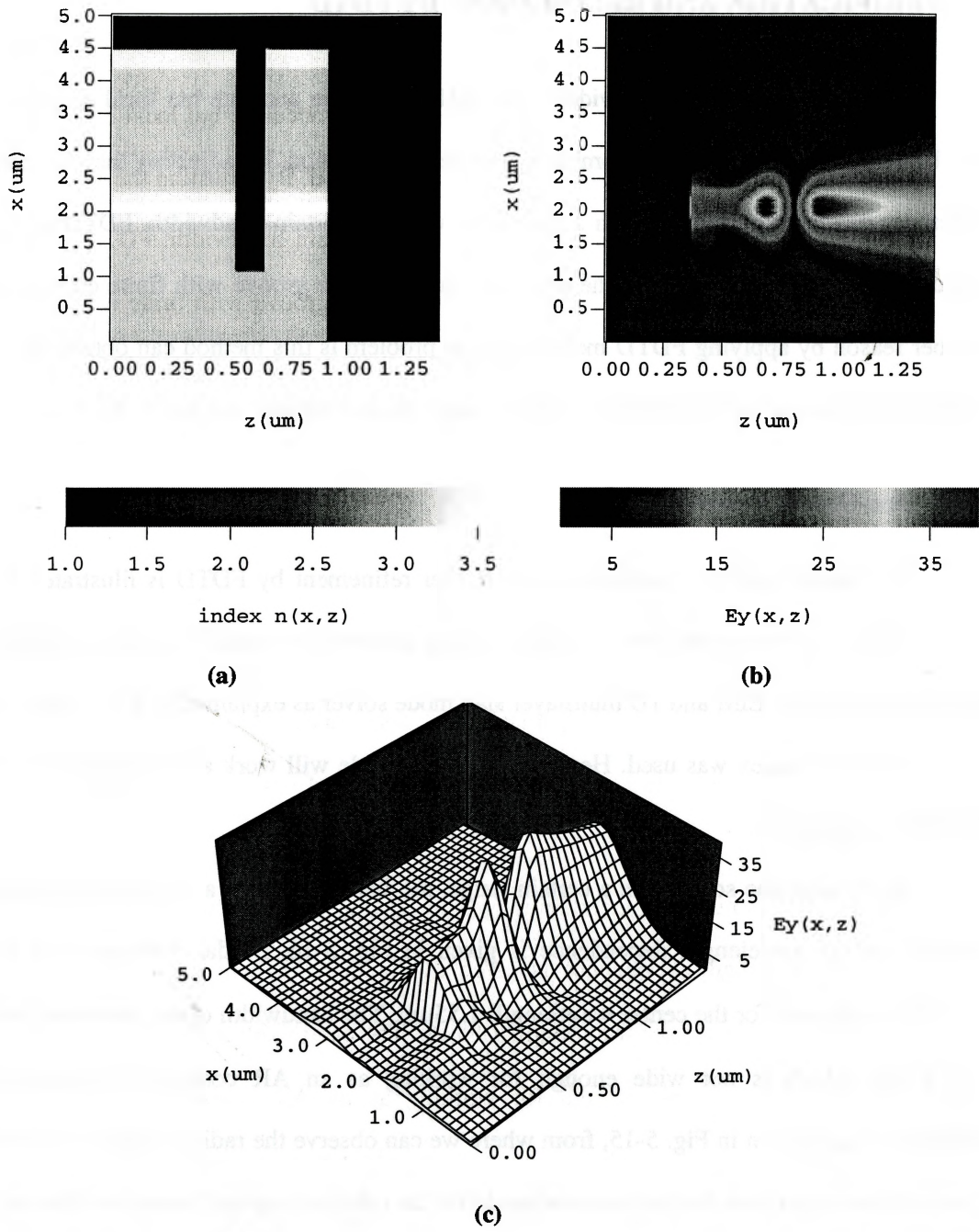
**Fig. 5-15 Steady state Ey field distribution for the waveguide with one design example of one etching groove at one end. (a) Refractive index distribution; (b)Field distribution in color plot; (c) Field distribution in surface plot. The parameters are chosen as $d_L$=0.116µm, $d_H$=0.272µm**

## 5.4 VERIFICATION AND REFINEMENT BY FDTD

From the initial design provided with TMM, the more accurate but local design can be done by using FDTD method and combined with refining method. By adjusting the variables, the reflectivity can be expected to reach a low value within a certain bandwidth. FDTD can easily pick up any discontinuities within the structure, including the groove with finite etching depth. Another reason by applying FDTD method for our problem is this method can obtain the steady state distribution, and all the physics involving mode interactions can be clearly observed.

### 5.4.1  One-Groove Design

The model used for verification and further refinement by FDTD is illustrated in Fig. 5-14, with the 2D waveguide with one deep etching groove at the end. The waveguide mode is obtained by combing EIM and 1D multilayer slab mode solver as explained in 5.3.1.1 part, where only the effective index was used. Here, the resulting mode will work as the incident mode for the FDTD propagation.

By refining the solution in a certain range, the final design for a one-groove structure is obtained and its wavelength dependence is given in Fig. 5-16. Modal reflectance as low as $6.5 \times 10^{-5}$ is obtained for the center wavelength 1.55µm. The bandwidth of the interested range is only 17nm, which is not wide enough for working as an AR coating. The steady field distributions are shown in Fig. 5-15, from where we can observe the radiation mode components are significant larger than the fundamental mode for the reflected region. Similar to what we have experienced with AR coating in Chapter, when the active layer thickness is small, the reflected field has the similar phenomenon. This radiation loss results in a lower reflectivity.
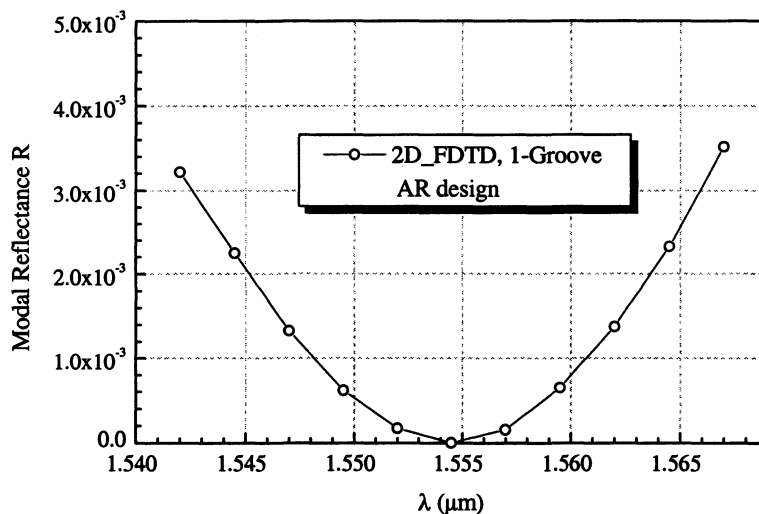
**Fig. 5-16 Modal reflectance wavelength dependence of one design example of the one-etching groove structure simulated by FDTD, with parameters chosen as $d_{L1}$=0.121μm, $d_{H1}$ = 0.272μm, the reflectivity at center wavelength R (1.55μm)= 1.2E-5.**

## 5.4.2  Two-Groove Design
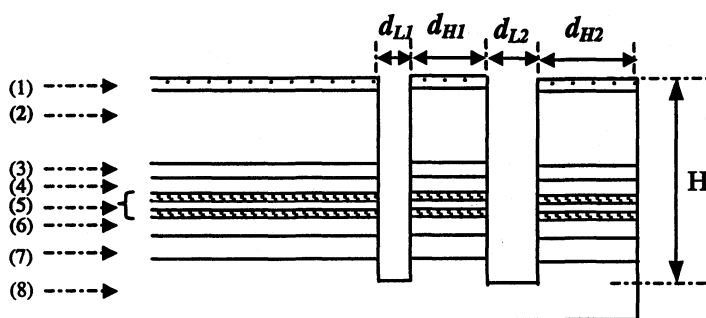


**Fig. 5-17 Schematic diagram of two-groove structure simulated by FDTD method**

By increasing one groove, and using the initial design obtained by TMM design in the previous part, we can verify and obtain a more accurate design for the two-groove structure as shown in Fig. 5-17
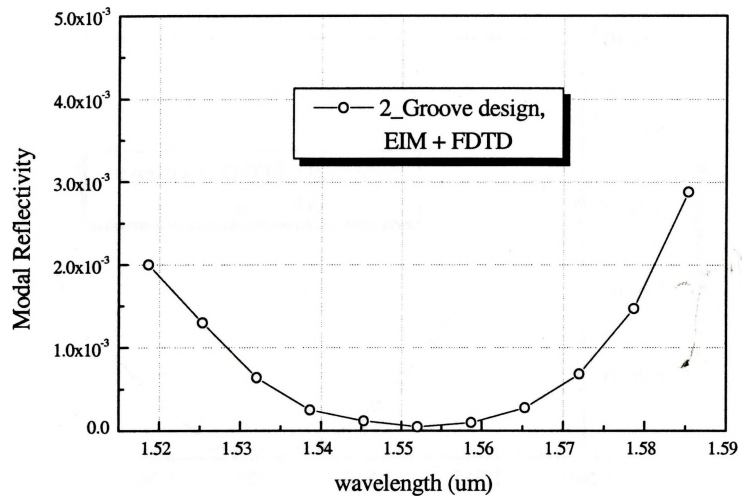
**Fig. 5-18 Modal reflectance wavelength dependence of a design example of the two-etching-groove structure, simulated by FDTD, with parameters chosen as $d_{L1}$=0.116µm, $d_{H1}$ = 0.267µm, $d_{L2}$=0.452µm, $d_{H2}$=0.236µm, the reflectivity at centre wavelength R (1.55µm)= 6.2×10⁻⁵.**



index n(x,z)

**(a)**

Ey(x,z)

**(b)**
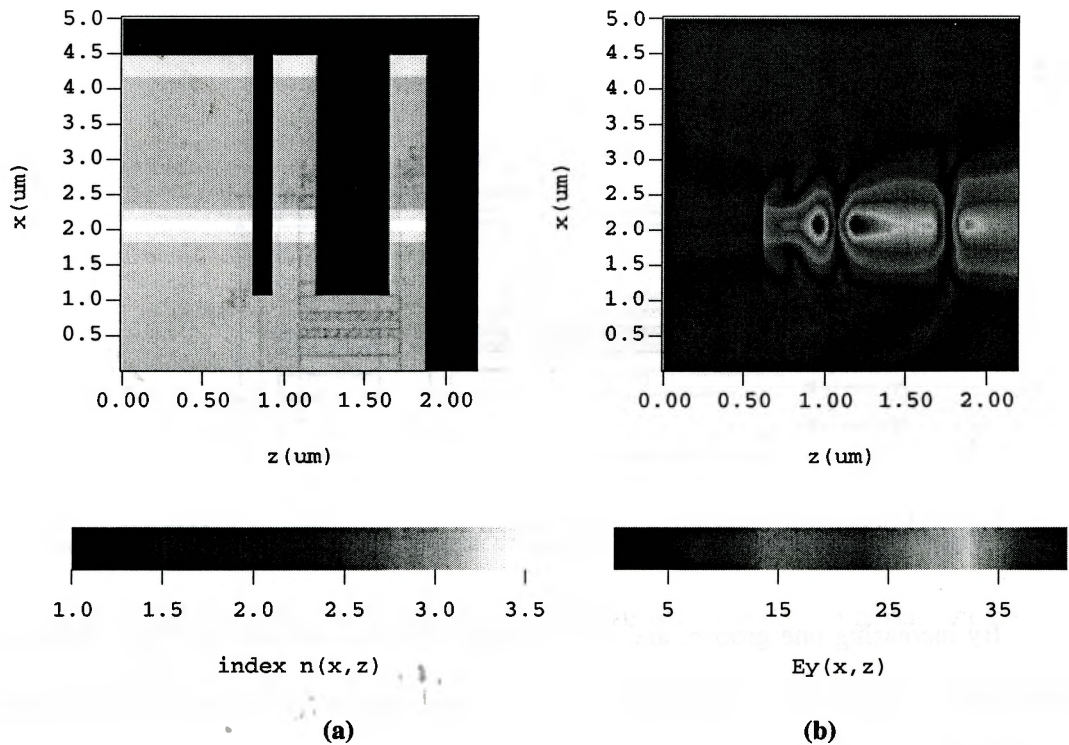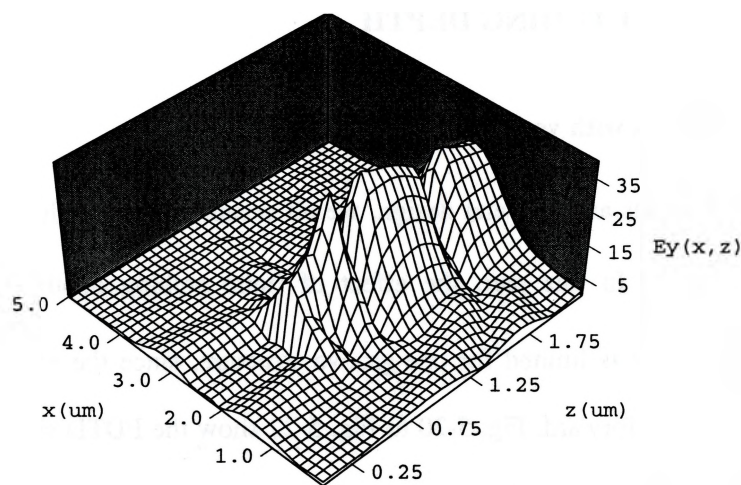
(c)

**Fig. 5-19 Steady state $E_y$ field distribution for the waveguide with two etching grooves at one end. (a) refractive index distribution; (b)Field distribution in color plot; (c) Field distribution in surface plot.**

After repetitive computation of the modal reflectance of the two-groove structure based on the initial design results obtained by TMM, and combining a refining method, the final design for the two-groove deep-etched waveguide structure is obtained with the index and field distribution shown in Fig. 5-19. The wavelength dependence is shown in Fig. 5-18, a modal reflectance with $6.2 \times 10^{-5}$ is obtained for single wavelength 1.55μm. And the bandwidth is extended to be 45nm, which is a great feature. In the previous part, by using TMM we obtained the broadband design with multiple etching grooves. And in this part, the design results obtained by FDTD prove that by applying multiple grooves, the bandwidth did get broadened. Further investigation can be conducted with more groove structure. However, since the time-consuming nature of FDTD method makes it not suitable for a design tool, but better for a verification tool as we have employed. A more efficient numerical tool is desired in order to reach a compromise between the accuracy and efficiency.

## 5.5  EFFECT OF THE ETCHING DEPTH

### 5.5.1   Field distributions with various etching depth

For all the previous analysis and design, we all assume a deep-etching structure, which

satisfy $H > H_0 \approx 3.4\mu m$. In this part, the effect of finite etching depth H is studied. For

simplicity, our study on H is limited for one-groove structure, since the extension to multiple

groove structure is straightforward. Fig. 5-20 to Fig. 5-22 show the FDTD simulation results for

three different etching depth, $H = 1.0\mu m$, $H = 2.5\mu m$, and $H = 4.5\mu m$, respectively.



(a)                                          (b)
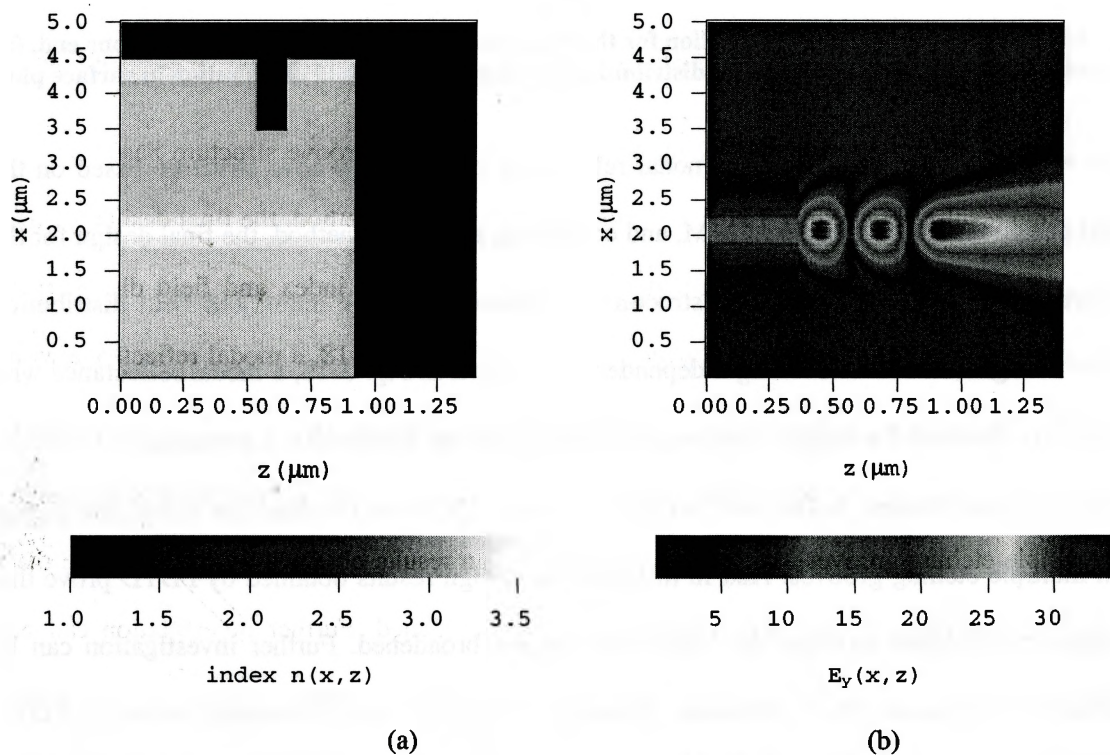
**Fig. 5-20 Steady state Ey field distribution for the shallow etching case with H=1.0μm. (a) Index distribution; (b) Ey field distribution R=0.37 in this case.**

**(a)**                                                    **(b)**
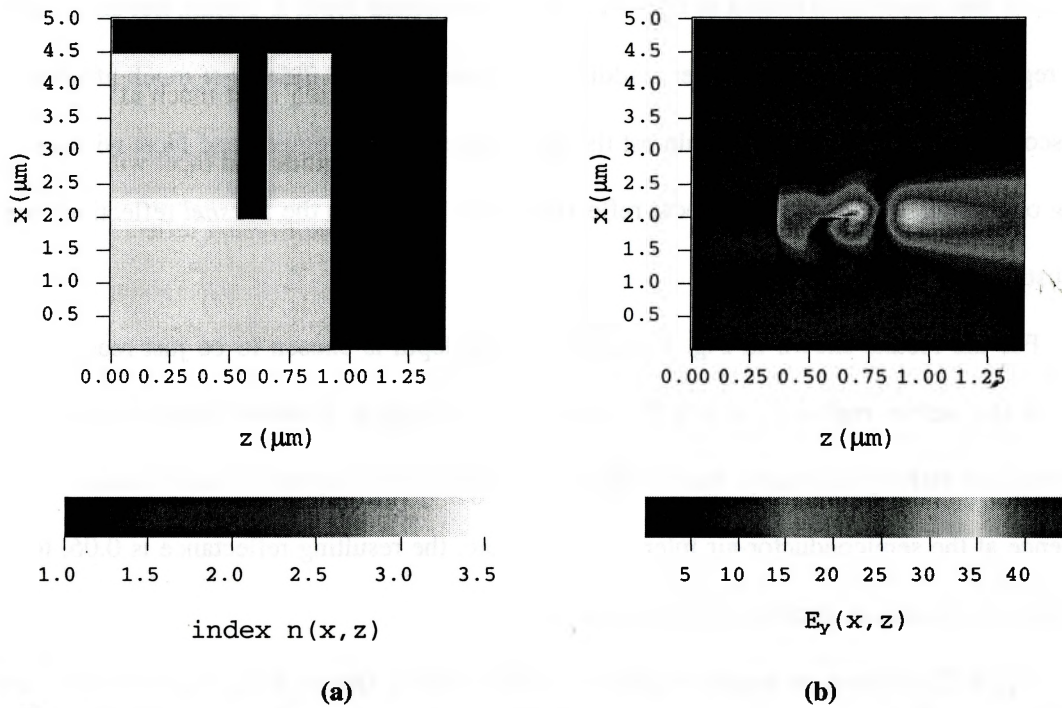
**Fig. 5-21 Steady state Ey field distribution for the moderate etching case with $H$=2.5μm. (a) Index distribution; (b) Ey field distribution. R = 0.067 in this case.**



**(a)**                                                    **(b)**
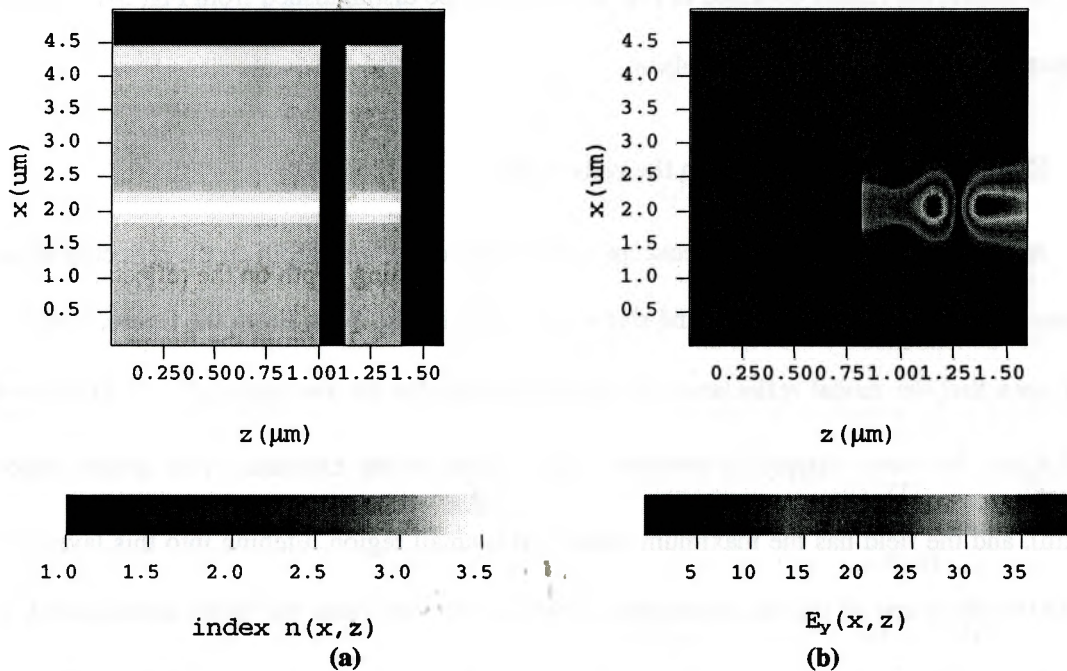
**Fig. 5-22 Steady state $E_y$ field distribution for the full etching case with $H$=4.5μm. (a) Index distribution; (b) $E_y$ field distribution. $R = 1.0 \times 10^{-4}$ in this case.**

For the distribution shown in Fig. 5-20, since the etching depth is 1.0μm, not entering the active region, still staying in the upper cladding InP layer, the field didn't get much affected by this discontinuity. This structure has almost the same effect as a waveguide end facet without any etching or coating. The calculated modal reflectance 0.37 is close to the *Fresnel* reflectivity with InP substrate.

For the results shown in Fig. 5-21, the etching depth is chosen to be just reaching the center of the active region. The steady state field distribution distorted sharply at the air-semiconductor etching boundary. Part of the light is radiated (in optics, it can be described as divergence at the semiconductor-air interface); therefore, the resulting reflectance is 0.06, lower than a shallow grating as shown in the previous figure.

Fig. 5-22 refers to the results in the case of full etching. Due to that the structure we have chosen for this analysis is an optimized structure for deep-etched antireflective waveguide grating structure, the results obtained in Fig. 5-22 can not be distinguished from Fig. 5-15, where the etching depth was chosen as $H_0 = 3.4$μm.

## 5.5.2   Effect of the etching depth on the reflectance

In order to gain a continuous concept of the effect of etching depth on the reflectance, we calculate this dependence by FDTD, and show the results in Fig. 5-23. From the figure, it can be clearly seen that the modal reflectance changed smoothly for the two ends ($H < 1.5 \mu m$, and $H > 3.4 \mu m$, but very sharply in between. This is due to the extremely thin active region (0.15μm), and the field has the maximum value in this small region. Etching into this layer will result in the sharp end of the electromagnetic field. For the two ends, the fields almost decay to

very small values, the small variations with etching depth is reasonable. This also tells us why the waveguide grating only applies at both ends, either shallow grating or deep-etched grating.
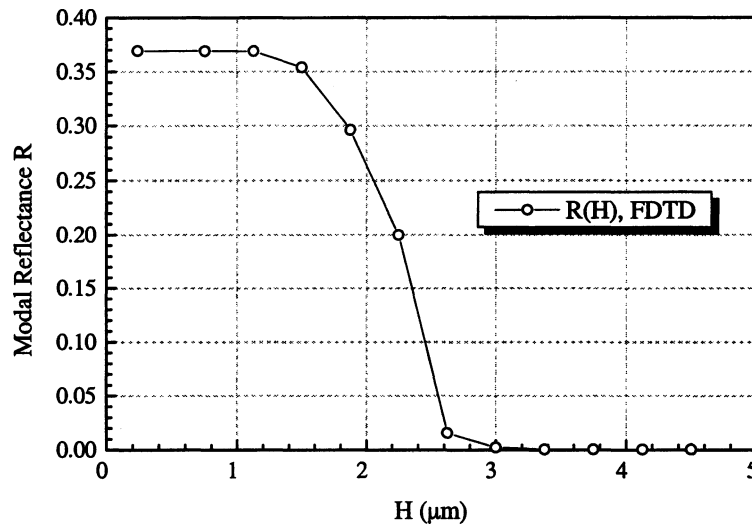


**Fig. 5-23 Modal reflectance as a function of the etching depth H.**

## REFERENCE:

[1]  T. Tamir, *Integrated Optics*, 2nd. Topics Appl. Phys., vol.7, Chap. 1, Springer, New York 1979.

[2]  R. G. Hunsperger, *Integrated Optics: Theory and Technology*, Springer-Verlag, New York 1982, ch.1.

[3]  M. Dagenais, Robert F. Leheny, and John Crow, *Integrated Optoelectronics, Quantum Electronics Principles and Applications*, Academic Press Ltd., 1995, ch. 7, 14, 15.

[4]  Larry A Coldren, Scott W. Corzine, *Diode lasers and photonic integrated circuits*, and 6, John Wiley & Sons, Inc., 1995, Ch. 3.

[5]   T. L. Kock and U. Koren, "Semiconductor photonic integrated circuits," *IEEE J. Quantum Electron.*, vol.27, no.3, pp.641-653, Mar. 1991.

[6]   C. A. Brackett, "Dense wavelength division multiplexing networks: Principles and applications, "*IEEE J. Selected Area Commun.*, vol. 8, pp. 948-964, 1990.

[7]   K. C. Shin, M. Tamura, A. Kasukawa, N. Serizawa, S. Kurihashi, S. Tamura, and S. Arai, "Low threshold current density operation of GaInAsP–InP laser with multiple reflector microcavities," *IEEE Photon. Technol. Lett.*, vol. 7, pp. 1119–1121, 1991.

[8]   P. Vettiger, et al, "Full wave technology – A new approach to large-scale laser fabrication and integration," *IEEE J. Quantum Electron.*, vol.27, no.6, pp.1319-1331, June 1991.

[9]   I. Vurgaftman and J. Singh, "Laser cavity mirror imperfections and reflectivity: A time-dependent numerical approach," *Appl. Phys. Lett.*, vol. 66, pp. 288–290, 1995.

[10] T. Baba, M. Hamasaki, et al, "A novel short-cavity laser with deep-grating distributed Bragg reflectors," *Jpn, J. Appl. Phys.*, vol.35, pp. 1390-1394, 1996.

[11] Y. Yuan, T. Brock, P. Bhattacharya, C. Caneau, and R. Bhat, "Edge-emitting lasers with short-period semiconductor/air distributed Bragg reflector mirrors," *IEEE Photon. Technol. Lett.*, vol.9, no.7, pp.881-883, July 1997.

[12] R. Jambunathan and J. Singh, "Design studies for distributed Bragg reflectors for short-cavity edge-emitting lasers," *IEEE J. Quantum Electron.*, vol.33, pp.1180-1189, July 1997.

[13] T. Mukaihara, et al, "1.3 μm GaInAsP lasers integrated with butt-coupled waveguide and high reflective semiconductor/air Bragg reflector (SABAR)," *Electron. Lett.*, vol.34, pp.882-883, 1998.

[14] T. Mukaihara, et al, "Integrated GaInAsP laser diodes with monitoring photodiodes through semiconductor/air Bragg reflector (SABAR)", *IEEE J. Select. Quantum Electron*, vol. 5, no.3, pp.469-475, May/June, 1999.

[15] P. Modh, N. Eriksson, M.Q.Teixeiro, A.Larsson, and T. Suhara, "Deep-etched distributed Bragg reflector lasers with curved mirrors-experiments and modeling", *IEEE J. Quantum Electron.*, vol.37, pp.752-761, June 2001.

[16] H. A. Macleod, *Thin-Film Optical Filters*, 1$^{st}$ ed. (1982), 2$^{nd}$ ed. (1985), 3$^{rd}$ ed. (2001), Chap. 1-4, McGraw-Hill, New York.

[17] A. Thelen, *Design of optical interference coatings*, McGraw-Hill Optical and Electro-Optical Engineering Series, Chap. 1-5, McGraw-Hill, 1989.

[18] B. Broberg and S. Lindgren, "Refractive index of $In_{1-x}Ga_xAs_yP_{1-y}$ layers and InP in the transparent wavelength region," *J. Appl. Phys.*, vol.55, pp.3376-3381, 1984.

[19] A. Yariv, Quantum Electronics, 2nd ed. New York: Wiley, 1975, pp.512.

[20] M. S. Stern, "Semivectorial polarized finite difference method for optical waveguides with arbitrary index profiles," *IEE Proc. J.* 135, pp.56-63, 1988.

[21] J. Buus, "The effective index method and its application to semiconductor lasers," *IEEE J. Quantum Electron.*, QE-18, pp.1279-1286, 1982.

[22] A. Hardy, "Formulation of two-dimensional reflectivity calculations based on the effective-index method", *J. Opt. Soc. Am.* Part A, vol.1, no.5, pp. 550-555, May 1984.

[23] S. T. Chu, W. P. Huang, and S. K. Chaudhuri, "Simulation and analysis of waveguide based optical integrated circuits," *Comp. Phys. Commun.*, vol.68, pp.451-484, 1991. J. P. Berenger, "A perfectly matched layer for the absorption of electromagnetic waves," *J. Comput. Phys.*, vol.114, pp.185-200, 1994.

[24] B. Chen, D. G. Fang and B. H. Zhou, "Modified Berenger PML absorbing boundary condition for FD-TD meshes," *IEEE Microwave and Guided Wave Lett.*, vol. 5, pp. 399-401, Nov., 1995.

[25] W. P. Huang, S. T. Chu and S. K. Chaudhuri, "A semivectorial finite-difference time-domain method," *IEEE Photon. Technol. Lett.*, vol. 3, pp. 803-806, Sept. 1991.

[26] W. C. Chew and W. H. Weedon, "A 3-D perfectly matched medium from modified Maxell's equations with stretched coordinates," *Microwave and Optical Tech. Lett.*, vol. 7, pp. 599-604, Sept. 1994.

[27] D. Zhou, W. -P. Huang, C. -L. Xu, D.G. Fang,, B. Chen, "The perfectly matched layer boundary condition for scalar finite-difference time-domain method", IEEE Photon. Technol. Lett., pp. 454-456, May. 2001.

[28] Y. Suematsu, S. Arai, and K. Kishino, "Dynamic single-mode semiconductor lasers with a distributed reflector," *J. Lightwave Technol.*, vol. LT-1, pp.161-176, 1983.

[29] C. Vassalo, "Rigorous and approximate calculations of antireflection layer parameters for travelling-wave diode laser amplifiers", *Electronics Lett.*, vol.21, no.8, Apr. 1985.

[30] T. Sitoh, T. Mukai, and O. Mikami, "Theoretical analysis and fabrication of antireflection coatings on laser-diode facets," *IEEE J. Lightwave Technol.*, vol. LT-3, pp.288-293, 1985.

[31] C. Vassallo, "Polarization-independent antireflection coatings for semiconductor coatings for semiconductor optical amplifiers," *Electronic Lett.*, vol.24, no.1, pp.61-62, Jan. 1988.

[32] L. Atternas and L. Thylen, "Single-layer antireflection coating of semiconductor lasers: polarization properties and the influence of the laser structure", *IEEE J. Lightwave Technol.*, vol. LT-7, no. 2, pp.426-430, 1989.

[33] C. Vassallo, "Theory and practical calculation of antireflection coatings on semiconductor laser diode optical amplifiers", *Optical Amplifier Commun., IEE Proc.*, vol.137, pt. J, no.4, pp.193-202, Aug. 1990.

[34] D. M. Braun, and R. L. Jungerman, "Broadband multiplayer antireflection coating for semiconductor laser facets," *Opt. Lett.*, vol.20, no.10, pp.1154-1156, 1995.

[35] C. Cole, "Broadband antireflection coatings for spaceflight optics," *Ph.D thesis* (#R7123), University of reading, UK. Sept. 1995.

[36] R. Prakasam, S. Fox, et al, "Practical approach to design and fabrication of antireflection coatings for semiconductor optical amplifiers", *IEEE Photon. Technol. Lett.*, vol.8, no.4, pp.509-511, Apr. 1996.

[37] D. J. Gallant, M. L. Tilton, D. J. Bossert, J. D. Barrie, and G. C. Dente, "Optimized single-layer antireflection coatings for semiconductor lasers", *IEEE Photon. Technol. Lett.*, vol.9, pp.300-302, Mar. 1997.

[38] J. Lee, T. Tanaka, S. Uchiyama, et. al, "Broadband double-layer antireflection coatings for semiconductor laser amplifiers", *Japan J. Appl. Phys.*, vol.36, pp.L52-L54, Jan.1997.

[39] J. Lee, T. Tanaka, S. Sasaki, S. Uchiyama, "Novel design procedure of broadband multilayer antireflection coatings for optical and optoelectronic devices", *IEEE J. Lightwave Technol.*, vol. LT-16, no.5, pp.884-891, 1998.

[40] J. Lee, T. Kamiya, "Improved characterization of multilayer antireflection coatings for broad-band semiconductor optical amplifiers", *IEEE J. Lightwave Technol.*, vol. LT-18, pp.2158-2166, 2000.

[41] J. Yamauchi, M. Mita, S. Aoki, and H. Nakano, "Analysis of antireflection coatings using the FD-TD method with the PML absorbing boundary condition," IEEE Photon. Technol. Lett., vol.8, pp.239-241, 1996.

[42] P. Sewell, M. Reed, T. M. Benson, and P.C. Kendall, "Full vector analysis of two-dimensional angled and coated optical waveguide facets," IEEE J. Quantum Electron., vol.33, pp.2311-2318, Dec. 1997.

[43] G. -R. Zhou, X. Li and W. -P. Huang, "Design and simulation of deep-etched antireflective waveguide gratings", paper submitted for the publication of *IEEE Photon. Technol. Lett.*, Aug. 2001.

[44] G. -R. Zhou, X. Li, "Design of deep-etched antireflective waveguide gratings for optoelectronics devices", paper submitted for the publication of *International Conference on Laser and Electro-Optics,* CLEO 2002, Optical Society of America, Nov. 2001.

# 6 Deep-Etched High-Reflective Waveguide Gratings

## 6.1 INTRODUCTION

### 6.1.1 Deep-etched distributed Bragg Gratings (DBR)

Conventional edge-emitting semiconductor lasers are fabricated through cleaving, resulting in mirror reflectivities in the range of 0.3~0.4. Monolithic integration excludes cleaved facets as feedback elements for the laser resonator. One of the integration-compatible alternatives is deep-etched distributed Bragg reflectors (DBRs) formed from the cavity material itself and a few number of air gaps created via etching. Deep-etched semicondutor/air DBRs (SABARs) act as 1-D photonic bandgap structures.

It has been reported theoretically and experiementally that high reflectivity over a wide range of wavelengths and angles of incidence can be provided by SABAR, with only a few numbers of periods [9]-[13].

Schematically, a SABAR structure can be depicted as in Fig. 6-1, both 3-D and 2-D views, and several mirrors are formed by deep-etched the waveguide by certain distance $d_{gap}$.

127
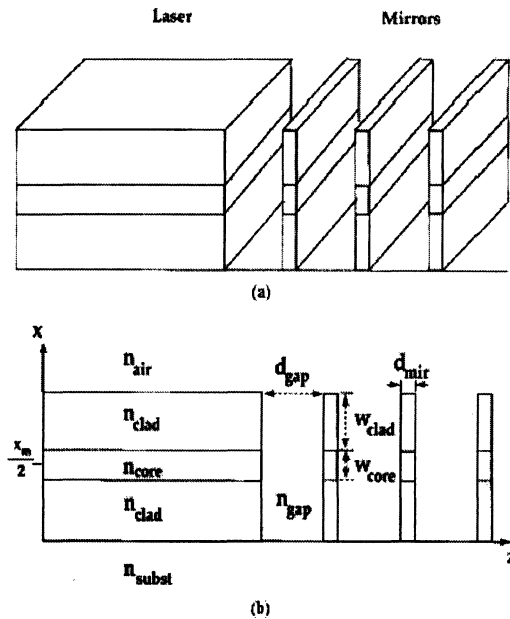
Fig. 6-1 (a) A three-dimensional visualization of the basic structure for the model used in its study and (b) a two-dimensional projection of (a) with the corresponding parameters labelled [13].

In our study in this chapter, instead of using the structures that have been studied in published literatures, we chose the same structure, which we used for design the antireflection (AR) grating for semiconductor optical amplifier. In this chapter, with the same waveguide structure, we can design a high-reflective (HR) grating, used to form edge-emitting laser mirrors. The conclusions obtained in this chapter should be useful to the design with different structures.

From the experiences we have gained from Chapter 4 with HR coatings. A stack of high and low index layers with the thickness as quarter wave optical thickness (QWOT) should provide high-reflectivity.

In this chapter, the HR design will also be divided into two parts: HR design with TMM, and HR design with FDTD method [6],[7]. Results from both approaches are compared with the effect of number of periods and etching depth on the reflectance. Results from both strategies

show that a three-groove deep-etched waveguide grating (uniform grating) is a good choice for

building a SABAR.

## 6.2 HR DESIGN BY TMM
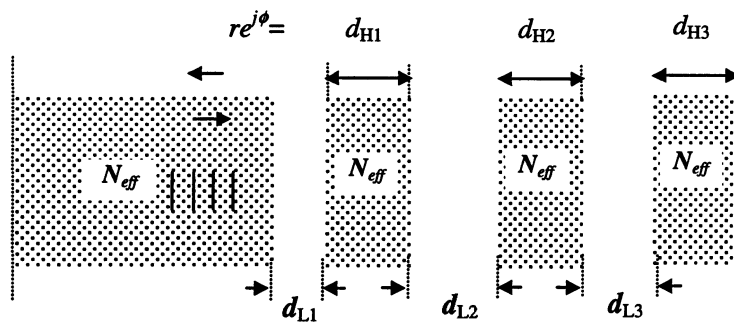


**Fig. 6-2 Schematic diagram for a deep-etched waveguide grating structure with three etching grooves.**

As shown in Fig. 6-2, the deep-etched waveguide grating structure, which we have

studied in Chapter 5 is replotted here. In order to reach a high-reflection, we chose a uniform

periodic grating structure with air gap and mirror width chosen as $1/4\lambda_0$ and $3/4N_{eff}\lambda_0$, same as

[13] respectively. $\lambda_0$ is the center wavelength, and we chose it as $1.55\mu m$.

The effect of number of periods on the reflectance are studied in Fig. 6-3, by increasing

the number of periods (grooves) from 1, to 3, to 7. The reflectance increases quickly from 0.9 to

0.99 when the period number increases from 1 to 3. When the period number increases further

from 3 to 5, to 7, the effect on reflectance is not very obvious, same with the bandwidth.
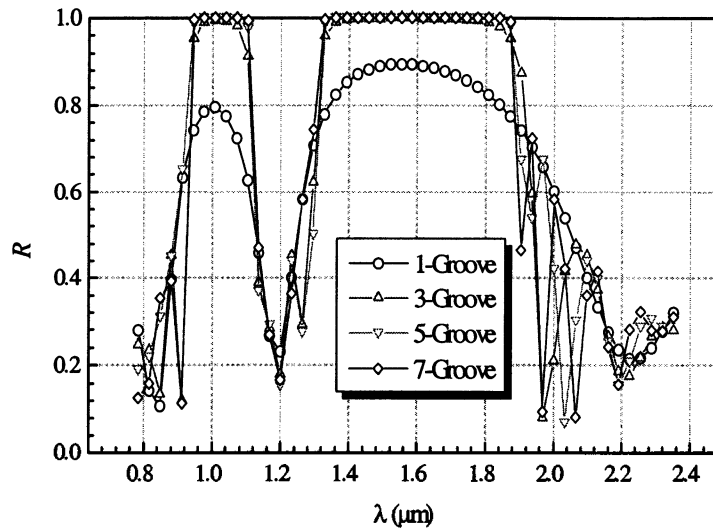
**Fig. 6-3 Reflectance wavelength dependence for structures with different number of groove/periods.**
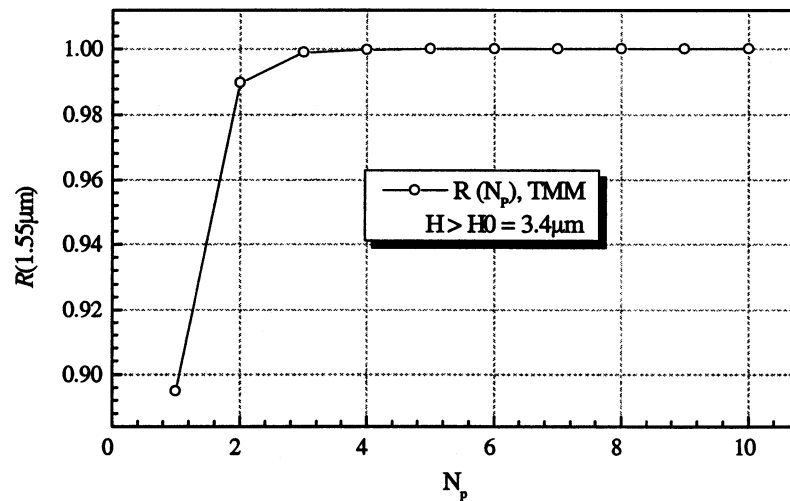


**Fig. 6-4 Reflectance at 1.55μm varies as a function of number of periods, simulated by TMM.**

By fixing the wavelength to be 1.55μm, we can study the effect of number of grating periods $N_P$ on the center wavelength reflectance as shown in Fig. 6-4. It is seen that the

reflectance quickly jumps from 0.88 to 0.99 when the grating number increases from 1 to 3. The

reflectance will saturate at 0.999 (almost 1.0) with adding the number of gratings. This prediction

in TMM shows the reflectance will increase with $N_P$, but will saturate when $N_P$ is larger than 3.

In this sense, $N_P$ more than 3 is not necessary.

## 6.3  VERIFICATION BY FDTD METHOD

In order to give a more reliable design, FDTD is needed to simulate the whole structure.

Same as what we have dealt with AR design in Chapter 5. Since TMM already predicts a good

HR design with (L3H) stack, the same structure can be used for FDTD verification. The results

are shown in Fig. 6-5.
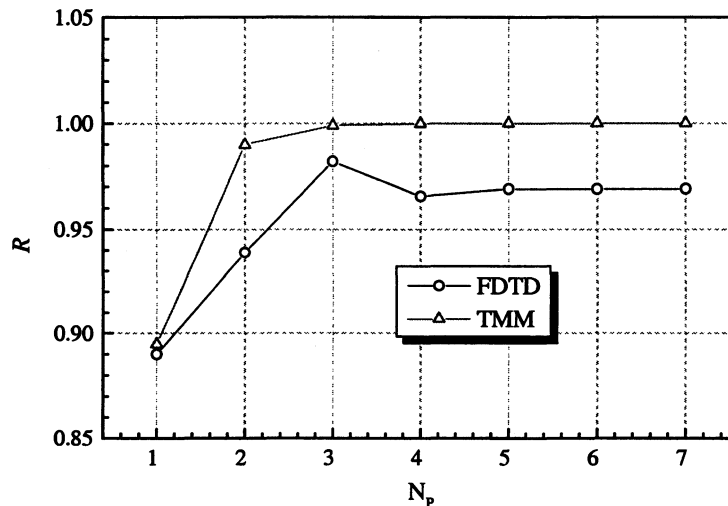


**Fig. 6-5 Reflectance at 1.55μm varies as a function of number of periods, simulated by FDTD, results
done by TMM are also shown for comparison.**

Fig. 6-5 also shows the reflectance will increase from 0.88 to 0.982 when the grating

periods increase from 1 to 3. But when the period numbers increases to 4, it drops to 0.97 and

then with the increasing of the NP, the reflectance will not change accordingly, but maintain a reflectance with 0.97.

Fig. 6-6 to Fig. 6-8 have shown the field distributions for deep-etched waveguide gratings with different choices of NP (1, 3, 6). For all the cases, the grating configurations are chosen as $1/4\lambda_0$ and $3/(4N_{eff}\lambda_0)$ or (L3H), 3(L3H), 6(L3H). From the field distributions, they all get large components reflected back. What's left in the right side of the incident plane is very small, for these three cases.

## 6.3.1 Effect of Period Numbers on the Reflectance
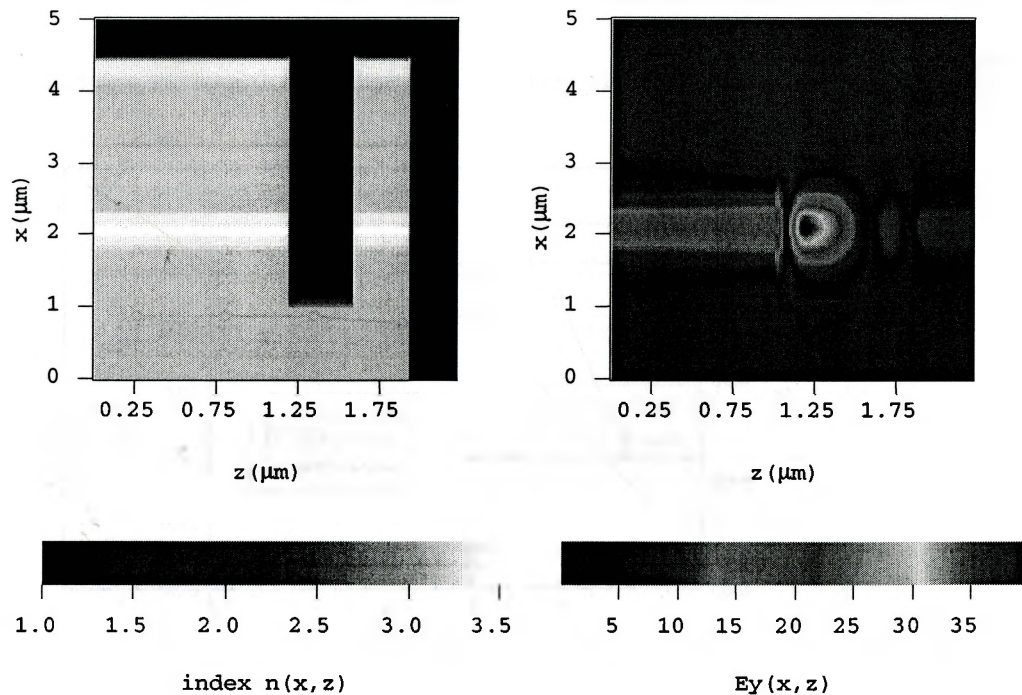


**Fig. 6-6 Design examples for a One-groove deep-etched waveguide structure. (a) Index distributions; (b) Steady state field distributions in color plot; (c) state steady field distribution in surface plot.**
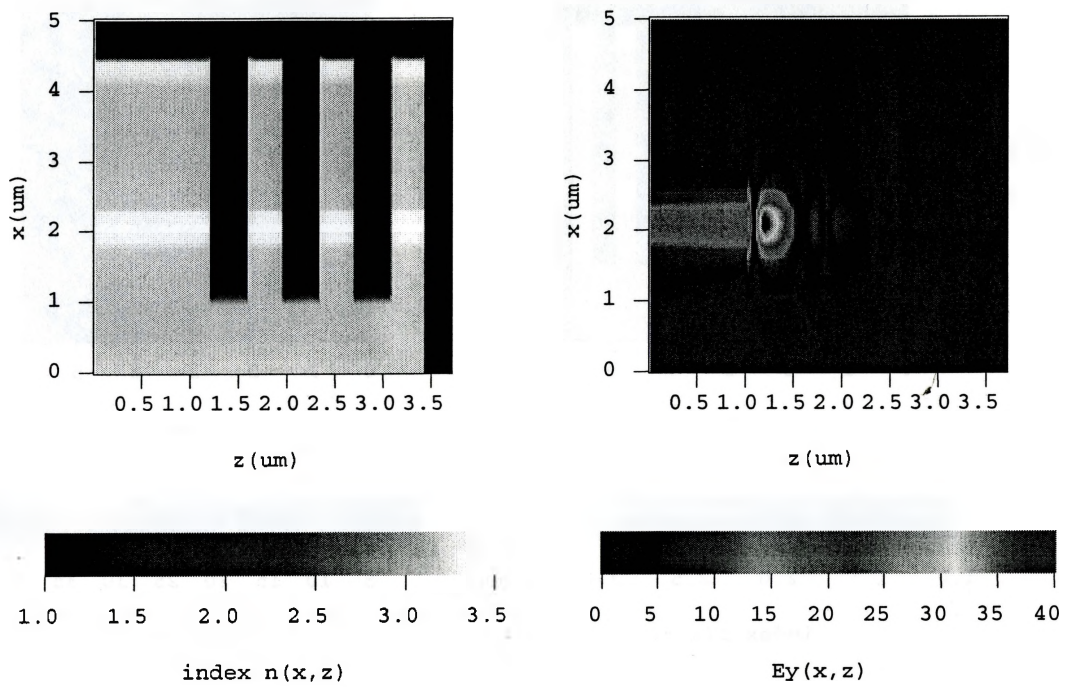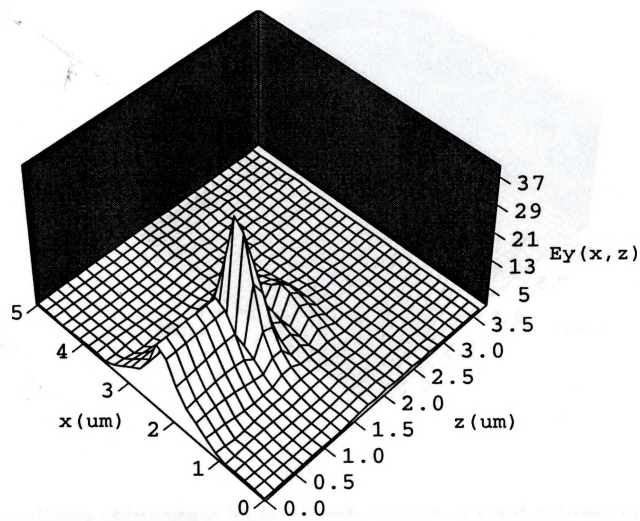
**Fig. 6-7 Design examples for a 3-groove deep-etched waveguide grating structure. (a) Index distributions; (b) Steady state field distributions in color plot; (c) state steady field distribution in surface plot.**

**(a)**



**(b)**



**(c)**
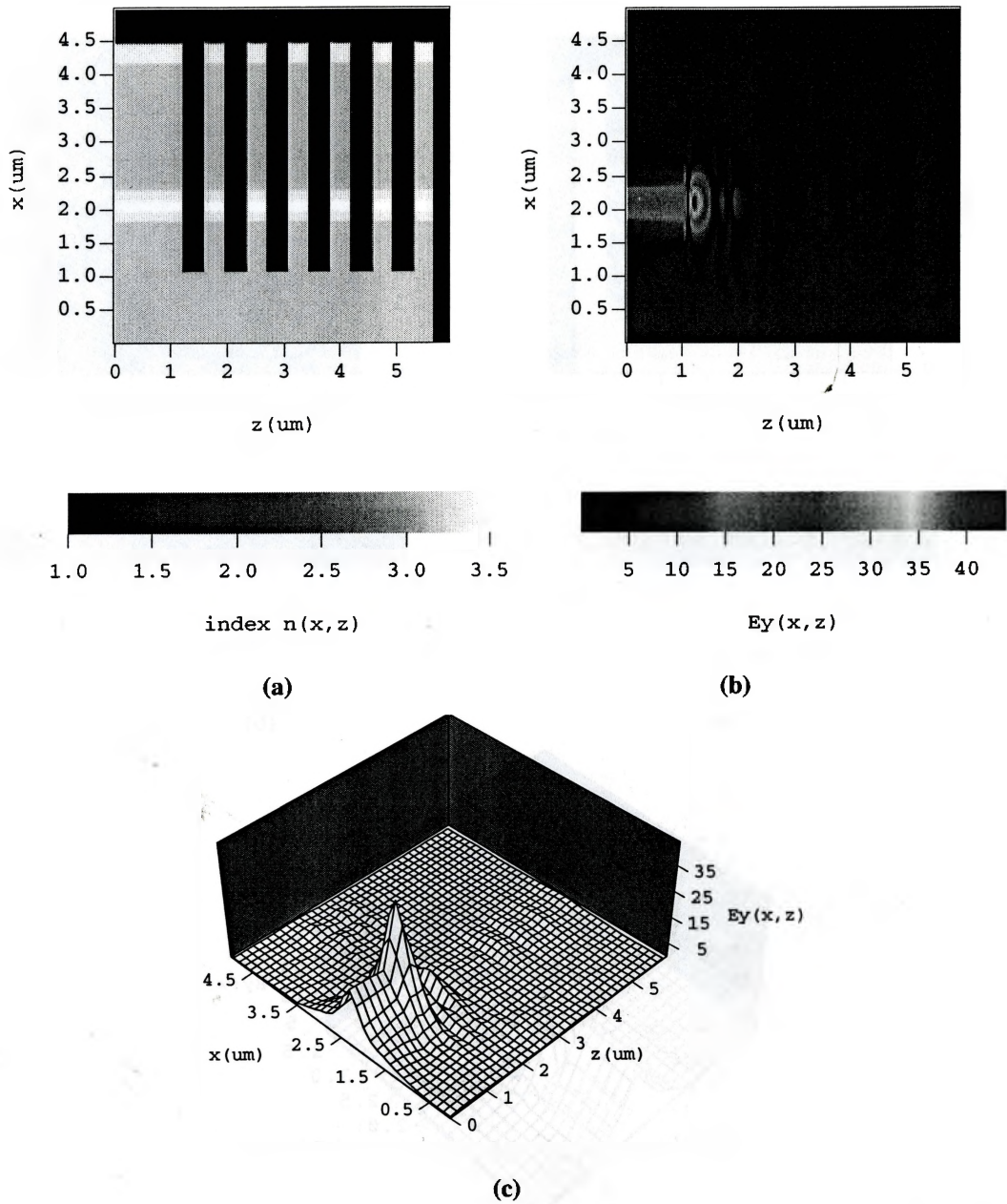
**Fig. 6-8 Design examples for a 6-groove deep-etched waveguide grating structure. (a) Index distributions; (b) Steady state field distributions in color plot; (c) state steady field distribution in surface plot.**

### 6.3.2 Effect of the Finite Etching Depth

We also studied the effect of etching depth on the reflectance, using FDTD method. What have showed in Fig. 6-9 and Fig. 6-10 are the field distributions for the one-groove structure with two different etching depths. Again we have observed the field distortion or beam divergence when the etching ends in the active region. Some parts of the field are radiated into cladding and the substrate and therefore the reflected field component is decreased, which is not expected in HR design.
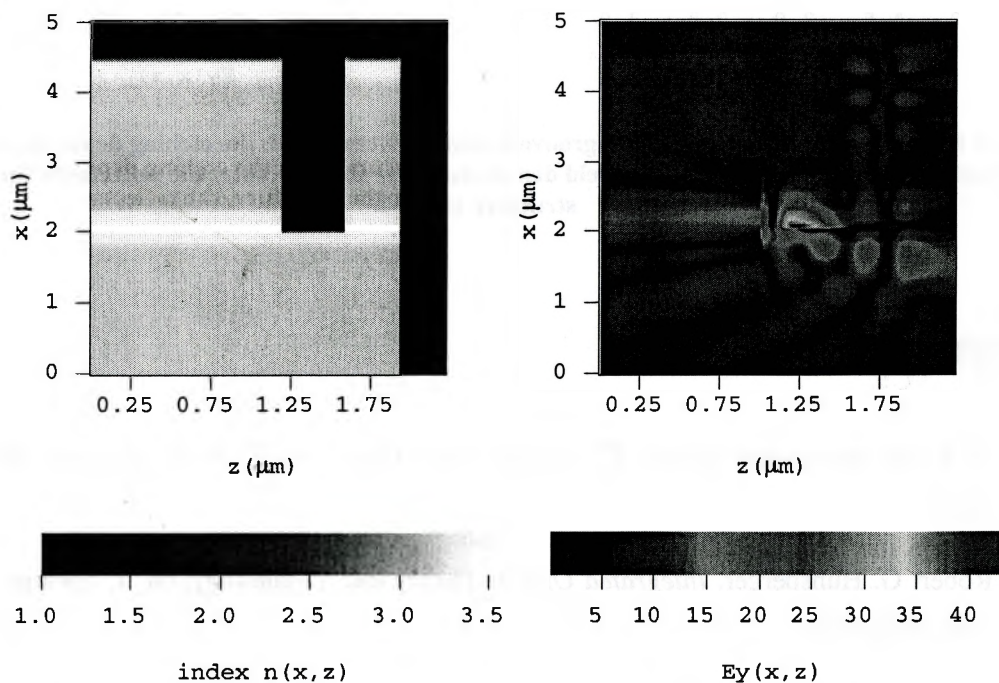


**Fig. 6-9 (a) Index distribution for a one-groove etching structure with the etching depth as 2.5μm (in the active region); (b) Steady state field distributions for the structure, the reflectance is 0.347.**
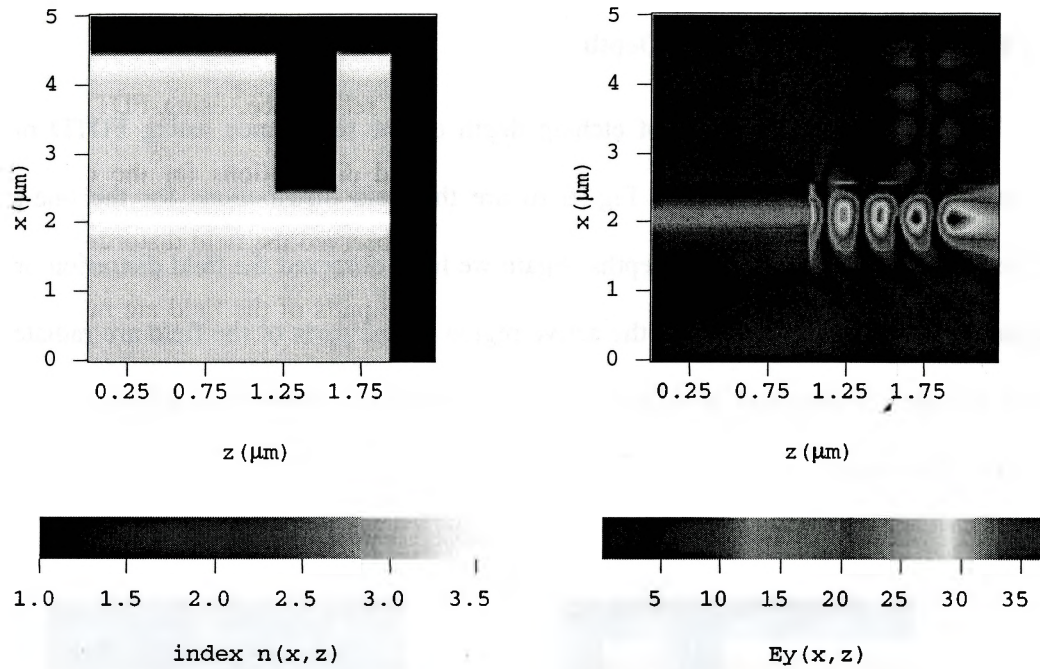
Fig. 6-10 (a) Index distribution for a 1-groove etching structure with the etching depth as 2.0μm (in cladding region); (b) Steady state field distributions for the structure, the reflectance for this structure is 0.374.

# REFERENCE

[1]  T. Tamir, *Integrated Optics*, 2<sup>nd</sup>. Topics Appl. Phys., vol.7, Ch. 1, Springer, New York 1979.

[2]  Robert G. Hunsperger, *Integrated Optics: Theory and Technology*, ch. 1, Springer-Verlag, New York 1982.

[3]  M. Dagenais, R. F. Leheny, and J. Crow, Integrated Optoelectronics, Quantum Electronics Principles and Applications, Academic Press Ltd., 1995.

[4]  Larry A Coldren, Scott W. Corzine, *Diode lasers and photonic integrated circuits*, ch. 3 and 6, John Wiley & Sons, Inc., 1995.

[5] B. Broberg and S. Lindgren, "Refractive index of $In_{1-x}Ga_xAs_yP_{1-y}$ layers and InP in the transparent wavelength region," *J. Appl. Phys.*, vol.55, pp.3376-3381, 1984.

[6] S. T. Chu, W. P. Huang, and S. K. Chaudhuri, "Simulation and analysis of waveguide based optical integrated circuits," *Comp. Phys. Commun.*, vol.68, pp.451-484, 1991.

[7] J. P. Berenger, "A perfectly matched layer for the absorption of electromagnetic waves," *J. Comput. Phys.*, vol.114, pp.185-200, 1994.

[8] P. Vettiger, et al, "Full wave technology – A new approach to large-scale laser fabrication and integration," *IEEE J. Quantum Electron.*, vol.27, no.6, pp.1319-1331, June 1991.

[9] I. Vurgaftman and J. Singh, "Laser cavity mirror imperfections and reflectivity: A time-dependent numerical approach," *Appl. Phys. Lett.*, vol. 66, pp. 288–290, 1995.

[10] T. Baba, M. Hamasaki, et al, "A novel short-cavity laser with deep-grating distributed Bragg reflectors," *Jpn, J. Appl. Phys.*, vol.35, pp. 1390-1394, 1996.

[11] Y. Yuan, T. Brock, P. Bhattacharya, C. Caneau, and R. Bhat, "Edge-emitting lasers with short-period semiconductor/air distributed Bragg reflector mirrors," *IEEE Photon. Technol. Lett.*, vol.9, no.7, pp.881-883, July 1997.

[12] R. Jambunathan and J.Singh, "Design studies for distributed Bragg reflectors for short-cavity edge-emitting lasers," *IEEE J. Quantum Electron.*, vol.33, pp.1180-1189, July 1997.

[13] P. Modh, N. Eriksson, M.Q.Teixeiro, A.Larsson, and T.Suhara, "Deep-etched distributed Bragg reflector lasers with curved mirrors-experiments and modeling", *IEEE J. Quantum Electron.*, vol.37, pp.752-761, June 2001.

[14] J. Yamauchi, M. Mita, S. Aoki, and H. Nakano, "Analysis of antireflection coatings using the FD-TD method with the PML absorbing boundary condition," *IEEE Photon. Technol. Lett.*, vol.8, pp.239-241, 1996.

[15] J. Yamauchi, H. Kanbara, and H. Nakano, "Analysis of optical waveguides with high-reflection coatings using the FD-TD method," *IEEE Photon. Technol. Lett.*, vol.10, pp.11-13, 1998.

# 7 Conclusions

Based on the comprehensive and systematic study of the conventional antireflection (AR) coating for semiconductor optical amplifier (SOA) and the high-reflection (HR) coating for semiconductor lasers, a new deep-etched waveguide structure which is appealing for photonic monolithic integration is proposed and theoretically studied in this thesis. The numerical results simulated by finite difference time domain (FDTD) approach show that a power reflectivity in the order of $10^{-5}$ at $1.55\mu m$ and a bandwidth of 45nm are achievable if a multiple-groove structure is employed.

We expect that more research will be carried out in putting this technology forward by further theoretical study and experimental verifications if possible. We foresee that this research will lead to the following development:

1) Application of optimization algorithms to the design of deep-etched antireflective waveguide gratings. Possible choices could be space mapping (SM) technique and other robust optimization engines.

2) Toleration Sensitivity studies. The difficulty of considering structure toleration sensitivity using FDTD can be overcome by introducing other algorithms, such as adjoint gradient method, etc.